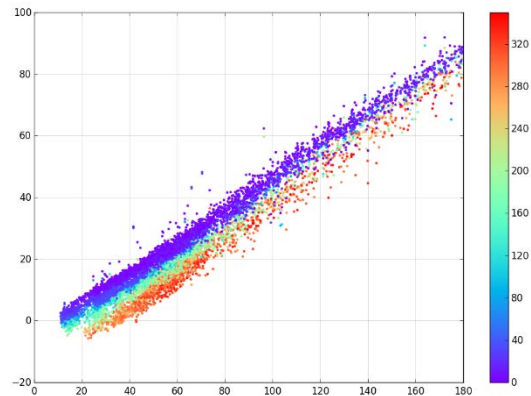
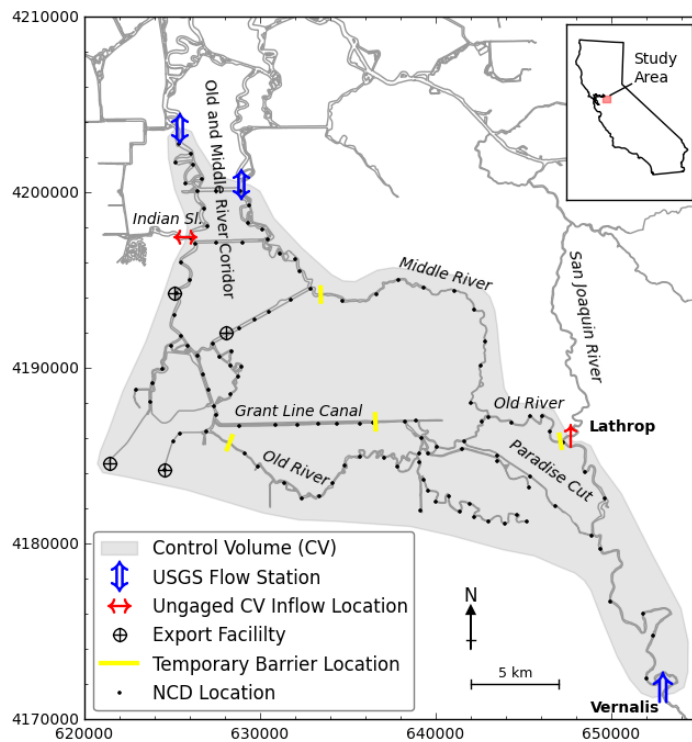


A Water Balance Model to Estimate Flow through the Old and Middle River Corridor, Sacramento–San Joaquin Delta, California

Technical Memorandum

MWD Task Order 02, Subtask 5, Agreement No. 143936

October 2015



Prepared For:
Metropolitan Water District of Southern
California
1121 L Street
Sacramento, CA 95814
Contact:
Paul Hutton, PhD
phutton@mwdh2o.com
(916) 650-2620

Prepared By:
Resource Management Associates
4171 Suisun Valley Road, Suite J
Fairfield, CA 94534
Contact:
Stephen Andrews, PhD
steve@rmanet.com
(707) 864-2950



Executive Summary

Tidally-averaged (hereafter referred to as subtidal) flow through the Old and Middle River (OMR) corridor is an important metric for describing hydrodynamics in the interior Sacramento–San Joaquin Delta. As a result of south Delta water diversions, net flow through the corridor is typically in a landward (southerly) direction except during times of high San Joaquin River inflow to the Delta. This so called “reverse flow” impacts Delta transport patterns and has implications for water quality and ecology in the region. OMR flow is used in several important regulatory contexts. Accurate methods are therefore necessary to predict future OMR flows given expected hydrological and export conditions.

A water balance approach is applied to predict subtidal flows in Old River and Middle River. OMR flow is calculated as the residual flow in a control volume centered on the south Delta: $\text{OMR flow} = \text{San Joaquin River flow at Vernalis} - \text{San Joaquin River flow downstream of the head of Old River} \pm \text{Indian Slough flow at Old River} - \text{net channel depletions} \pm \text{change in subtidal storage}$. Results from long-term (1990–2012) DSM2 simulations are used to develop a linear regression relating Indian Slough flow to OMR flow. Piecewise linear regressions are similarly developed to relate San Joaquin River flow downstream of the head of Old River to San Joaquin River flow at Vernalis for different south Delta barrier configurations and Vernalis flow classes.

The change in subtidal storage term accounts for the cyclic filling and draining of the control volume. The detailed dynamics which govern subtidal flows and water levels are reviewed, and a simplified representation is adopted. Variation in subtidal storage within the control volume is considered to vary due to fortnightly variation in subtidal water level (spring-neap tidal cycling), net Delta inflows, and barometric pressure. Changes in subtidal water levels are converted to flows using a hypsographic curve developed for the south Delta control volume.

In addition to the presented water balance model, which gives separate consideration to different south Delta barrier configurations, Vernalis flow classes, and subtidal flow, a second formulation of the method is derived whereby all unknown regression coefficients are fit directly in one step using a non-linear optimization method. This analysis is referred to as the “direct-fit” method and is provided as ancillary support for the original water balance method.

An error analysis is performed to estimate the accuracy of the water balance method, the direct-fit water balance method, and the DSM2 hydrodynamic model in predicting OMR flows. Flows are compared against USGS observed values on both a 5-day and a 14-day average basis. The water balance method with subtidal storage flows is found to perform with accuracy comparable to DSM2 and represents a significant improvement over existing empirical methods. Its use is recommended in place of existing empirical approaches. The addition of the

subtidal storage term appreciably improves the accuracy of the method, but does requires additional forecast information for future net Delta inflow and barometric pressure. The direct-fit water balance approach has similar accuracy as the piecewise approach, and has the added advantage of requiring fewer model coefficients.

The water balance approach of analyzing flow divisions and accounting for subtidal storage has broad applicability to the Delta. Some potential applications include: improving net Delta outflow estimates by accounting for subtidal storage in the Delta, verifying the accuracy of estimated subtidal flow at USGS monitoring stations by forming control volumes and accounting for subtidal storage, and estimating net channel depletions using a water balance approach incorporating observed flows and estimated storage.

Table of Contents

Executive Summary.....	i
Introduction	1
Literature Review.....	2
Subtidal Water Levels	2
Subtidal Flow through Channel Junctions	3
Methods.....	4
Control Volume Approach to Estimating OMR Flow	4
Subtidal Water Level Analysis.....	12
A Direct Fit Approach to the Water Balance Method	13
Model Performance Metrics.....	14
Results.....	16
Statistical Relationships for Ungaged Control Volume Flows.....	16
Subtidal Water Level Analysis.....	28
Direct Fit Water Balance Approach	35
Discussion.....	36
References	39
Appendix A: Calculation of a Hypsographic Curve for the South Delta Control Volume	42
Appendix B: Yearly Old River at Bacon Island Stage Comparison Plots.....	48
Appendix C: Yearly OMR Flow Comparison Plots.....	71

List of Figures

Figure 1 Control volume map for estimation of OMR flow.	10
Figure 2 South Delta net channel depletions (NCD) as a percentage of total Delta NCD	11
Figure 3 Observed flow at Old River at Bacon Island station as a function of observed flow at Middle River at Middle River station	15
Figure 4 DSM2-predicted Indian Slough and OMR flow correlation and best fit line	19
Figure 5 DSM2-predicted flow in Paradise Cut as a function of San Joaquin flow at Vernalis.....	20
Figure 6 Dependence of DSM2-modeled San Joaquin River flow downstream of HOR on San Joaquin flow at Vernalis, during low flow conditions, and the presence or absence of the HOR barrier.	21
Figure 7 Dependence of DSM2-modeled San Joaquin River flow downstream of HOR on San Joaquin flow at Vernalis and the presence or absence of south Delta temporary barriers for agriculture, for times when the HOR barrier is not installed	22
Figure 8 Dependence of DSM2-modeled San Joaquin River flow downstream of HOR on San Joaquin flow at Vernalis and south Delta diversions, for times when the HOR barrier and Grant Line Canal barriers are not installed.	23
Figure 9 Comparison of methods to estimate San Joaquin River flow downstream of HOR.....	24
Figure 10 Statistical comparison of observed and model-predicted flows on the San Joaquin River downstream of HOR	25
Figure 11 Comparison of OMR estimation method to observed data for DSM2, water balance with and without the subtidal storage term, and direct fit water balance. 5-day average.	26
Figure 12 Comparison of OMR estimation method to observed data for DSM2, water balance with and without the subtidal storage term, and direct fit water balance. 14-day average.	27
Figure 13 Power spectrum for DSM2 predicted stage at Old River at Bacon Island.....	32
Figure 14 South Delta subtidal water level statistical model fit.....	33
Figure 15 Seasonal trends in 5-day average water balance model standard error.	34
Figure 16 RMA 3D San Francisco Estuary Model grid section clipped to south Delta control volume boundary.....	43
Figure 17 Detail of clipped RMA 3D San Francisco Estuary Model grid depths in the area of Woodward Island.....	44
Figure 18 Hypsographic curve data and linear fit for the south Delta control volume region. ...	45
Figure 19 RMA 3D San Francisco Estuary Model grid section clipped to south Delta control volume downstream of temporary agricultural barriers.....	46
Figure 20 Hypsographic curve data and linear fit for the south Delta control volume region downstream of temporary agricultural barriers.....	47

List of Tables

Table 1 Monthly average south Delta water diversions, 1990–2012.....	7
Table 2 DSM2 grid locations of major inflows, outflows, and withdrawals used in the water balance model calibration.	8
Table 3 South Delta temporary barrier operations, 1990–2012.	9
Table 4 Statistical model constants for San Joaquin River flow downstream of HOR.	18
Table 5 OMR water balance model constants without subtidal storage term	18
Table 6 Standard error of OMR flow models.....	19
Table 7 Subtidal water level statistical model parameters.	30
Table 8 Seasonal trends insouth Delta NCD and 5-day average water balance model errors.....	31
Table 9 Direct fit water balance statistical model constants.	35

Introduction

Tidally-averaged (hereafter referred to as subtidal) flow through the Old and Middle River (OMR) corridor is an important metric for describing hydrodynamics in the interior Sacramento–San Joaquin Delta (Delta). As a result of south Delta water diversions, net flow through the corridor is typically in a landward (southerly) direction except during times of high San Joaquin River inflow to the Delta. This so called “reverse flow” impacts Delta transport patterns and water residence times and thus has implications for water quality and ecology in the region (Glibert et al. 2014). Movement of water from north to south generally improves water quality in the OMR corridor by pulling high quality water from the Sacramento River into the interior Delta. However, during periods of low net Delta outflow, this flow pattern tends to pull saline water from the western Delta into the interior. Salvage of the federally-threatened delta smelt (*Hypomesus transpacificus*) in export facilities has been correlated with reverse OMR flows (Grimaldo et al. 2009). As a result, flow restrictions have been imposed on OMR as part of the U.S. Fish and Wildlife Service Long Term Biological Opinion’s Reasonable and Prudent Alternative (USFWS 2008) to limit the potential for smelt entrainment. OMR flow restrictions are also incorporated in the National Marine Fishery Service Biological Opinion (NMFS 2009).

Because of the aforementioned restrictions, water managers need methods to accurately estimate OMR flows for projected future conditions. A simple water balance model is an efficient and conceptually clear approach to meet this need. Hutton (2008) developed a water balance model to estimate OMR flows and provided a comparison with previously available statistical models (Snow 1986; Ruhl et al. 2006). Water balance models are available in the DAYFLOW program (CDWR 1986) to describe a variety of subtidal flows in the Delta. Notably, Delta outflow is estimated by a water balance method to comply with flow requirements imposed by the State Water Resources Control Board (SWRCB 1999). This approach, referred to as the Net Delta Outflow Index, neglects changes in subtidal storage in the Delta by assuming that inflows and outflows balance on a daily basis. Oltmann (1998) compared this index with net flows estimated by flow monitoring and found it to be accurate at moderate to high flows but less accurate at low flows. Potential sources of error in the water balance method were cited as effects of the spring-neap cycle, variability in barometric pressure, and uncertainty in net channel depletions, herein referred to as Delta NCD (Oltmann 1998). Although not directly mentioned by Oltmann (1998), measurement error is also inherent in determining statistically significant small net flows in the presence of much larger estuarine tidal flows (Jay et al. 1997).

Simple water balance methods which assume inflows and outflows balance may be improved by considering changes in subtidal storage. In addition to the spring-neap cycling and variation in barometric pressure mentioned by Oltmann, subtidal water levels can also be influenced by

the magnitude of river inflows or diversions, regional and local winds, and hydraulic structure operations. Because of the complex channel connectivity of the Delta and the depth and flow dependent effects of bottom friction, these subtidal water level forcing factors can interact to affect subtidal flows in non-linear ways.

This technical memorandum details the derivation, assumptions, and evaluation of a water balance method to estimate flows through the Old and Middle River corridor. Explicit consideration to changes in subtidal storage is given. The following section reviews the most current literature on subtidal water levels and subtidal flows through channel junctions. The control volume is defined and the water balance model formulation is derived in the Methods section. An analysis of subtidal water levels is introduced in order to account for changes in subtidal storage. Ungaged inflows and outflows to the control volume are estimated based on statistical regressions derived from long-term DSM2 model simulations. The water balance model is evaluated compared to USGS observed data in the Results section. Error metrics and summary figures are shown to compare the performance of DSM2 and the water balance model with and without subtidal storage. Lastly, implications of the presented methods and results are explored in the Discussion section.

Literature Review

Subtidal Water Levels

The spring-neap cycle of subtidal water level referred to by Oltmann (1998) has been widely observed in estuaries (LeBlond 1978). This variability is associated with compound tides and occurs at frequencies related to those of astronomical tidal constituents (Parker 2007). For example, variation at the frequency of the principle lunar tide (M_2) minus the frequency of the principle solar tide (S_2), referred to as the compound tide constituent MS , is related to variations in tidal range over the spring-neap cycle and associated changes in subtidal friction (Buschman et al. 2009). This constituent has the same frequency as the astronomical constituent MS_f , but is created by hydrodynamic effects, not astronomical forcing. Since these hydrodynamic effects are generated by bottom friction, they depend on river flow, tidal amplitude, and the non-linear interactions that develop between the two (Buschman et al. 2009; Godin 1999). A simple description of the spring-neap cycle of subtidal water levels is that the higher flow velocities during spring tides result in increased friction; an increased subtidal water level slope is therefore required to transport river water seaward (Buschman et al. 2009). Positive river flow is not a requirement for this process. The large tidal range during spring tides results in a large landward Stokes drift balanced by a seaward Stokes drift compensation flow which, like river flow, is driven by a subtidal water level slope (Jay and Flinchem 1997). Therefore, like river flow, this Stokes drift compensation flow is also impeded by increased

friction resulting in spring-neap variability. Furthermore, Stokes drift and Stokes drift compensation flow are not always in balance. Sassi and Hoitink (2013) found substantial landward water flux in periods of peak Stokes drift corresponding to spring tides. When river flow is present, its magnitude similarly influences water levels, subtidal friction, and generation of compound tides. The overall subtidal water level variation therefore cannot be represented solely by a harmonic analysis (Jay and Flinchem 1997). Hydrodynamic models and complex analytical models (e.g., Buschman et al. 2009) can estimate these effects to accurately predict water levels. However, Buschman et al. (2009) report that the pragmatic approach proposed by Godin (1999), whereby subtidal water level is estimated as a linear function of tidal range and net river flow, was also able to reproduce observations.

Not only do river flows influence the generation of compound tides, they also directly influence water level even in the absence of tides. Subtidal water level is further influenced by barometric pressure, local and coastal wind, and operations within the Delta. In South San Francisco Bay, Walters (1982) found that subtidal water level variations were generated by non-local coastal forcing, primarily related to barometric pressure, and that local wind contributed only a small amount of setup. Operations that influence water levels in the interior Delta are diversions for the Central Valley Project (CVP), State Water Project (SWP), and Contra Costa Water District (CCWD), temporary barrier installation, and Delta NCD. Delta NCD is particularly uncertain (Siegfried et al. 2014) and may constitute a substantial portion of net flows during low inflow conditions.

Subtidal Flow through Channel Junctions

The water balance model for OMR flow requires estimation of subtidal flow division at channel junctions. Observed subtidal flow division depends on local water surface slopes, channel geometry and friction, and tidal amplitude (Buschman et al. 2010). One reason for tidal variation is that Stokes drift and Stokes drift compensation flow, both of which vary with tidal amplitude, can be distributed unevenly in branching channels (Sassi et al. 2012). A portion of the water volume transported landward by Stokes drift in one channel may flow into an adjacent channel at a junction and return as Stokes drift compensation flow by a different pathway. Previous modeling in the Delta (URS 2007, Fleenor and Bombardelli 2013), however, has been successful at predicting flows and salinity without accounting for variability in flow divisions with tidal range. This suggests that variability in subtidal flow through junctions with tidal range may be weak in the Delta.

Observed flow divisions at a junction can change dramatically due to temporary barrier installation. A barrier is typically installed at the head of Old River (HOR) in the fall and spring and is intended to benefit migrating San Joaquin River Chinook salmon (*Oncorhynchus tshawytscha*). When the HOR barrier is not in place, the net downstream flow at the Old River–

San Joaquin River junction predominantly travels down Old River (at low San Joaquin flows) or is split approximately evenly (at higher San Joaquin flows). With the HOR barrier in place, flow into Old River is restricted and about 80% of the flow continues in the San Joaquin River. Temporary agricultural barriers are typically placed at three locations (on Old River, Middle River, and Grant Line Canal) during the summer months in order to raise water levels and keep local agricultural intakes underwater. These structures restrict flow, but allow some water over and through them, altering local water surface slopes and affecting flow splits.

Methods

Control Volume Approach to Estimating OMR Flow

OMR flow was calculated as the residual flow in a control volume centered on the south Delta (Figure 1). Flow may enter or exit the control volume through river channels at the San Joaquin River at Vernalis, the San Joaquin River downstream of the HOR split (near Lathrop), Indian Slough, and Old River and Middle River at Bacon Island. The motivation for defining the control volume in this way was to make use of the long term USGS-measured flow records dating back to 1923 at Vernalis and 1987 at Old and Middle Rivers. A CDWR flow gage at Lathrop was operational between late 2004 and early 2012.

Major diversion points from the control volume are the Clifton Court Forebay (SWP) intake, the Jones Pumping Plant (CVP), and CCWD facilities on Old River and Victoria Canal. Agricultural diversion and return flows (i.e. Delta NCD) are estimated by CDWR at multiple locations throughout the control volume. The magnitude of these sources and sinks are driven by a variety of climatic and landscape factors as well as farm-scale water management decisions. Monthly average values for these diversions is shown in Table 1.

Conservation of fluid volume within the control volume dictates that, at a given time step, inflows must be offset by outflows and changes in storage.

$$Q_{omr} \equiv Q_{old} + Q_{mid} = Q_{vns} - Q_{lrp} - Q_{ind} - Q_{div} - \frac{\Delta V}{\Delta t} \quad (1)$$

where

- Q_{omr} = combined Old and Middle River flows
- Q_{old} = Old River flow at Bacon Island
- Q_{mid} = Middle River flow at Bacon Island
- Q_{vns} = San Joaquin River flow at Vernalis
- Q_{lrp} = San Joaquin River flow downstream of HOR
- Q_{ind} = Indian Slough flow at Old River

Q_{div} = south Delta diversions, the sum of Delta exports and NCD in the control volume
 ΔV = change in water volume over time Δt

Flow is considered positive in the seaward direction; this is north for most channels and west for Indian Slough. South Delta diversions are considered positive when water is removed from the control volume. South Delta diversions and San Joaquin River flow at Vernalis are considered known for planning purposes.

Since long-term flow records are not available for Indian Slough and the San Joaquin River at Lathrop, they were estimated by linear regression with Q_{omr} and Q_{vns} , respectively, using the results of DSM2 simulations. The linear regression equations can be expressed as

$$Q_{lrp} = aQ_{vns} + c \quad (2)$$

$$Q_{ind} = a'Q_{omr} + c' \quad (3)$$

where a and a' are dimensionless fitting parameters, and c and c' are fitting parameters with units $m^3 s^{-1}$. Substituting in to Equation 1 results in

$$Q_{omr} = A_{wb}Q_{vns} + B_{wb}Q_{div} + C_{wb} - \frac{\Delta V}{\Delta t} \quad (4)$$

where A_{wb} and B_{wb} are dimensionless parameters, and C_{wb} has units $m^3 s^{-1}$.

Two long-term DSM2 simulations were performed, the results of which were used to estimate the fitting parameters in Equations 2 and 3. The first was a historical simulation, using observed values for boundary inflows and major diversions. The time period chosen was 1990 through 2012, the longest period with CDWR verified boundary flow records and input files available at the time of this work. From this record, two time periods were excluded: Jan–Feb 1997, because of flooding conditions on the San Joaquin River around Vernalis, and Jun–Dec 2004, because of the Jones Tract levee failure and subsequent pump-out. Both time periods include anomalous flows into and out of the control volume that are not accounted for in Equation 1. The second DSM2 simulation was similar to the historical case, but did not include SWP and CVP diversions. The intention of including this simulation data was to encompass a broader range of operational conditions in the regressions, so that non-historical operational regimes could be evaluated for planning purposes without relying on extrapolation in the water balance model.

The specific version of DSM2 used in this study was v8.0, which underwent a full recalibration effort in 2009 (CH2M Hill 2009). Model flow data were output at Indian Slough at Old River (DSM2 channel node 236), Old and Middle River at Bacon Island (channel nodes 106, 144, and 145), and the San Joaquin River at Lathrop (channel node 8). Raw 15 minute output data were tidally filtered using a Godin filter in order to obtain net flows, and then daily averaged to

create a manageable number of data points for the two full 23 year time-series. Indian Slough flow was regressed against OMR flow because of their proximity and similarity in hydraulic behavior. San Joaquin River flow at Lathrop was statistically related to San Joaquin River flow at Vernalis by linear regression. A full list of the DSM2 output locations used in the analysis is given in Table 2.

At high flows, a portion of the San Joaquin River flow upstream of the Old River junction spills over an overflow weir connecting the San Joaquin River to Paradise Cut. Due to the presence of this weir, relationships of San Joaquin River flow at Lathrop to San Joaquin River flow at Vernalis were developed for multiple ranges of San Joaquin River inflow. The effect of barrier operation on the San Joaquin River–Old River flow split was accounted for by obtaining different best fit regression equations for filtered time-series when barriers were in place or absent. Specific cases were considered with all barriers out, with the Grant Line Canal barrier in and HOR barrier out, and with the HOR barrier in. Because of different prevailing hydraulic conditions and construction designs, the fall HOR barrier installation was treated separately from the spring HOR barrier. South Delta diversions were also included in the regression because of their effect on local water surface slopes in all cases except the highest San Joaquin flows and when the spring HOR barrier is installed. Temporary barrier installation and removal dates are presented in Table 3.

Delta island diversion and return flows were calculated by CDWR and provided as DSM2 boundary conditions. NCD in the south Delta control volume consistently averaged around 20% of the total Delta NCD (Figure 2).

Table 1 Monthly average south Delta water diversions, 1990–2012. Negative net channel depletions in winter months are the result of high precipitation compared to agricultural diversions.

Month	San Joaquin R at Vernalis (m ³ s ⁻¹)	South Delta NCD (m ³ s ⁻¹)	SWP (m ³ s ⁻¹)	CVP (m ³ s ⁻¹)	CCWD Total (m ³ s ⁻¹)
January	135	-7	130	95	4
February	180	-7	108	97	5
March	181	2	101	90	3
April	200	8	63	58	3
May	185	14	35	42	5
June	128	24	69	80	8
July	82	28	139	110	8
August	53	19	150	110	7
September	55	10	138	112	5
October	68	7	105	105	3
November	53	5	96	98	3
December	71	2	116	90	3

Table 2 DSM2 grid locations of major inflows, outflows, and withdrawals used in the water balance model calibration. South Delta NCD were estimated from CDWR’s DICU model.

Data Type	Data Location	DSM2 Channel or Node Number	Observed or Computed Data
River Flow	Old River at Bacon Is	Channel 106	Computed
River Flow	Middle River at Middle River	Channels 144 and 145	Computed
River Flow	San Joaquin River at Vernalis	Node 1	Observed
River Flow	Indian Sl at Old R	Channel 236	Computed
River Flow	San Joaquin River below HOR at Lathrop	Channel 8	Computed
Diversion	Clifton Court Forebay	Node 72	Computed
Diversion	Jones Pumping Plant	Node 181	Observed
Diversion	CCWD Intake at Old R	Node 80	Observed
Diversion	CCWD Intake at Victoria Canal	Node 191	Observed
Diversion	South Delta NCD	Diversions/returns from several nodes	Computed
Temporary Barrier Operation	Head of Old River Fish Barrier	Channel 54	Observed
Temporary Barrier Operation	Grant Line Canal Agricultural Barrier	Channel 206	Observed
Temporary Barrier Operation	Old River Agricultural Barrier	Channel 79	Observed
Temporary Barrier Operation	Middle River Agricultural Barrier	Channel 134	Observed

Table 3 South Delta temporary barrier operations, 1990–2012.

Year	HORB (Spring)		HORB (Fall)		Old River		Middle River		Grant Line Canal	
	In	Out	In	Out	In	Out	In	Out	In	Out
1990	---	---	11-Sep	27-Nov	---	---	4-Apr	29-Sep	---	---
1991	---	---	12-Sep	23-Nov	25-Aug	28-Sep	4-Apr	27-Sep	---	---
1992	22-Apr	5-Jun	10-Sep	3-Dec	20-Apr	30-Sep	8-Apr	28-Sep	---	---
1993	---	---	10-Nov	6-Dec	1-Jun	28-Sep	16-Jun	23-Sep	---	---
1994	23-Apr	18-May	7-Sep	29-Nov	24-Apr	4-Oct	24-Apr	29-Sep	---	---
1995	---	---	---	---	7-Aug	29-Sep	10-Aug	11-Oct	---	---
1996	---	---	3-Oct	20-Nov	5-Jun	29-Sep	19-May	29-Sep	10-Jul	3-Oct
1997	10-Apr	15-May	---	---	16-Apr	1-Oct	4-Apr	27-Sep	4-Jun	26-Sep
1998	---	---	---	---	---	---	---	---	---	---
1999	---	---	---	---	25-May	27-Sep	18-May	30-Sep	3-Jun	23-Sep
2000	15-Apr	31-May	3-Oct	8-Dec	16-Apr	29-Sep	16-Apr	30-Sep	1-Jun	28-Sep
2001	25-Apr	30-May	6-Oct	25-Nov	26-Apr	14-Nov	21-Apr	14-Nov	9-May	12-Nov
2002	15-Apr	24-May	4-Oct	21-Nov	15-Apr	18-Nov	15-Apr	20-Nov	7-Jun	17-Nov
2003	15-Apr	16-May	22-Sep	5-Nov	14-Apr	14-Nov	15-Apr	11-Nov	10-Jun	10-Nov
2004	12-Apr	21-May	20-Sep	2-Nov	15-Apr	8-Nov	12-Apr	10-Nov	4-Jun	11-Nov
2005	---	---	28-Sep	7-Nov	31-May	9-Nov	12-May	7-Nov	12-Jul	14-Nov
2006	---	---	---	---	17-Jul	15-Nov	7-Jul	17-Nov	19-Jul	20-Nov
2007	20-Apr	22-May	17-Oct	9-Nov	18-Apr	6-Nov	10-Apr	19-Nov	10-May	7-Nov
2008	---	---	16-Oct	3-Nov	4-Jun	3-Nov	21-May	5-Nov	26-Jun	10-Nov
2009	---	---	---	---	23-Jun	3-Nov	19-Jun	16-Nov	1-Jul	29-Oct
2010	---	---	---	---	2-Jun	20-Oct	21-May	28-Oct	6-Jul	14-Oct
2011	---	---	---	---	10-Jun	10-Oct	5-Jun	11-Oct	14-Jul	19-Oct
2012	1-Apr	4-Jun	---	---	31-Mar	20-Oct	16-Mar	23-Oct	4-May	18-Oct

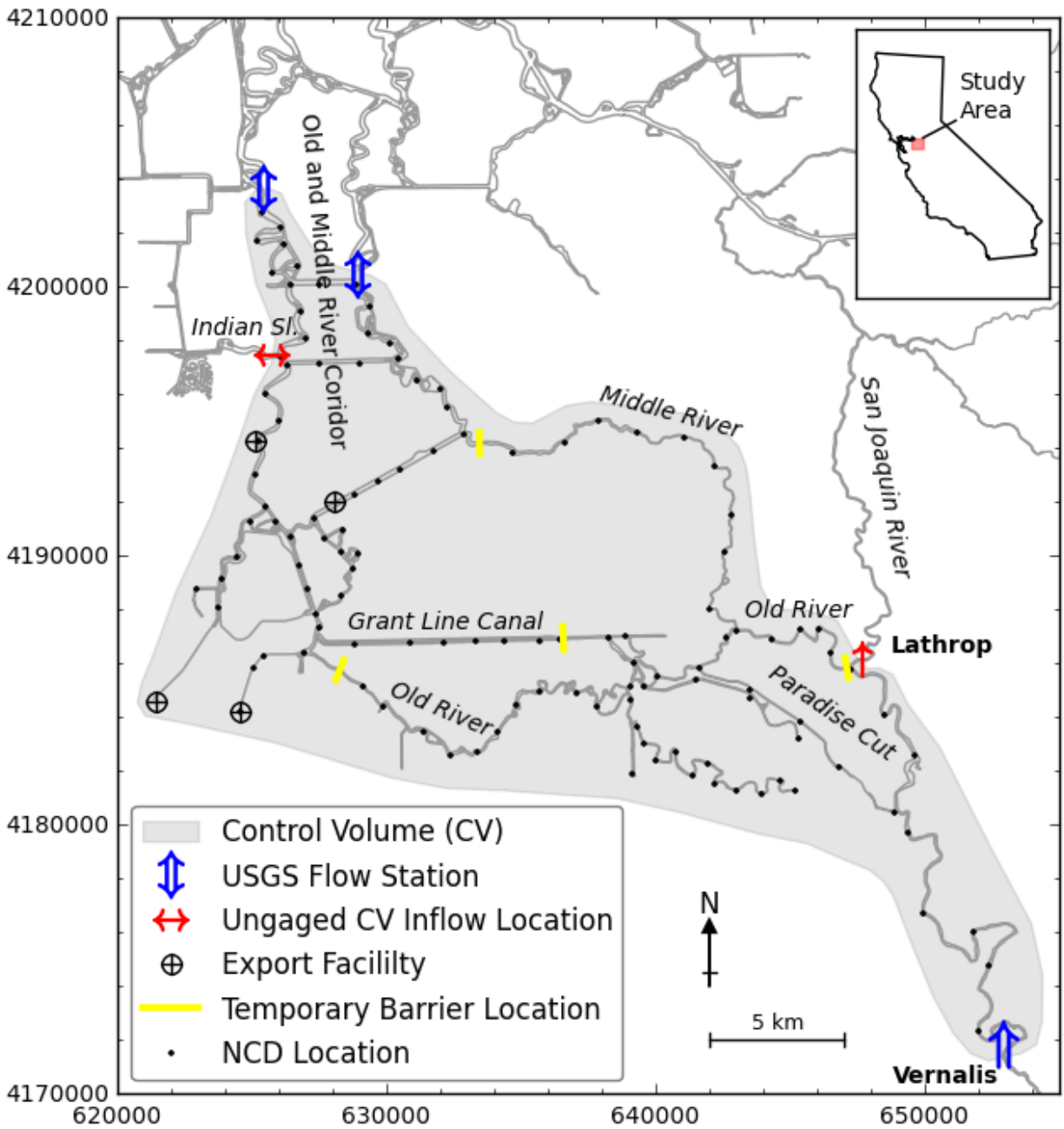


Figure 1 Control volume map for estimation of OMR flow. Coordinate system is UTM, Zone 10 (m).

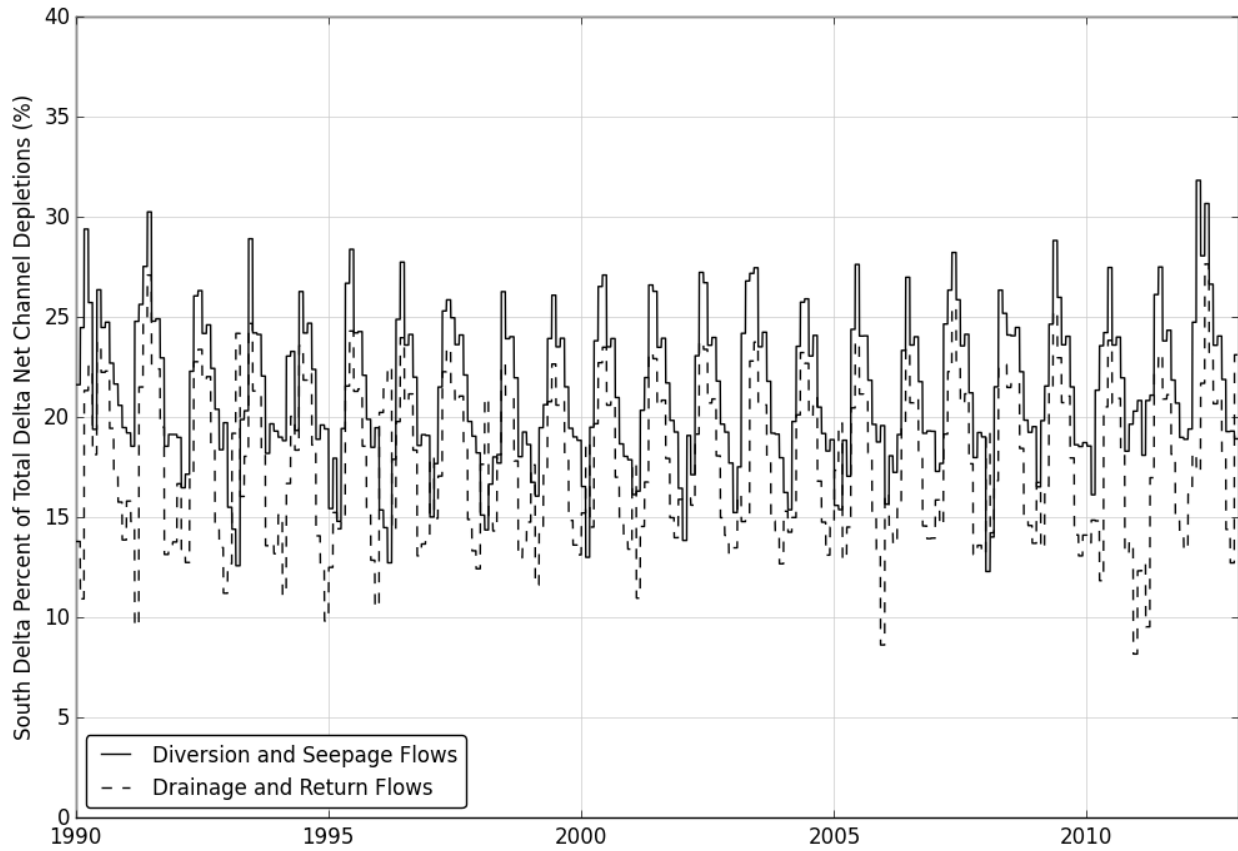


Figure 2 Net channel depletions (NCD) within the south Delta control volume (see Figure 1), as a percentage of total Delta NCD.

Subtidal Water Level Analysis

The final term in Equation 1 takes into account changes in subtidal storage in the control volume. Our approach followed Godin (1999), who estimated a linear effect of river flow on subtidal water level in addition to a periodic spring-neap influence. A linear effect of barometric pressure, acknowledged by Godin (1999) to have a significant effect on subtidal water level, was also included, resulting in:

$$\eta_0 = \sum_i^{N_i} A_i \cos(\sigma_i t + \phi_i) + a_0 Q_{inflow} + b_0 P + c_0 \quad (5)$$

where η_0 is the subtidal water level in m, A_i is the amplitude of the compound tide constituent i in m, σ_i is the frequency of the i^{th} constituent in radians day⁻¹, ϕ_i is the phase of the i^{th} constituent in radians, Q_{inflow} is Delta inflow in m³ s⁻¹, P is barometric pressure in millibars, a_0 is a fitting parameter in m⁻² s, b_0 is a fitting parameter in m millibars⁻¹, and c_0 is a fitting parameter in m. The empirical coefficients were determined by fitting Equation 5 to water level records predicted by the DSM2 simulations using a nonlinear least squares optimization approach (Levenberg 1944). While b_0 is known in theory and may be specified a priori by assuming hydrostatic pressure, Walters (1982) reported that the effect of barometric pressure observed on South San Francisco Bay subtidal water level is greater than expected. Therefore this parameter was retained. Pressure data were obtained from NOAA Station 9414290, located on the south side of the Golden Gate inlet. This data series was supplemented with measurements from the San Francisco International Airport prior to 1996 and where data gaps in the NOAA record existed. The Delta inflow record was developed by summing daily river inflows provided as DSM2 boundary conditions. Wind effects were found to be negligible based on a correlative analysis of wind speed and stress components to water level using a wind record from NOAA Station 9414290. For this reason, wind effects were not included in Equation 5.

Prior to fitting, a power spectrum analysis of water levels indicated three distinct amplitude peaks at periods greater than 25 hours, corresponding to the shallow water interactions of the K_1 and O_1 tides (constituent KO, period 328 hours), the M_2 and S_2 tides (constituent MS, period 354 hours), and the M_2 and N_2 tides (constituent MN, period 661 hours). Therefore, three amplitudes (A_i) and three phases (ϕ_i) were determined in Equation 5. For convenience the time origin (time = 0 days) of the estimated phases was taken to be Jan 1, 1900 at 00:00 in Pacific Standard Time.

Equation 5 does not consider nodal factors to account for variations in tidal amplitude during the 18.61 year lunar node cycle. These node factors are important for the primary astronomical tidal constituents but are more ambiguous for compound tides. They are neglected here for

simplicity. In order to examine this assumption, a harmonic analysis was performed using the Vtide tidal harmonic analysis and prediction package (Foreman et al. 2009). The Vtide package was run in analysis mode to calculate amplitudes for the spring-neap constituents. These were then isolated (all other tidal constituent amplitudes were set equal to zero) and the Vtide package was run in prediction mode in order to construct a water surface elevation time-series reflecting only the spring-neap tidal cycle. The improvement in fit to subtidal water level using Vtide was negligible, so Equation 5 was retained for conceptual simplicity and to allow simultaneous fitting of water level as a function of compound tides, Delta inflow, and barometric pressure.

The specific water surface elevation time-series used for the harmonic analysis was a 23-year long (1990 through 2012) DSM2-predicted stage record at the Old River at Bacon Island station. Other locations throughout the control volume were tested, and results at this station were found to be similar to results at other stations located downstream of the temporary agricultural barriers. The DSM2 stage time-series was analyzed instead of the observed USGS stage at that location because of its long-term record without the complications of missing data.

The subtidal water level predicted using Equation 5 was converted to water volume using a relationship derived from a hypsographic curve of the southern Delta control volume:

$$V = 14.916 \times 10^6 * \eta_0 + 28.845 \times 10^6 \quad (6)$$

where V is the water volume in m^3 and η_0 is water surface elevation in m, NAVD88. This approach implicitly assumes that subtidal water level is constant through the control volume. The bathymetry data used to derive this relationship were aggregated by CDWR from multiple bathymetric surveys (Wang and Ateljevich 2012). Detailed information on the derivation of Equation 6 is given in Appendix A. The change in subtidal storage term needed for Equation 1 was calculated using centered differences.

A Direct Fit Approach to the Water Balance Method

The water balance method as presented is conceptually clear and founded on physical principles, including discrete configurations of the physical system (e.g., barrier installation or channel connectivity) and subtidal storage in the control volume. Separate statistical regressions were performed for Equations 2, 3, and 5, which were then substituted into Equation 1 in order to obtain Q_{omr} predictions for different flow and barrier installation cases. The subtidal storage parameters were not fit to match Q_{omr} directly, but were fit to match a subtidal water level record which was then converted to storage volume using Equation 6. A

total of 18 parameters are present before subtidal storage is considered, and an additional nine parameters are introduced to account for subtidal storage.

An alternative approach is to fit parameters to directly optimize fit to OMR flow instead of developing regressions at individual junctions. In this direct fitting approach all relevant parameters are estimated by nonlinear optimization of a single equation. To derive this equation, Equations 2, 3, 5, and 6 were substituted into Equation 1, and parameters were combined. The effect of Paradise Cut was incorporated by inclusion of a threshold flow at Vernalis, above which the slope of the Q_{omr} dependence on Q_{vns} changes. This guarantees a continuous relationship between Q_{omr} and Q_{vns} . Barrier effects were represented as stepwise changes in the slope of the relationship between Q_{vns} and Q_{omr} . The resulting equation is:

$$Q_{omr} = AQ_{vns} + \max(0, Q_{vns} - D)A' + BQ_{div} + I_s A_s Q_{vns} + I_f A_f Q_{vns} + I_g A_g Q_{vns} + \sum_i^{N_i} A'_i \cos(\sigma_i t + \phi'_i) + a_1 \frac{\Delta Q_{inflow}}{\Delta t} + b_1 \frac{\Delta P}{\Delta t} + C \quad (7)$$

where A , A' , B , A_s , A_f , A_g , are dimensionless fitting parameters, A'_i and ϕ'_i are the unknown amplitudes in $\text{m}^3 \text{s}^{-1}$ and phases in radians of the compound tide constituents, a_1 is a fitting parameter in days, b_1 is a fitting parameter in $\text{m}^3 \text{s}^{-1} \text{millibars}^{-1} \text{day}$, and C and D are fitting parameters in $\text{m}^3 \text{s}^{-1}$. I_s , I_f , and I_g are indicator functions for different barrier operations. I_s takes a value of one during periods of spring HOR barrier installation and zero otherwise. I_f is the analogous indicator function for fall HOR barrier installation, and I_g is the indicator function for periods when only the Grant Line Canal barrier is installed. OMR flows related to subtidal changes in control volume storage are now directly dependent on changes in Delta inflow and atmospheric pressure.

Several simplifications were made in the derivation of Equation 7. Terms including barrier indicator function effects on the slope of the relationship between Q_{omr} and Q_{div} were neglected, and only one breakpoint in the slope of the Q_{vns} and Q_{omr} relationship was considered. These simplifications reduced the number of fitting parameters from 27 to 16 by removing terms implicitly included in Equations 2 and 3 which are expected to have small effects on the prediction of OMR flow. The parameters of Equation 7 were fit using the differential evolution optimization approach (Storn and Price 1997).

Model Performance Metrics

Predictions from the water balance approach and the DSM2 hydrodynamic model were compared to USGS observed OMR flow. Fifteen minute discharge data were obtained directly from the USGS in April 2015 for the Old River at Bacon Island (USGS station number 11313405)

and Middle River at Middle River (11312676) stations. These data were tidally filtered using a Godin filter and then daily-averaged. Both records include periods during which a sensor was malfunctioning and no data were recorded. A more complete record was generated by developing a piecewise linear regression between the two stations and filling in missing data using the regression. Periods excluded from the DSM2 analysis were also excluded from the regression analysis for the same reasons. A piecewise linear relationship was used in order to account for different prevailing hydraulic conditions during strongly negative flows (Figure 3). The slopes and location of the breakpoint were determined using the differential evolution non-linear optimization method (Storn and Price 1997).

Predicted and observed data were compared on both a 5-day and 14-day running-average basis. For the empirical models, period averages of San Joaquin River flow at Vernalis and south Delta diversions were used to compute average OMR flow. For DSM2, predicted OMR flow was averaged over the period. The purpose of this averaging was to examine the accuracy of each method without the additional scatter caused by large day-to-day flow variations. Additionally, both averaging periods have importance in regulatory contexts, including the Reasonable and Prudent Actions under the USFWS and NMFS Long Term Biological Opinions.

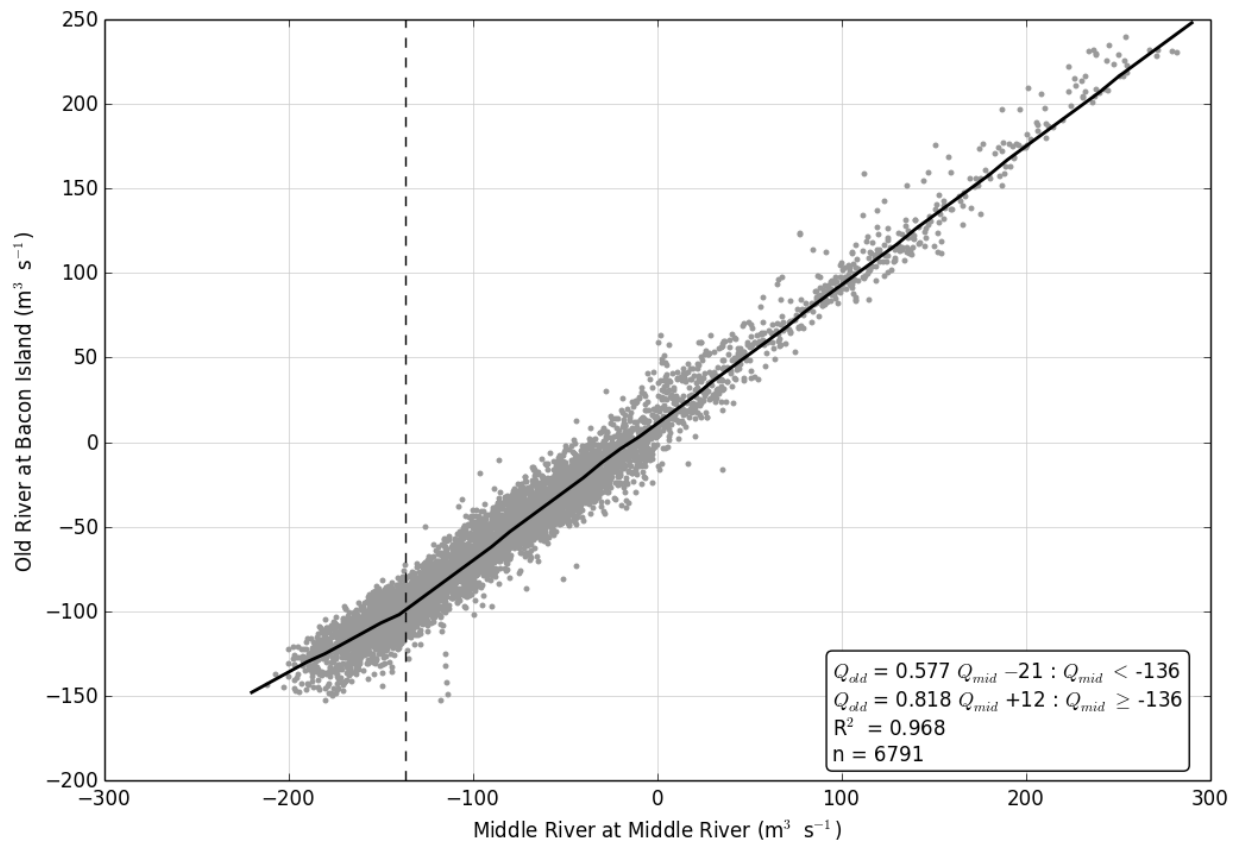


Figure 3 Observed flow at USGS Old River at Bacon Island station as a piecewise linear function of observed flow at USGS Middle River at Middle River station.

Results

Statistical Relationships for Ungaged Control Volume Flows

The relationship between Indian Slough and OMR flow is shown in Figure 4. Subtidal Indian Slough flow averages about 6% of OMR flow. An implication of this is that a slightly less than one-to-one relationship exists between negative OMR flows and the magnitude of south Delta diversions. An improved regression could be developed by accounting for the effect of local NCD in Indian Slough. However, the local diversion term is omitted for simplicity and because its contribution to the accuracy of the Indian Slough flow estimate has a small effect on the estimate of OMR flow.

The relationship between San Joaquin River flow at Vernalis and Paradise Cut is shown in Figure 5. There is a change point in the relationship at $467 \text{ m}^3 \text{ s}^{-1}$ ($16,500 \text{ ft}^3 \text{ s}^{-1}$) when flow begins to spill over the overflow weir connecting the San Joaquin River to Paradise Cut. At $818 \text{ m}^3 \text{ s}^{-1}$ ($28,900 \text{ ft}^3 \text{ s}^{-1}$), expansions in the San Joaquin River flow area and the geometry of the weir lead to smaller increases in Paradise Cut flow with increases in San Joaquin flow. The exact location of these change points was determined by fitting a piecewise linear function to the data using a non-linear least squares optimization method (Levenberg 1944). The resulting relationship forms the basis for different $Q_{vns}-Q_{trp}$ regressions based on San Joaquin River flow. During high flow conditions when Paradise Cut is active, the temporary barriers are typically not installed due to concerns of localized flooding.

Figure 6 shows the effect of the head of Old River (HOR) barrier on the San Joaquin–Old River flow split. For San Joaquin flows at Vernalis below $468 \text{ m}^3 \text{ s}^{-1}$, an approximately even flow split occurs when the HOR barrier is not installed. When the barrier is installed, flow into Old River is restricted and San Joaquin flow past Stockton is higher for a given San Joaquin flow at Vernalis. The magnitude of this effect differs between the spring and fall barrier installations; a “full” barrier implementation is typically installed in the spring, and a “partial” barrier install in the fall.

During periods when the HOR barrier is not installed, the Grant Line Canal barrier affects the San Joaquin–Old River flow split (Figure 7). When the Grant Line Canal barrier is installed, it raises water levels in the south Delta, which influence the water surface slope near the junction and cause more water to flow down the San Joaquin River. All of the temporary agricultural barriers are usually installed and removed within a month of one another. Limited data during periods when the Grant Line Canal barrier was installed and Old and Middle River barriers were not suggests the Grant Line Canal barrier has a much larger effect on the split than either of the other two. The Grant Line Canal barrier is also closer to the junction (~ 14 river km) than the Old (~ 29 river km) or Middle (~ 26 river km) River barriers. For these reasons, the installation of the

Grant Line Canal barrier is treated as different cases in the $Q_{vns}-Q_{lrp}$ regressions while the remaining agricultural barriers are not.

When neither the HOR barrier nor the Grant Line Canal barrier is installed, south Delta diversions have a noticeable influence on the San Joaquin–Old River flow split (Figure 8). As diversions increase, more flow is pulled into the Old River channel from the San Joaquin River. At very low Vernalis flows, pumping may even cause reverse flows in the San Joaquin River downstream of HOR. The influence of diversions on the flow split is also important for low San Joaquin River flow conditions during which the fall HOR barrier or the Grant Line Canal barrier are installed (dependence not shown in figures), and was considered for the regression analysis. At higher San Joaquin River flow conditions, the influence of south Delta diversions on the flow split is less important.

The resulting $Q_{vns}-Q_{lrp}$ regressions for different barrier configurations and flow thresholds are given in Table 4. Figure 9 and Figure 10 compare the statistical model for San Joaquin River flow downstream of HOR to the DSM2 model results upon which it was based, and observed data at Lathrop (CDWR-operated gage) and Garwood Bridge (USGS-operated gage located approximately 18 river km downstream of HOR). The statistical model has similar accuracy to DSM2 (Figure 10), and both compare well to the two sets of observed data. The model suggests that a $100 \text{ m}^3 \text{ s}^{-1}$ increase in south Delta diversion results in a $2.93 \text{ m}^3 \text{ s}^{-1}$ decrease in San Joaquin River flow downstream of HOR and a commensurate increase in Old River flow. The San Joaquin River flow downstream of HOR regressions were algebraically combined with the Indian Slough correlations in Equation 1 to create a model for OMR flow without the change in storage term. These coefficients are given in Table 5.

Error metrics for DSM2 and the water balance model in predicting observed OMR flow are presented in Figure 11 and Figure 12, and in Table 6. DSM2 shows the highest accuracy, with 71% of 5-day average predictions falling within $\pm 15 \text{ m}^3 \text{ s}^{-1}$ ($530 \text{ ft}^3 \text{ s}^{-1}$) of observed. The water balance approach without subtidal flow has 65% of predictions falling within $\pm 15 \text{ m}^3 \text{ s}^{-1}$. Both methods are off by greater than $35 \text{ m}^3 \text{ s}^{-1}$ ($1200 \text{ ft}^3 \text{ s}^{-1}$) only a small percent (1–4%) of the time. DSM2 predictions are generally more negative than observed, with 61% of model predictions having a negative residual. The water balance approach is not as biased, with 46% of predictions having a negative residual. When comparing to observed data on a 14-day average basis (Figure 12), the short-term variations in subtidal storage are averaged out, and the water balance model without subtidal storage approaches DSM2 accuracy.

Table 4 Statistical model constants for San Joaquin River flow downstream of HOR:
 $Q_{lrp} = \alpha * Q_{vns} + \beta * Q_{div} + \gamma$. N is the number of points used in the regression. R^2 is the coefficient of determination. SE is the standard error of the estimate. R^2 and standard error are computed in comparison to calculated DSM2 flow values.

Q_{vns} ($m^3 s^{-1}$)	HOR barrier	GLC barrier	α (-)	β (-)	γ ($m^3 s^{-1}$)	N	R^2	SE ($m^3 s^{-1}$)
< 467	Out	Out	0.501	-0.0293	-4.7	9952	0.996	0.1
467–818	Out	Out	0.260	0	100.0	636	0.991	0.6
> 818	Out	Out	0.338	0	38.3	98	0.956	6.6
All	In (fall)	In/Out	0.736	-0.0132	-0.9	1358	0.960	0.2
All	In (spring)	In/Out	0.890	0	-5.5	780	0.959	0.7
All	Out	In	0.522	-0.0211	0.7	3432	0.976	0.1

Table 5 OMR water balance model constants without change in control volume storage term:
 $Q_{omr} = A_{wb} * Q_{vns} + B_{wb} * Q_{div} + C_{wb}$.

Q_{sjr} ($m^3 s^{-1}$)	HOR barrier	GLC barrier	A_{wb} (-)	B_{wb} (-)	C_{wb} ($m^3 s^{-1}$)
< 467	Out	Out	0.471	-0.915	6.8
467–818	Out	Out	0.698	-0.943	-92.1
> 818	Out	Out	0.624	-0.943	-33.8
All	In (fall)	Out	0.249	-0.931	3.2
All	In (spring)	Out	0.104	-0.943	7.6
All	Out	In	0.451	-0.923	1.7

Table 6 Standard error of OMR flow models. Predictions are compared to USGS observed data using 5-day/14-day running-averages. Units are $\text{m}^3 \text{s}^{-1}$.

Q_{vns} ($\text{m}^3 \text{s}^{-1}$)	HOR barrier	GLC barrier	N	5-day/14-day Average Model Standard Error			
				DSM2	Water Balance w/o Subtidal Storage	Water Balance w/ Subtidal Storage	Direct Fit Water Balance
< 467	Out	Out	4919	13.1/11.1	15.4/11.8	14.2/11.4	14.3/11.4
467–818	Out	Out	315	16.3/12.9	20.8/14.6	19.9/14.4	19.0/13.9
> 818	Out	Out	48	25.5/23.7	28.8/23.7	29.7/24.8	29.6/24.5
All	In (fall)	In/Out	670	12.9/10.7	14.8/11.7	14.1/11.7	14.1/11.6
All	In (spring)	In/Out	384	14.3/11.9	15.9/11.6	14.7/11.5	14.5/11.5
All	Out	In	1665	14.2/12.8	15.3/13.1	14.7/13.1	15.4/13.8
All	All	All	8001	14.2/12.3	16.5/13.2	15.6/13.0	15.8/13.3

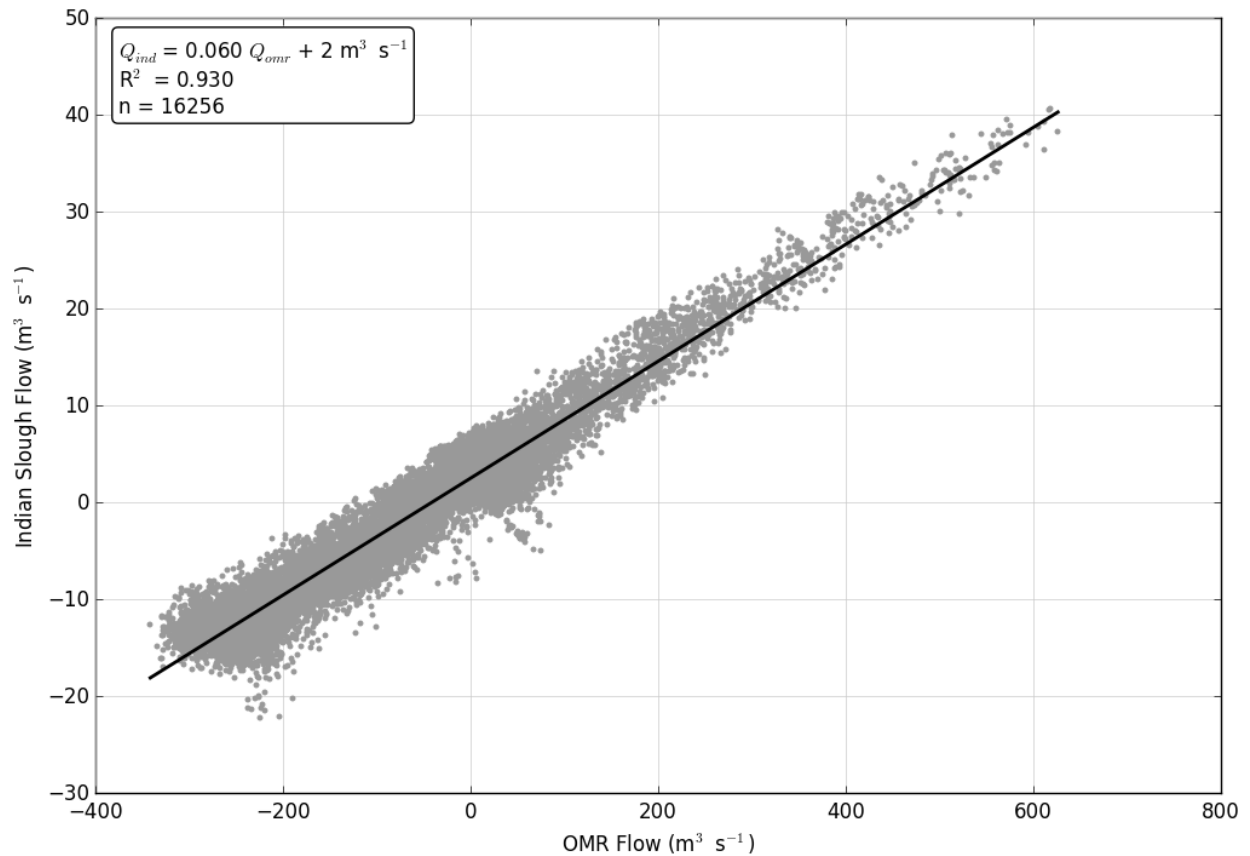


Figure 4 DSM2-predicted Indian Slough and OMR flow correlation and best fit line.

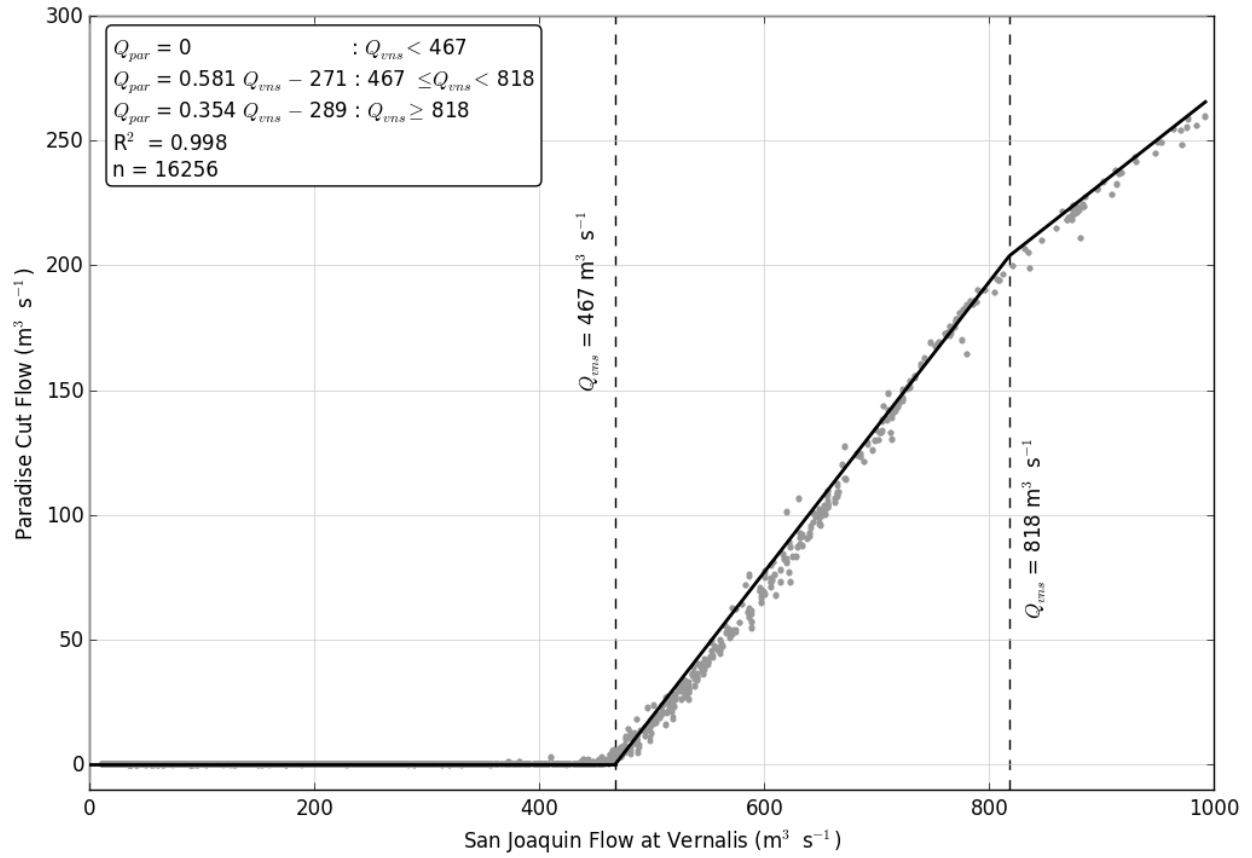


Figure 5 DSM2-predicted flow in Paradise Cut as a piecewise linear function of San Joaquin flow at Vernalis. Vertical lines are shown at $Q_{vns} = 467 \text{ m}^3 \text{ s}^{-1}$, where the overflow weir into Paradise Cut begins to spill and $Q_{vns} = 818 \text{ m}^3 \text{ s}^{-1}$, where river and weir geometry cause a change in slope.

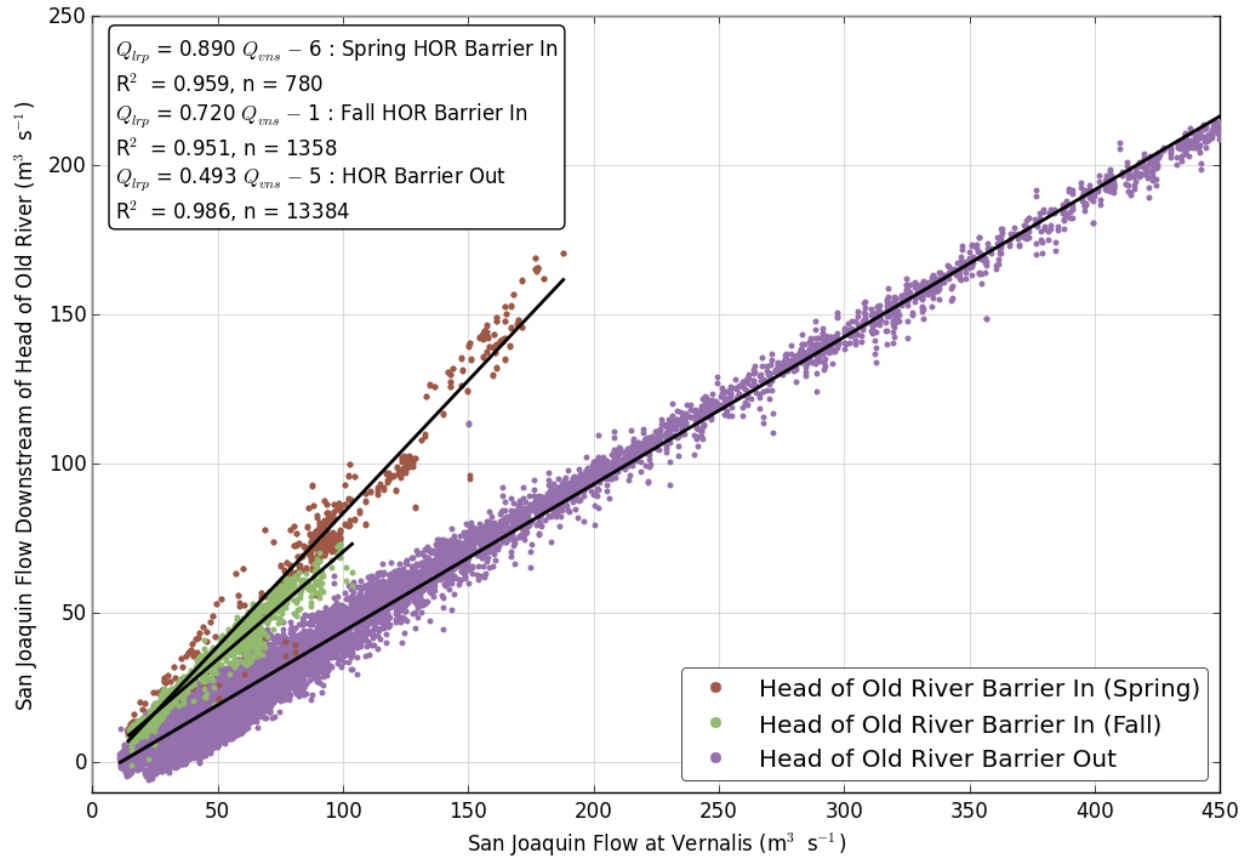


Figure 6 Dependence of DSM2-modeled San Joaquin River flow downstream of HOR on San Joaquin flow at Vernalis, during low flow conditions, and the presence or absence of the HOR barrier.

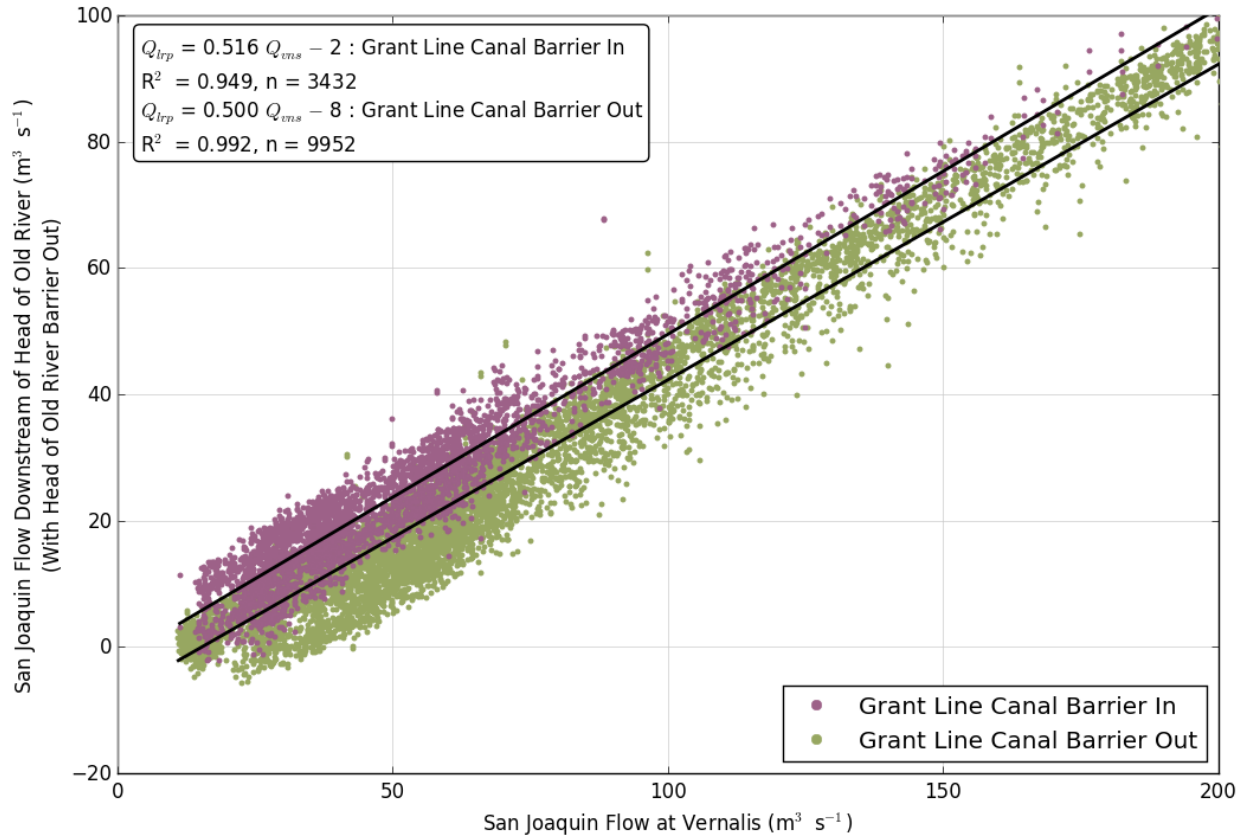


Figure 7 Dependence of DSM2-modeled San Joaquin River flow downstream of HOR on San Joaquin flow at Vernalis and the presence or absence of south Delta temporary barriers for agriculture, for times when the HOR barrier is not installed. The installation of the Grant Line Canal barrier has a significant effect on the regression. When the Grant Line Canal barrier is installed, the presence or absence of the other barriers have only a minor effect.

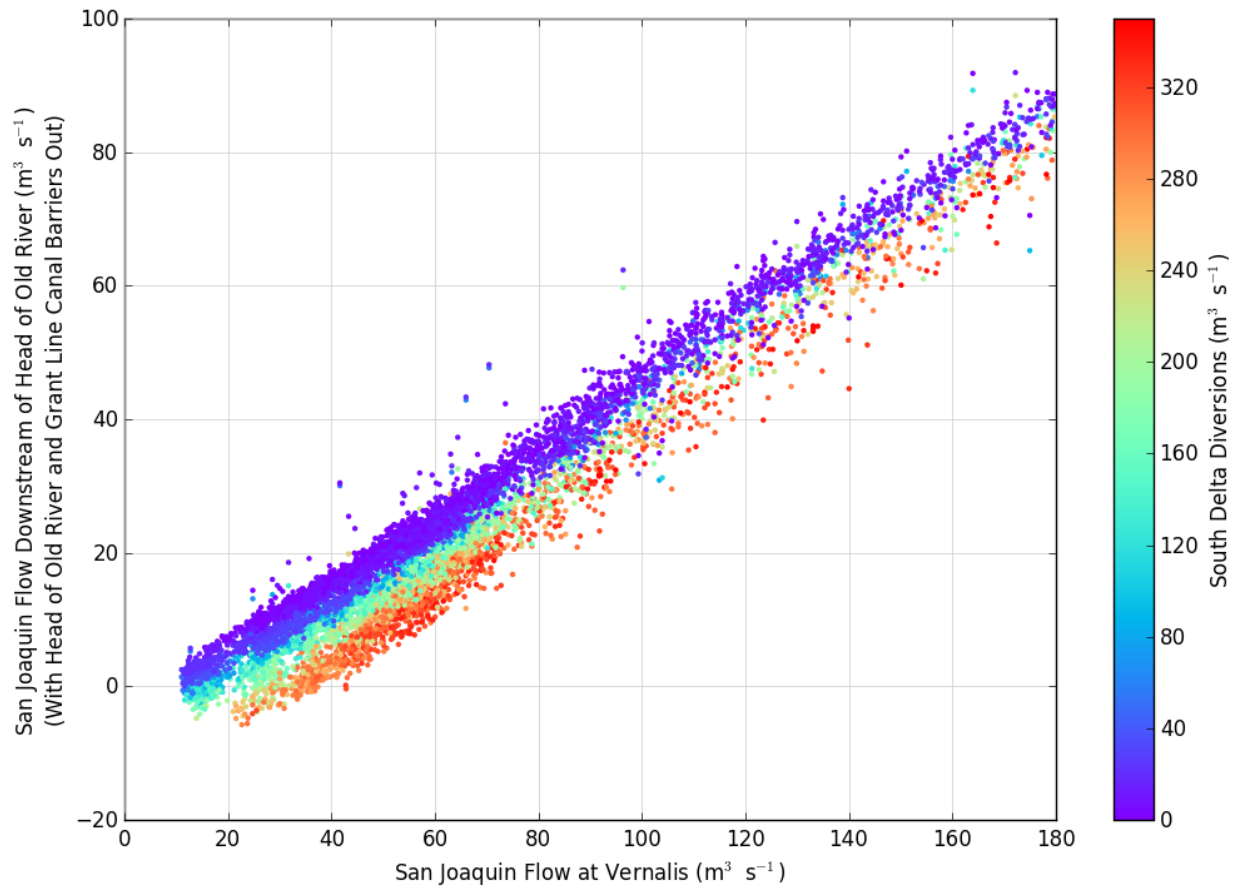


Figure 8 Dependence of DSM2-modeled San Joaquin River flow downstream of HOR on San Joaquin flow at Vernalis and south Delta diversions, for times when the HOR barrier and Grant Line Canal barriers are not installed.

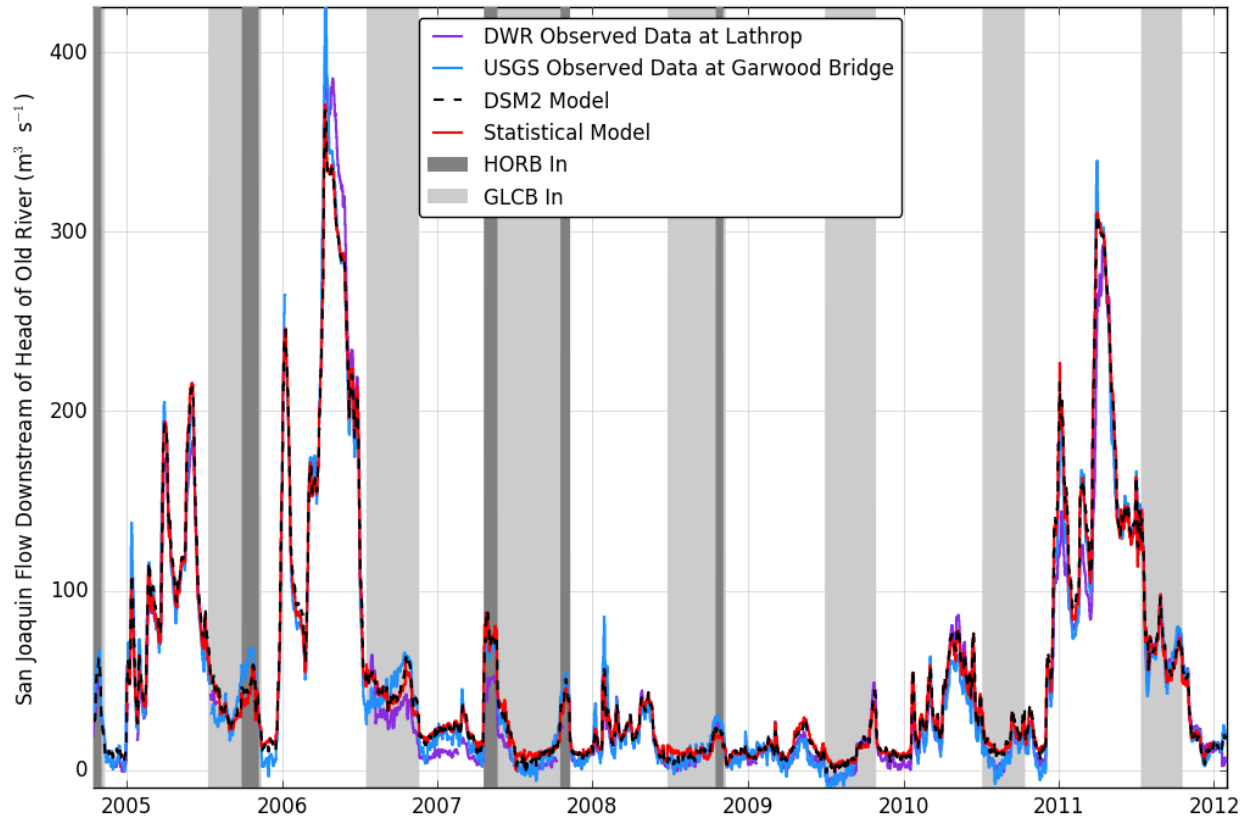


Figure 9 Comparison of methods to estimate San Joaquin River flow downstream of HOR. DSM2 model and the statistical model given in Table 4 are compared against observed flow measured at Lathrop and Garwood Bridge.

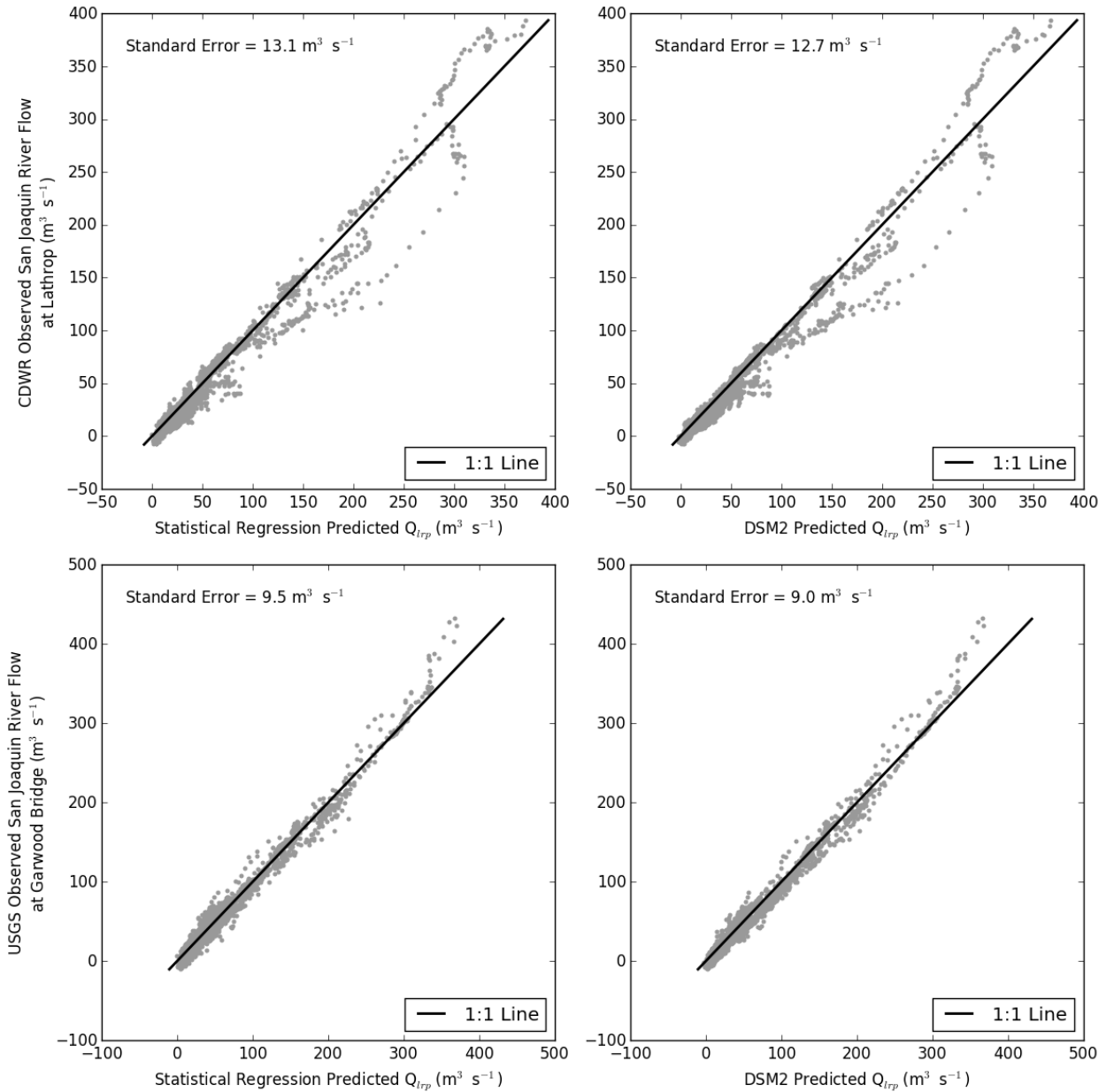


Figure 10 Statistical comparison of observed and model-predicted flows on the San Joaquin River downstream of HOR. DSM2 and the statistical model described in Table 4 are each compared to both CDWR observed data at Lathrop and USGS observed data at Garwood Bridge. Top two plots show model comparisons to the CDWR Lathrop gage. Bottom two plots show model comparisons to the USGS Garwood Bridge gage. Left plots show the statistical model accuracy. Right plots show the accuracy of DSM2.

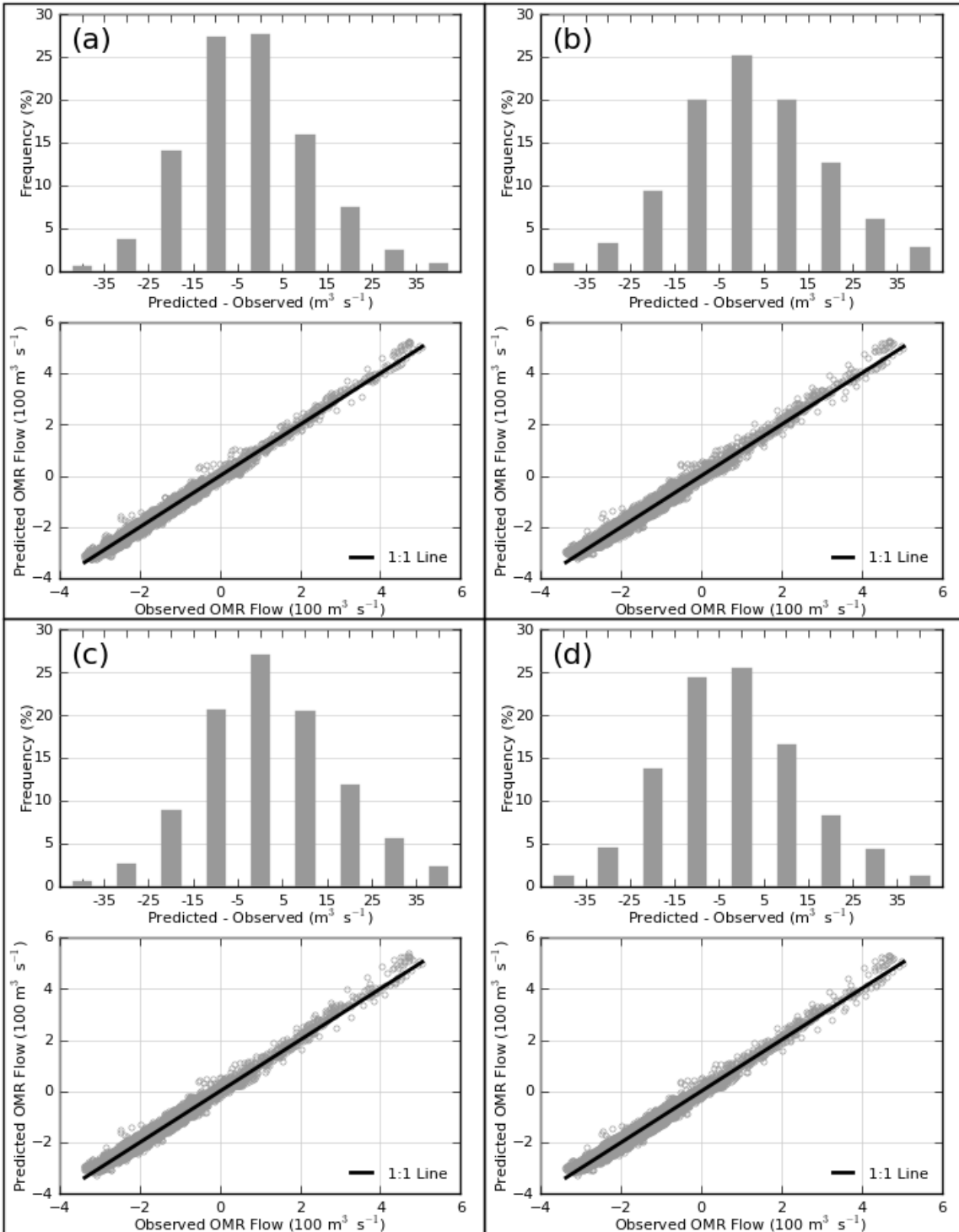


Figure 11 Comparison of OMR estimation method to USGS observed data: DSM2 (a), water balance model without the subtidal storage term (b), water balance model with the subtidal storage term (c), and direct fit water balance model (d). For each method, the lower plot shows paired data points and 1:1 line. Upper plots show the binned predicted minus observed differences. Results are compared on a 5-day average basis.

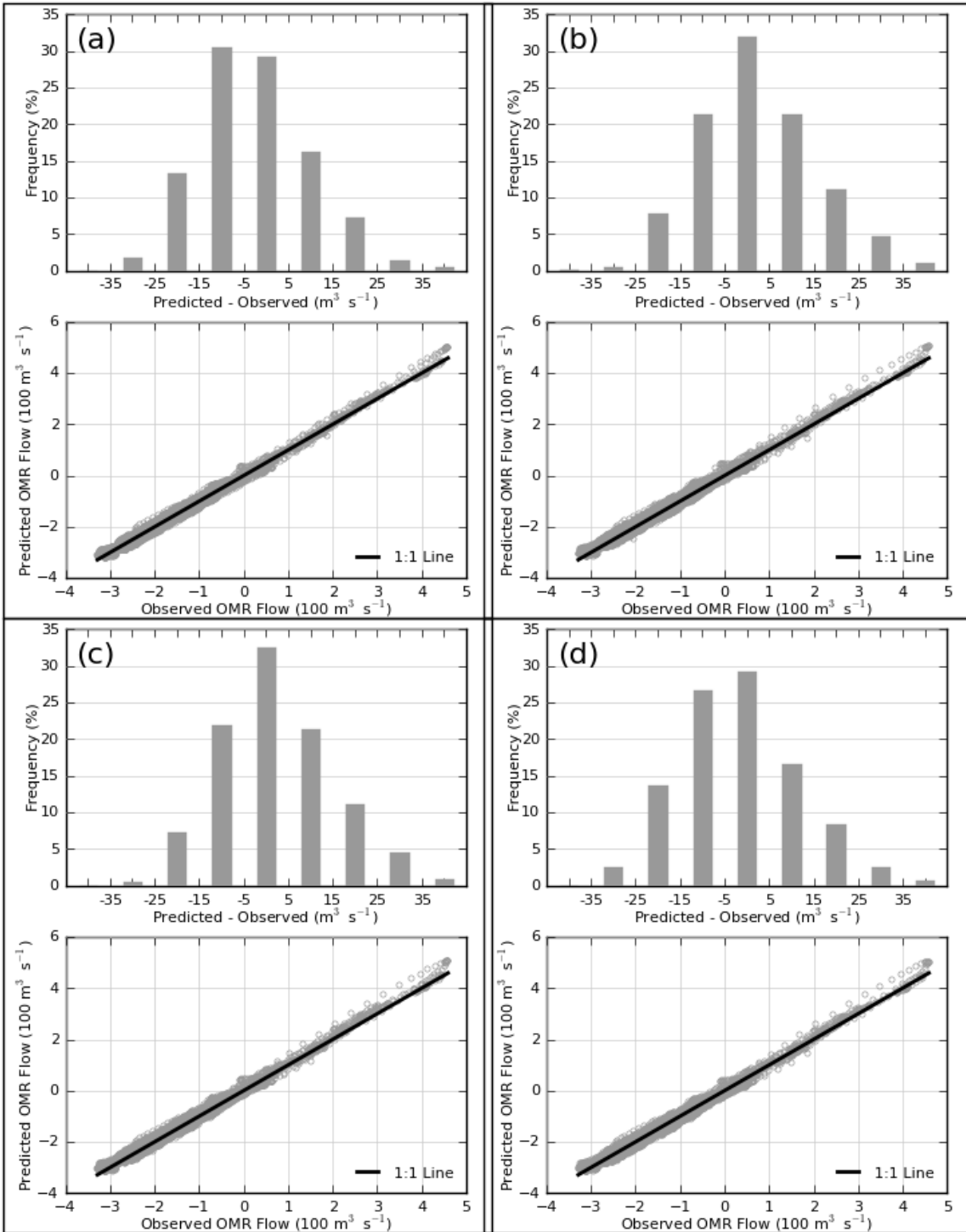


Figure 12 Comparison of OMR estimation method to USGS observed data: DSM2 (a), water balance model without the subtidal storage term (b), water balance model with the subtidal storage term (c), and direct fit water balance model (d). For each method, the lower plot shows paired data points and 1:1 line. Upper plots show the binned predicted minus observed differences. Results are compared on a 14-day average basis.

Subtidal Water Level Analysis

A power spectrum for the historical DSM2 computed stage at Old River at Bacon Island is shown in Figure 13. Power spectrums are simple ways to look at important frequencies in periodic data by plotting the amplitudes of harmonic components derived from a Fourier Transform of the data. Peaks in the power spectrum in Figure 13 indicate periods (or frequencies) that have the greatest influence on water levels. Around a period of 12 hours, three peaks in the power spectrum were found which correspond to the known semi-diurnal tidal constituents S_2 , M_2 , and N_2 (see Parker 2007, Table 2.2). Around 24 hours, two peaks in the spectrum were found which correspond to known semi-diurnal tidal constituents, K_1 and O_1 . These diurnal and semi-diurnal constituents are responsible for the large daily variations in water levels in San Francisco Bay. They directly relate to astronomical forcing; e.g., S_2 and M_2 relate to the daily effects of earth's rotation through the gravitational pull of the sun and the moon and are known as the principle solar and principle lunar tides, respectively. K_1 , O_1 , and N_2 relate to period cycling of the Earth-moon distance (perigee-apogee) and the angle of the moon relative to the Earth's equatorial plane (lunar declination).

Several of these diurnal and semi-diurnal constituents have very similar periods. When their time series are overlaid, these periodic signals slowly cycle in and out of phase, which creates a longer-term modulation. For example, the combined effects of the principle lunar and principle solar cycles create the monthly full moon-new moon lunar cycle, and the additive or counterbalancing effects of the sun and moon's gravity on the tides are widely regarded as causing the spring-neap tidal cycle. In actuality, this is an over-simplification. Although the interaction of M_2 and S_2 does contribute to the spring-neap cycling of water levels in the south Delta, there are two other tidal constituent interactions which also play a part. These interactions are referred to as compound tides and are given their own names based on the primary tidal constituents interacting: KO, MS, and MN. They were identified by locating peaks in the power spectrum shown in Figure 13 at periods longer than 30 hours. The periods of the compound tides equal the corresponding frequency differences between their interacting components.

In addition to relating to the interactions of the primary tides, the magnitude of compound tides in the Delta is related to non-linear hydrodynamic effects. When the amplitudes of the primary tides are in phase, higher tidal ranges lead to faster velocities in the Delta channels. These faster velocities result in increased bottom friction, which necessitate increased water surface slopes in the direction of downstream flow. In deeper water, tides also propagate faster, which results in further non-linearity in water levels.

To determine the amplitudes and phases for the tidal constituents KO, MS, and MN in Equation 5, a non-linear optimization fitting procedure was used. In this procedure, the sum of

the squared residuals between the DSM2 predicted Old River at Bacon Island stage and the Equation 5 predicted stage was minimized. The specific non-linear optimization method used to accomplish this is known as the Levenberg-Marquardt algorithm (Levenberg 1944), and was implemented in Python using the `curve_fit` function in the SciPy Optimize package¹. An initial guess is given, and the method iteratively searches for parameter set to minimize the sum of the squared residuals using a gradient descent method.

To determine the suitability of Equation 5 for the prediction of south Delta control volume water levels, each parameter was fit individually. After fitting the tidal constituent parameters using the non-linear optimization procedure described above, the residual water level was compared to Delta inflow (Figure 14, top); a strong correlation ($R^2 = 0.556$) was found. After fitting both the tidal constituents and a Delta inflow-dependent term (a_0), the residual water level was then compared to barometric pressure (Figure 14, center); a similarly strong correlation ($R^2 = 0.388$) was found, indicating both Delta inflow and pressure were suitable in Equation 5.

The DSM2 predicted and Equation 5 predicted subtidal water level for a representative year of the 23-year period is shown in Figure 14, bottom. Each term of Equation 5 is added incrementally and has a significant effect on the estimated subtidal water level. The standard error of the Equation 5 estimated water level is 0.132 m when only tidal constituent terms are considered. The error improves to 0.088 m when Delta inflow effects are also considered, and improves to 0.069 m for the complete Equation 5 including the barometric pressure effect. Values for the final fitting parameters are given in Table 7. Several alternative parameters were also considered, including natural logarithm and power law expressions for flow effects, regional and local wind, and south Delta diversions. None of these produced a substantial improvement in subtidal water level fit.

Yearly time series plots comparing the Equation 5 predicted stage at Old River at Bacon Island to the DSM2 predicted and USGS observed records are given in Appendix B. Over the course of the study period (1990–2012) an upward linear trend in the USGS observed stage data can be observed that is not captured in Equation 5. However, this trend is not important to capture in the context of the water balance method, as daily changes in control volume storage are much more important than incremental changes occurring over the period of record.

The subtidal water levels predicted by Equation 5 were converted to control volume storages using Equation 6, and were differenced in order to calculate the final flow term in Equation 1. Results from the water balance model with the inclusion of the subtidal storage term are shown in Table 6 and Figure 11 and Figure 12. Five-day average model accuracy within $\pm 15 \text{ m}^3 \text{ s}^{-1}$ is

¹ Documentation available from:
http://docs.scipy.org/doc/scipy/reference/generated/scipy.optimize.curve_fit.html

improved 3% to 68%, and standard error is reduced in all cases except for the highest San Joaquin flows. Fourteen-day average model accuracy is very close to the water balance method without the inclusion of subtidal storage, since the change in storage term approaches zero as longer averaging periods are considered.

In order to investigate seasonal bias in the water balance method, monthly averages of the 5-day standard error were calculated (Table 8 and Figure 15). No strong seasonal bias was observed.

Table 7 Subtidal water level statistical model parameters.

Parameter	Units	Value
A_{KO}	m	0.0469
A_{MS}	m	0.0433
A_{MN}	m	0.0256
ϕ_{KO}	radians	0.262
ϕ_{MS}	radians	-0.314
ϕ_{MN}	radians	-20.4
a_0	$m^{-2} s$	9.97×10^{-5}
b_0	m millibars ⁻¹	-0.0123
c_0	m	13.7

Table 8 Seasonal trends in San Joaquin River flow at Vernalis, south Delta NCD, and 5-day average water balance model errors, relative to observed USGS data.

Month	San Joaquin R at Vernalis ($\text{m}^3 \text{s}^{-1}$)	South Delta NCD ($\text{m}^3 \text{s}^{-1}$)	5-Day Average Water Balance with Subtidal Storage Model Standard Error ($\text{m}^3 \text{s}^{-1}$)
January	135	-7	13.7
February	180	-7	17.8
March	181	2	14.8
April	200	8	16
May	185	14	17.4
June	128	24	13.9
July	82	28	14.4
August	53	19	15.2
September	55	10	14.9
October	68	7	14.2
November	53	5	13.4
December	71	2	14.8

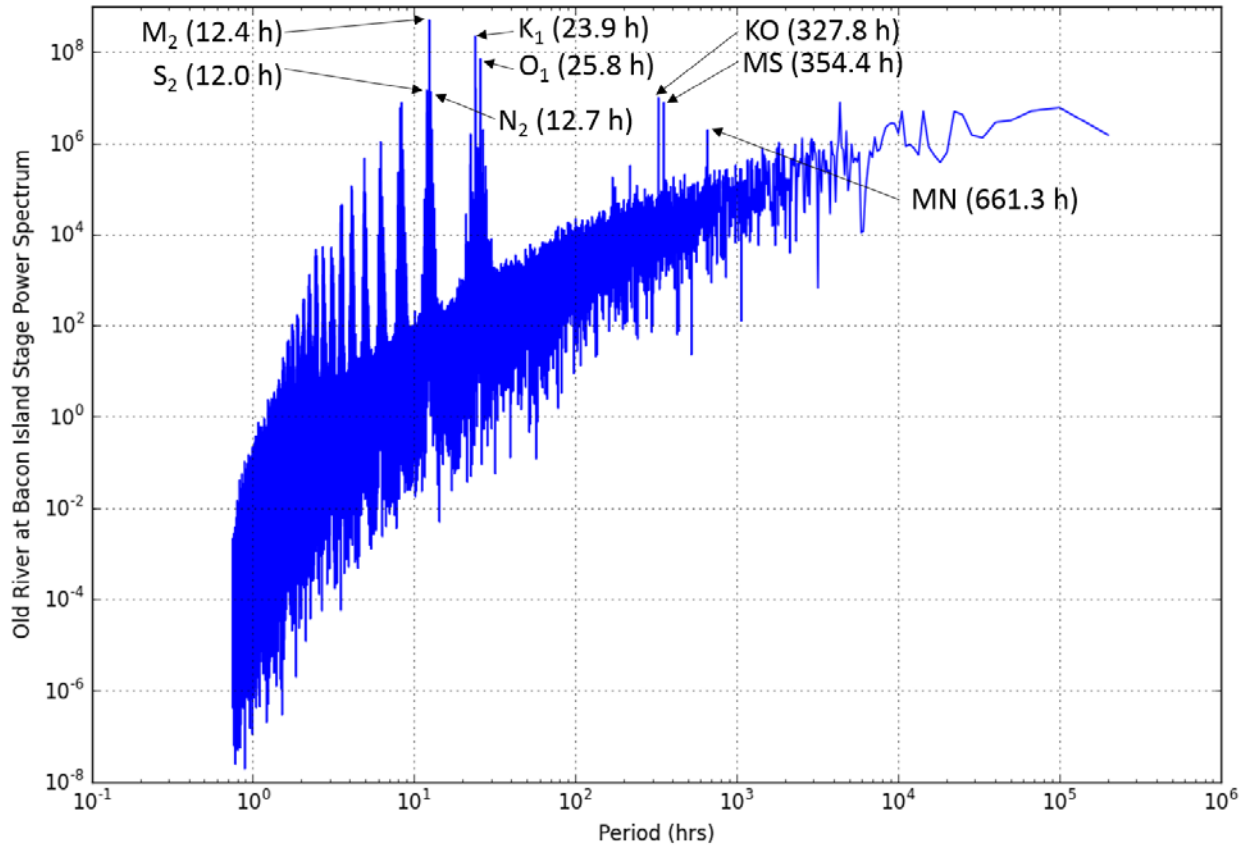


Figure 13 Power spectrum for DSM2 predicted stage at Old River at Bacon Island. Energy peaks corresponding to major tidal constituents for the region are called out. Important tidal constituents in longer-term (>30 hours) water level cycling include KO, MS, and MN, which result from non-linear interactions between major shorter-term constituents.

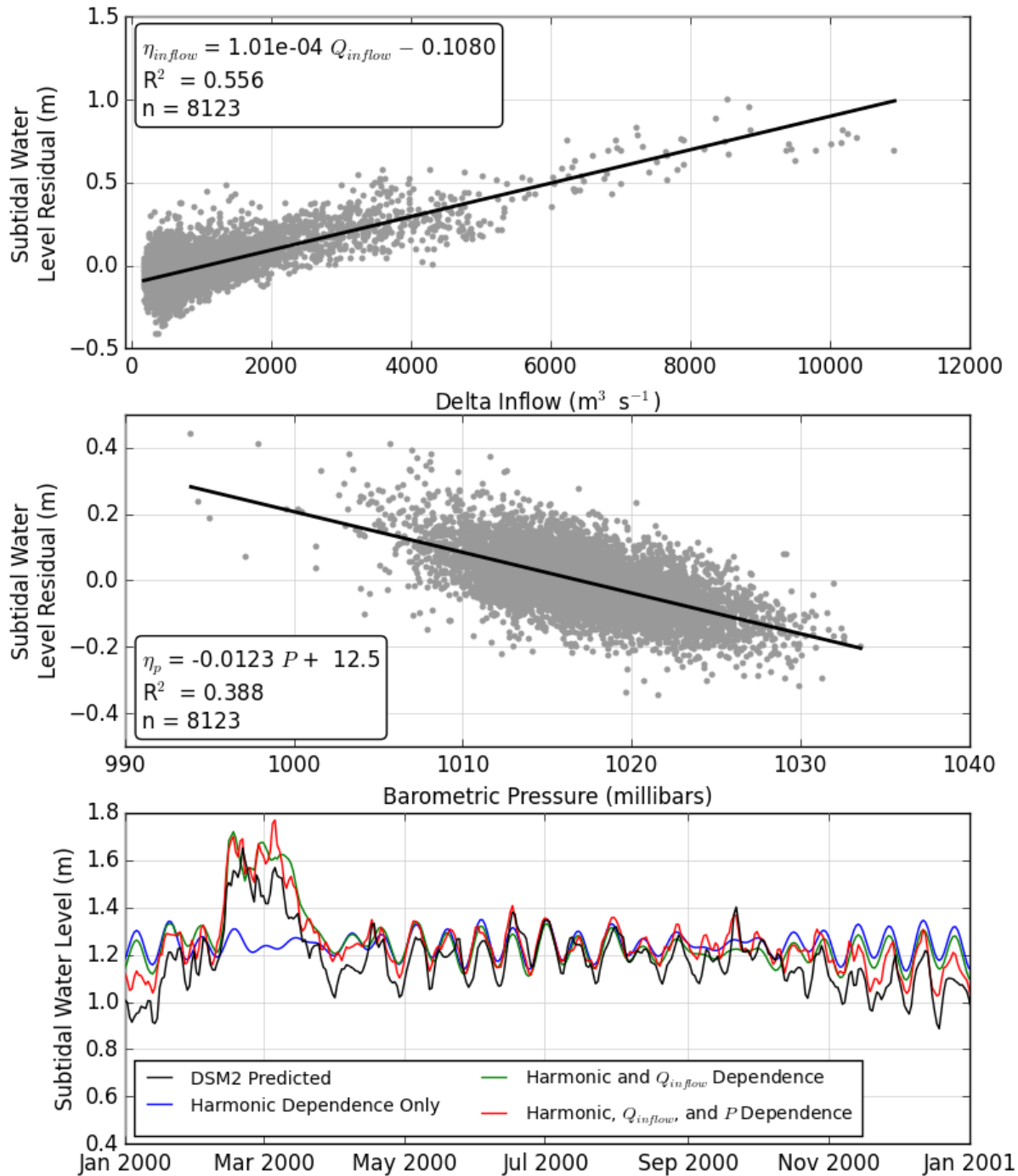


Figure 14 Top plot shows residual south Delta subtidal water level after accounting for tidal harmonic variability, versus Delta inflow. Middle plot shows residual water level after accounting for tidal harmonic variability and Delta inflow effects, versus barometric pressure. Bottom plot shows one year of subtidal water level predicted by both DSM2 and Equation 5. The blue line shows fitting using only the harmonic variability. The green line also includes the effect of Delta inflow, and the red line is the full Equation 5, including the effect of barometric pressure.

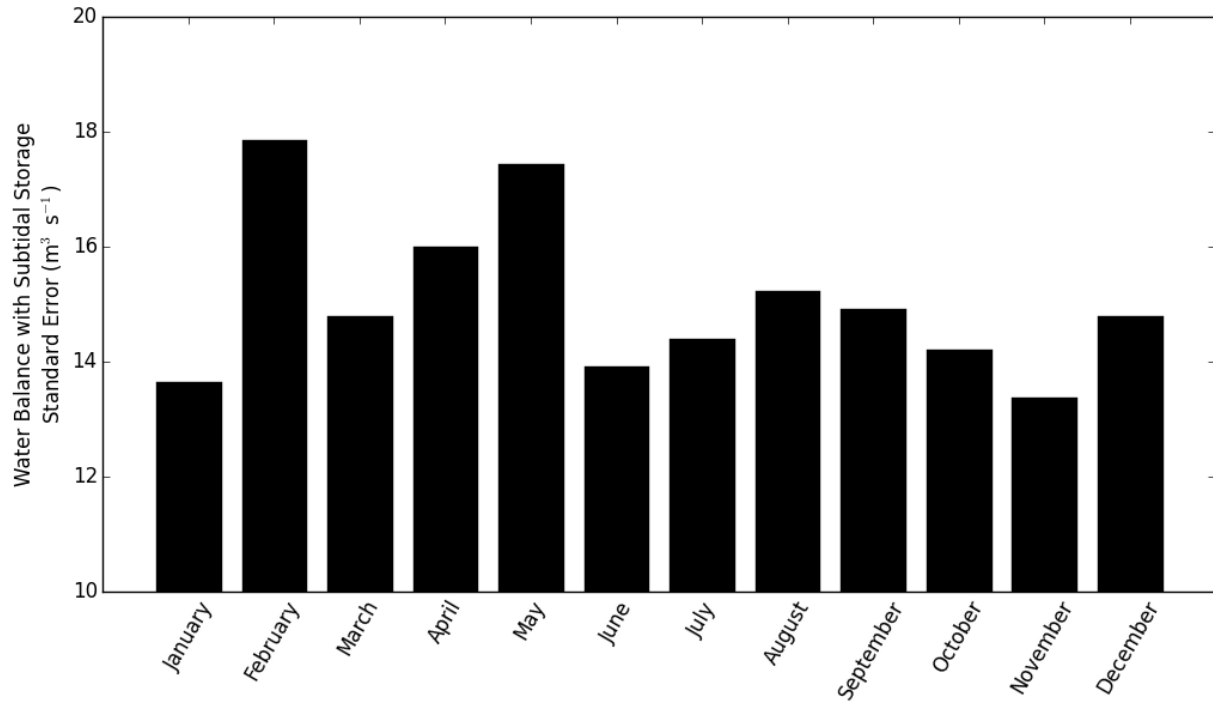


Figure 15 Seasonal trends in 5-day average water balance model standard error.

Direct Fit Water Balance Approach

The parameters estimated by the direct fit optimization approach are given in Table 9. Fitted slopes for the Q_{omr} dependence on Q_{vns} and Q_{div} are similar to those derived for the piecewise fit water balance model. A similar flow cutoff (parameter D in Equation 7) and change in Q_{omr} dependence on Q_{vns} at high flows were also found.

Table 6 and Figure 11 and Figure 12 suggest the direct fitting approach has similar accuracy to the piecewise fitting approach despite having a reduced set of parameters (16 instead of 27). The least accurate predictions were for periods with GLC barrier installation. In contrast to the piecewise fit water balance, the direct fit showed a tendency to underpredict OMR flows, similar to DSM2.

Yearly time series plots of OMR flow predicted by both the water balance model with subtidal storage and the direct fit method are shown in comparison to DSM2 predicted and USGS observed flows in Appendix C.

Table 9 Direct fit water balance statistical model constants.

Parameter	Units	Value
A	–	0.475
D	$\text{m}^3 \text{s}^{-1}$	438
A'	–	0.207
B	–	-0.910
A_s	–	-0.291
A_f	–	-0.388
A_g	–	-0.132
A'_{MS}	$\text{m}^3 \text{s}^{-1}$	3.62
A'_{MN}	$\text{m}^3 \text{s}^{-1}$	1.58
A'_{KO}	$\text{m}^3 \text{s}^{-1}$	4.93
ϕ'_{MS}	radians	-0.0301
ϕ'_{MN}	radians	-4.91
ϕ'_{KO}	radians	-0.310
a_1	day	-0.00949
b_1	$\text{m}^3 \text{s}^{-1} \text{millibars}^{-1} \text{day}$	1.39
C	$\text{m}^3 \text{s}^{-1}$	0.477

Discussion

Quantitatively, the most important improvement we present over previous statistical models of OMR flow is the development of distinct flow division ratings for conditions with and without barrier operations. Ratings the San Joaquin–Old River junction were found to vary with San Joaquin River flow and could be represented well by a continuous piecewise linear function. Linear and continuous piecewise linear fits were found to provide a good approximation of the DSM2 predicted flows. There is evidence of a spring-neap signal in the flow residuals (the difference between DSM2 predicted flows and flows predicted by flow division regressions) at Indian Slough in particular. This is consistent with the finding of Sassi and Hoitink (2013) that Stokes drift and the Stokes compensation flow can be distributed unevenly in individual channels; one channel can feed water volume from Stokes drift into Stokes compensation flow in an adjacent channel. This spring-neap cycle can be substantial in some tidal rivers, but the flow residual at Indian Slough is typically less than $5 \text{ m}^3 \text{ s}^{-1}$ (Figure 4), suggesting that spring-neap effects in the relationship of OMR flow to flow at this location are weak.

Accounting for changes in subtidal storage in the south Delta control volume contributes a significant improvement in prediction of subtidal OMR flow (Table 6). Tidal harmonic variability in subtidal water level was found to depend primarily on three compound tide constituents, similar to studies in other estuaries (Godin 1999). Significant additional variability in water level is contributed by Delta inflow and barometric pressure. Each of these effects was represented with a linear relationship following Godin (1999). The estimated coefficient of proportionality for water level variability with barometric pressure, b_0 , was $-0.0126 \text{ m millibar}^{-1}$, similar to the $0.01 \text{ m millibar}^{-1}$ expected from the “inverted barometer” effect (Gaspar and Ponte 1997). Large variation from the expected value of $0.01 \text{ m millibar}^{-1}$ with latitude was reported by Gaspar and Ponte (1997) who found substantial correlations between wind-driven sea level variation and barometric pressure. Walters (1982) also reported a stronger than expected barometric pressure effect in South San Francisco Bay, consistent with our fitting results.

Significant error (a standard error of 0.069 m) remains in estimating the subtidal water level predicted by DSM2. Part of this error is likely due to the simple relationships used to represent complex interactions between river flow and tidal flow. In addition, the Delta is a highly modified environment and anthropomorphic effects are significant. The detailed timing of operations at Clifton Court Forebay and Jones Pumping Plant is not currently accounted for in the water balance approach, which uses daily-average boundary conditions. Furthermore, even if the subtidal water level in Old River at Bacon Island were predicted perfectly, other sources of error would remain in predicting subtidal storage. One is the assumption that water level in Old River at Bacon Island is representative of water level in the south Delta. This appears to be a good first approximation, but some landward regions of the control volume are more fluviably

influenced than Old River at Bacon Island, so accounting for that spatial variation may afford some improvement in estimated storage, particularly at high Delta inflow. A more accurate relationship between subtidal water level and volume would also improve the storage estimate. The linear relationship in Equation 6 was developed assuming a constant water surface elevation throughout the south Delta control volume; a more accurate relationship might be derived from regressing control volume storage obtained from DSM2 to subtidal water level. The main advantage of using the DSM2 hydrodynamic model instead of the proposed water balance approach is improved prediction of storage in the south Delta.

The water balance approach of applying known flows and estimating unknown flows into and the control volume using Equations 2 and 3 is conceptually clear. But noting that the individual regressions are then substituted into Equation 4, and that Equations 5 and 6 can also be substituted into Equation 4, a single equation can be derived and then directly fit to optimize the model fit to observed or predicted OMR flow. This approach allows all parameters to be fit in a single optimization step instead of through a series of linear regressions. These parameters are fit by optimization to DSM2 predicted OMR flow using the differential evolution (Storn and Price 1997) optimization approach.

Equation 7 has conceptual advantages compared with the piecewise fitting approach. Notably this single equation shows the effect of all relevant parameters. The barrier effects can be immediately seen to be represented by a change in slope in the relationship of Q_{omr} to Q_{sjr} . This is consistent with Table 5 for the piecewise fitting results which indicates that the estimated changes to B_{wb} associated with barrier installation are small. In addition, the relationship of Q_{omr} to Q_{sjr} is continuous in Equation 7, while the piecewise fitting approach has discontinuous relationship at two values of Q_{sjr} . Table 6 indicates that despite several simplifications introduced in Equation 7, which decrease the total number of parameters from 27 to 16, the overall standard error of the OMR flow predictions differs little from the piecewise approach. These simplifications include only a single change in slope of Q_{omr} to Q_{sjr} as opposed to the two changes used in the piecewise fitting. The barrier effects were assumed to only change the slope of the relationship of Q_{omr} to Q_{sjr} and not the slope of the relationship of Q_{omr} to Q_{div} . The performance of the simplified approach supports the assumption that the primary effect of varied barrier and flow conditions is change in the slope of the relationship of Q_{omr} to Q_{sjr} . However, because the least accurate predictions of Equation 7 are for conditions with the GLC barrier, we conclude that the GLC barrier has some influence on the slope of the relationship between Q_{div} and Q_{omr} . A sensitivity test indicates that indeed a small improvement in overall accuracy can be achieved by adding one additional parameter to represent this slope change. However, since the difference was not large, we retained Equation 7 for conceptual simplicity.

While room for improvement of the water balance approach remains, the methods presented are quite accurate. It is a marked improvement over previous empirical approaches, and we recommend its adoption in place of those currently in use. Its accuracy in predicting 5-day average OMR flows approaches that of DSM2 and does not require a full hydrodynamic simulation of the Delta. Practically, the regressions in Table 5 provide a straightforward approach for managers to estimate OMR flows. The incorporation of the subtidal flow term requires more information, including forecasts of Delta inflow and barometric pressure, but these forecasts are typically available and the subtidal flow can be readily estimated using Equations 5 and 6.

Because errors shown in Figure 11 and Figure 12 are approximately Gaussian, confidence intervals can be estimated using the standard errors shown in Table 6. The water balance approach is less accurate in predicting OMR flows during high San Joaquin inflow conditions. This is largely a result of error in predicting the Old River–San Joaquin River flow split. At more typical San Joaquin River inflows the 5-day average standard error in the water balance estimate, without the subtidal flow term, is approximately $16.5 \text{ m}^3 \text{ s}^{-1}$, indicating that OMR flows can be predicted with 95% confidence to within $\pm 33 \text{ m}^3 \text{ s}^{-1}$. The inclusion of the subtidal flow term decreases the standard error by approximately $2 \text{ m}^3 \text{ s}^{-1}$.

The proposed approach of analyzing flow divisions and accounting for subtidal storage has broad applicability to the Delta. Several applications can be readily envisioned. One is to improve Delta outflow estimates by accounting for subtidal storage in the Delta. Another is checking the accuracy of estimated subtidal flow at USGS flow monitoring stations by forming control volumes and accounting for subtidal storage within these volumes. This procedure could identify flow stations that require improved calibration and quantify the uncertainty of observations. This would be of particular use in hydrodynamic model calibration. A demanding application that would only be possible with a highly accurate flow observation network is estimation of south Delta NCD using a water balance approach incorporating observed flows and estimated storage.

References

- [BAW] Bundesanstalt für Wasserbau. 2010. Mathematical Model UnTRIM² User Interface Description, Version May 2010 (1.1). Technical Report. Hamburg, Germany. Available from: http://wiki.baw.de/downloads/wasserbau/mathematische_verfahren/pdf/Simulationsverfahren_n_Kueste_untrim2-ui.pdf
- Buschman FA, Hoitink AJF, van der Vegt M, Hoekstra P. 2009. Subtidal water level variation controlled by river flow and tides. *Water Resour Res* 45: W10420. doi: <http://dx.doi.org/10.1029/2009WR008167>.
- Buschman FA, Hoitink AJF, van der Vegt M, Hoekstra P. 2010. Subtidal flow division at a shallow tidal junction. *Water Resour Res* 46: W12515. doi: <http://dx.doi.org/10.1029/2010WR009266>
- [CDWR] California Department of Water Resources. 1986. DAYFLOW program documentation and data summary user's guide. California Department of Water Resources, Sacramento. Available from: http://www.water.ca.gov/dayflow/docs/DAYFLOW_1986.pdf
- CH2M Hill. 2009. DSM2 recalibration. Prepared for California Department of Water Resources. 236 p. Available from: http://baydeltaoffice.water.ca.gov/downloads/DSM2_Users_Group/BDCP/DSM2_Recalibration_102709_doc.pdf
- Fleenor WE, Bombardelli F. 2013. Simplified 1-D Hydrodynamic and Salinity Transport Modeling of the Sacramento–San Joaquin Delta: Sea Level Rise and Water Diversion Effects. *San Francisco Estuary and Watershed Science* 11(4).
- Foreman MGG, Cherniawsky JY, Ballantyne VA. 2009. Versatile harmonic tidal analysis: improvements and applications. *J Atmos Ocean Technol* 26(4):806–817. doi: <http://dx.doi.org/10.1175/2008JTECHO615.1>
- Gaspar P, Ponte RM. 1997. Relationship between sea level and barometric pressure determined from altimeter data and model simulations. *J Geophys Res* 102(C1): 961–971. doi: <http://dx.doi.org/10.1029/96JC02920>
- Glibbert PM, Dugdale RC, Wilkerson F, Parker AE, Alexander J, Antell E, Blaser S, Johnson A, Lee J, Lee T, Murasko S, Strong S. 2014. Major – but rare – spring blooms in 2014 in San Francisco Bay Delta, California, a result of the long-term drought, increased residence time, and altered nutrient loads and forms. *J Exp Mar Biol Ecol* 460: 8–18. doi: <http://dx.doi.org/10.1016/j.jembe.2014.06.001>
- Godin G. 1999. The propagation of tides up rivers with special considerations on the Upper Saint Lawrence River Estuarine. *Coast Shelf Sci* 48(3), 307–324. doi: <http://dx.doi.org/10.1006/ecss.1998.0422>

- Grimaldo LF, Sommer T, Van Ark N, Jones G, Holland E, Moyle PB, Herbold B, Smith P. 2009. Factors affecting fish entrainment into massive water diversions in a tidal freshwater estuary: can fish losses be managed? *N Am J Fish Manag* 29: 1253–1270. doi: <http://dx.doi.org/10.1577/M08-062.1>
- Hutton P. 2008. A model to estimate combined Old & Middle River flows. Sacramento (CA): Metropolitan Water District of Southern California. 90 p.
- Jay DA, Flinchem EP. 1997. Interaction of fluctuating river flow with a barotropic tide: a demonstration of wavelet tidal analysis methods. *J Geophys Res* 102(C3): 5705–5720. doi: <http://dx.doi.org/10.1029/96JC00496>
- Jay DA, Uncles RJ, Largier J, Geyer WR, Vallino J, Boynton WR. 1997. A review of recent developments in estuarine scalar flux estimation. *Estuaries* 20(2): 262–280.
- LeBlond PH. 1979. Forced fortnightly tides in shallow rivers. *Atmosphere-Ocean* 17(3): 253–264. doi: <http://dx.doi.org/10.1080/07055900.1979.9649064>
- Levenberg K. 1944. A method for the solution of certain non-linear problems in least squares. *Q J Appl Math* 2(2): 164–168.
- [NMFS] National Marine Fisheries Service. 2009. Biological Opinion and Conference Opinion on the Long-Term Operations of the Central Valley Project and State Water Project. Technical memorandum from NMFS to U.S. Bureau of Reclamation. Available from: <https://nrm.dfg.ca.gov/FileHandler.ashx?DocumentID=21473>.
- Oltmann RN. 1998. Indirect measurement of delta outflow using ultrasonic velocity meters and comparison with mass-balance calculated outflow. Interagency Ecological Program for the Sacramento–San Joaquin Estuary Newsletter [Internet] 11(1). Available from: <http://www.water.ca.gov/iep/newsletters/1998/winter/Indirect%20Measurement%20of%20Delta%20Outflow%20Using%20Ultrasonic%20Velocity%20Meters.pdf>
- Parker BB. 2007. Tidal analysis and prediction. NOAA Special Publication NOS CO-OPS 3. Silver Spring, Maryland. Available from: http://tidesandcurrents.noaa.gov/publications/Tidal_Analysis_and_Predictions.pdf
- Ruhl C, Smith PE, Simi JJ, Burau JR. 2006. The pelagic organism decline and long-term trends in Sacramento–San Joaquin Delta hydrodynamics. Poster presented at: 4th Biennial CALFED Science Conference; Sacramento, CA.
- Sassi MG, Hoitink AJF. 2013. River flow controls on tides and tide-mean water level profiles in a tidal freshwater river. *J Geophys Res: Oceans* 118: 4139–4151. doi: <http://dx.doi.org/10.1002/jgrc.20297>

Sassi MG, Hoitink AJF, de Brye B, Deleersnijder E. 2012. Downstream hydraulic geometry of a tidally influenced river delta. *J of Geophys Res* 117: F04022. doi: <http://dx.doi.org/10.1029/2012JF002448>

Siegfried LJ, Fleenor WE, Lund JR. 2014. Physically based modeling of Delta Island Consumptive Use: Fabian Tract and Staten Island, California. *San Francisco Estuary and Watershed Science* 12(4). doi: <http://dx.doi.org/10.15447/sfews.2014v12iss4art2>

Snow J. 1986. CDWR Office memorandum communication to Richard Jones with subject title "New flow equations for the San Joaquin River at Stockton and for Old and Middle Rivers." April 17. 5 p.

[SWRCB] State Water Resources Control Board. 1999. Water Right Decision 1641, In the Matter of Implementation of Water Quality Objectives for the San Francisco Bay/Sacramento–San Joaquin Delta Estuary. Available from: http://www.swrcb.ca.gov/waterrights/board_decisions/adopted_orders/decisions/d1600_d1649/wrd1641.pdf

Storn R, Price K. 1997. Differential evolution – a simple and efficient heuristic for global optimization over continuous spaces. *J Glob Optim* 11(4): 341–359.

[URS and JR Benjamin Assoc.] URS Corporation, Jack R. Benjamin & Associates, Inc. 2007. Technical memorandum, topical area: water analysis module. Prepared for the California Department of Water Resources. Available from: http://www.water.ca.gov/floodsafe/fessro/levees/drms/docs/Water_Analysis_Module_TM.pdf

[USFWS] U.S. Fish and Wildlife Service. 2008. Formal Endangered Species Act Consultation on the Proposed Coordinated Operations of the Central Valley Project (CVP) and State Water Project (SWP). Technical memorandum from USFWS to U.S. Bureau of Reclamation. Available from: http://www.fws.gov/sfbaydelta/documents/SWP-CVP_OPs_BO_12-15_final_OCR.pdf

Walters RA. 1982. Low-frequency variations in sea level and currents in South San Francisco Bay. *J Phys Oceanogr* 12: 658-668. doi: [http://dx.doi.org/10.1175/1520-0485\(1982\)012%3C0658:LFVISL%3E2.0.CO;2](http://dx.doi.org/10.1175/1520-0485(1982)012%3C0658:LFVISL%3E2.0.CO;2)

Wang R, Ateljevich E. 2012. A continuous surface elevation map for modeling. In: Finch R, editor. 2012. Methodology for flow and salinity estimates in the Sacramento-San Joaquin Delta and Suisun Marsh, 33rd Annual Progress Report to the State Water Resources Control Board, California Department of Water Resources, Bay-Delta Office, Delta Modeling Section. Chapter 6. Available from: http://baydeltaoffice.water.ca.gov/modeling/deltamodeling/AR2012/Chapter%206_2012_Web.pdf

Appendix A: Calculation of a Hypsographic Curve for the South Delta Control Volume

A hypsographic curve for the south Delta control volume is necessary to relate subtidal water level, predicted using Equation 5, to the subtidal flows needed in the water balance model (Equation 1). A hypsographic curve was derived using bathymetric data contained in RMA's 3D San Francisco Estuary Model grid. The bathymetric data in this grid is given in UnTRIM .grd file format (BAW 2010) and was interpolated from the "San Francisco Bay and Sacramento–San Joaquin Delta DEM," Version 3, distributed by CDWR². Bathymetric data in this DEM was aggregated by CDWR from multiple independent bathymetric surveys using the methods described by Wang and Ateljevich (2012). Horizontal DEM resolution is a mixture of 2 m and 10 m in this region.

A section of the San Francisco Estuary Model grid corresponding to the boundaries of the south Delta control volume was isolated (Figure 16, Figure 17). From this, the total grid volume below a specified stage value was calculated for 50 stages within the typical stage range observed in the south Delta. A linear fit to the data points was calculated to obtain the stage-volume relationship given in Equation 6 (Figure 18).

A similar procedure was applied to derive a hypsographic relationship for the section of the south Delta control volume downstream of the temporary agricultural barriers (Figure 19, Figure 20). Water balance model calculations were run with this hypsographic curve used in place of the former during periods of time when all the temporary agricultural barriers were in place. The motivation for this was that, because of the flow restrictions provided by the barriers, this reduced control volume storage would better represent the area available to subtidal filling and draining. This procedure, however, yielded slightly less accurate results than using the full control volume relationship for the entire simulation period. The reason for this may be that, although the temporary barriers restrict subtidal flows on a short term scale, flows related to longer-term filling and draining of the region are able to move through the permeable barriers.

² Available from: <http://baydeltaoffice.water.ca.gov/modeling/deltamodeling/modelingdata/DEM.cfm>

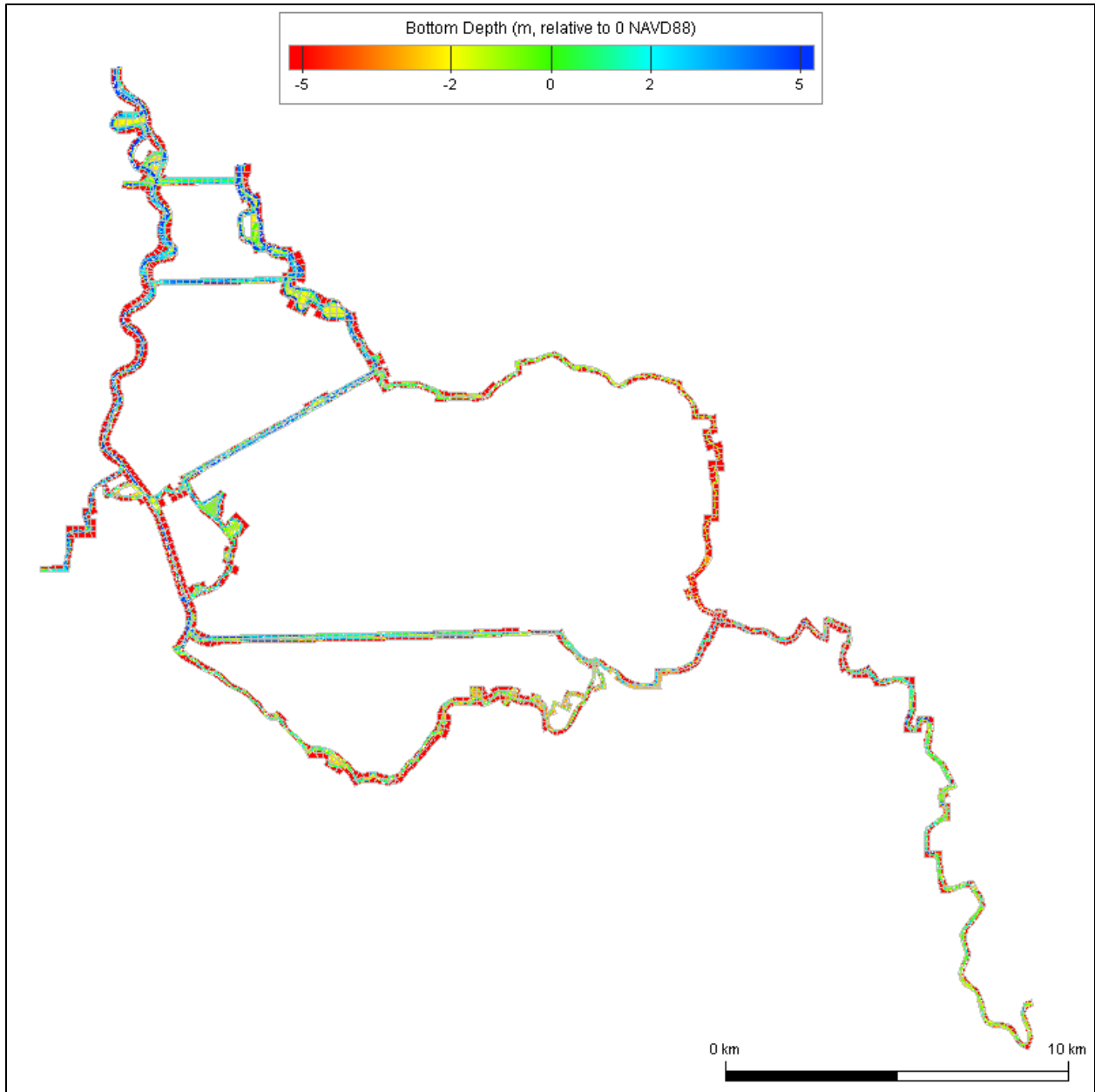


Figure 16 RMA 3D San Francisco Estuary Model grid section clipped to correspond to south Delta control volume boundary locations.

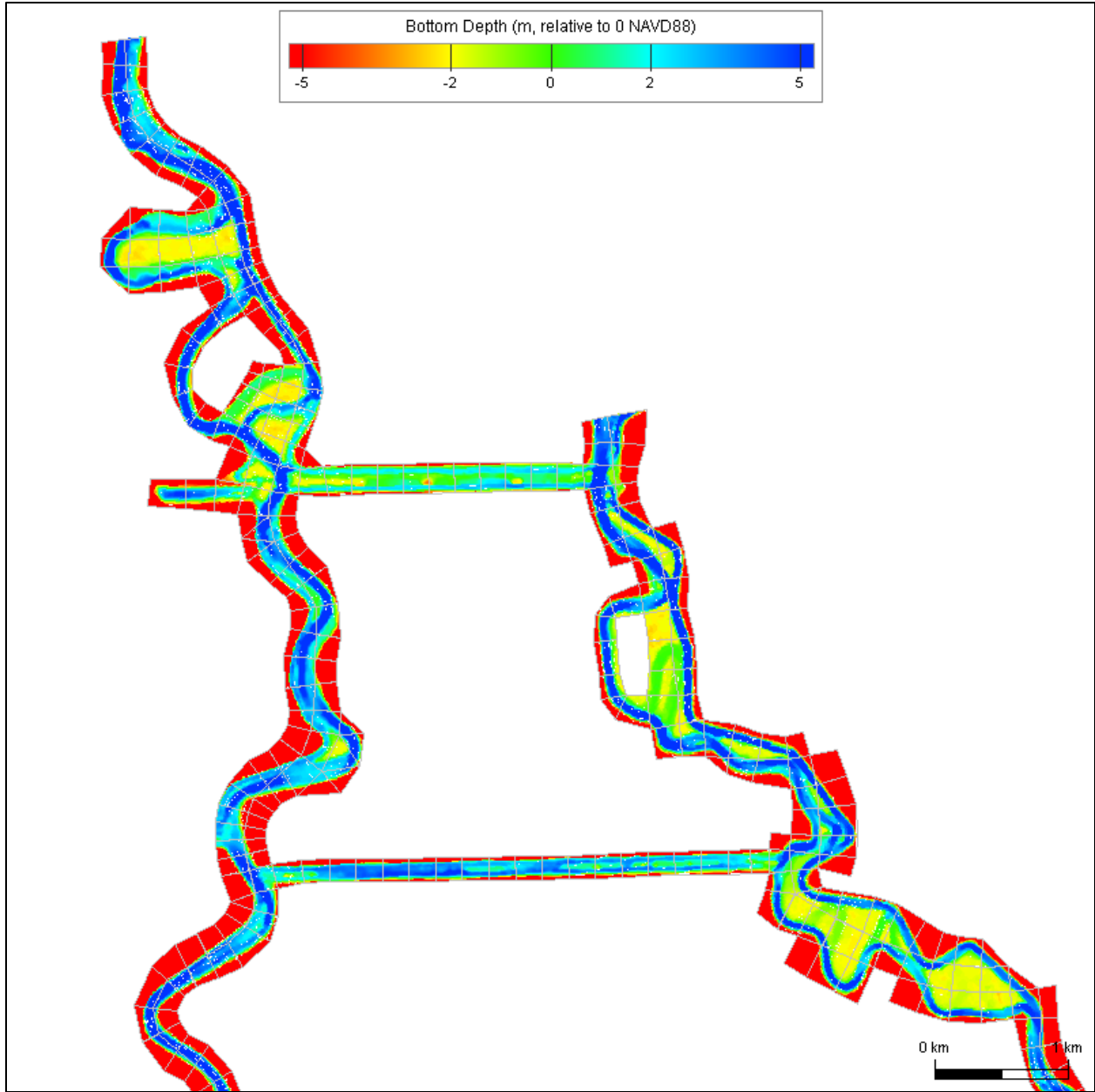


Figure 17 Detail of clipped RMA 3D San Francisco Estuary Model grid depths in the area of Woodward Island.

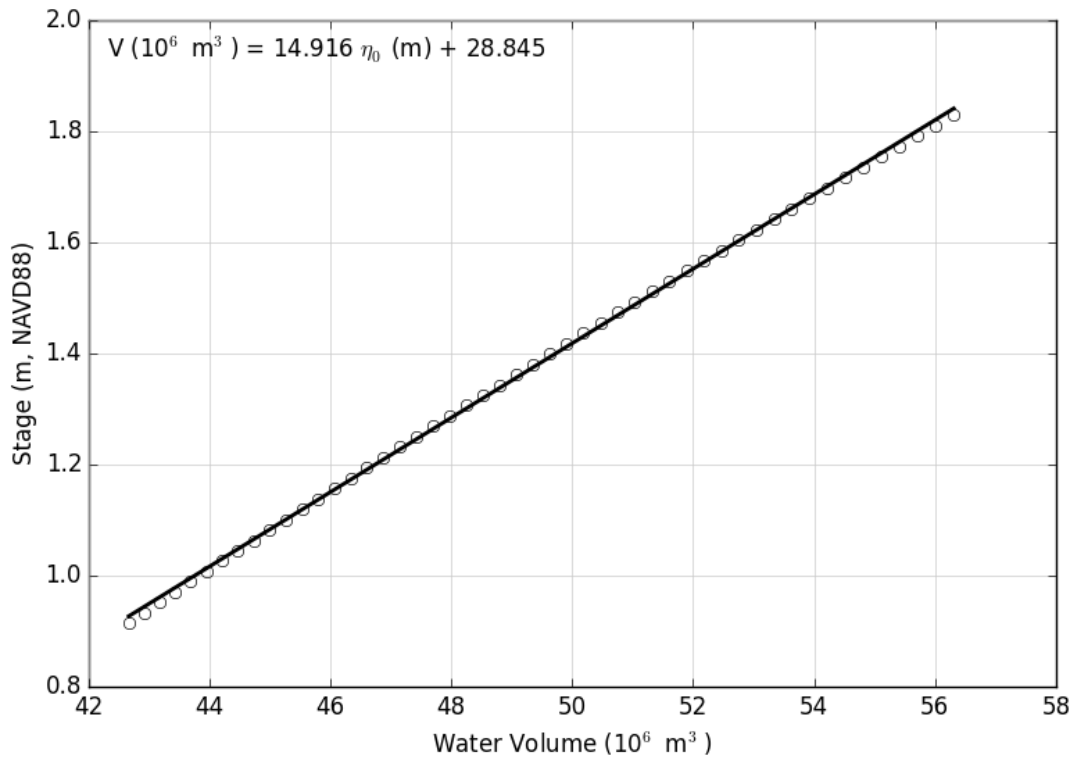


Figure 18 Hypsographic curve data and linear fit for the south Delta control volume region.

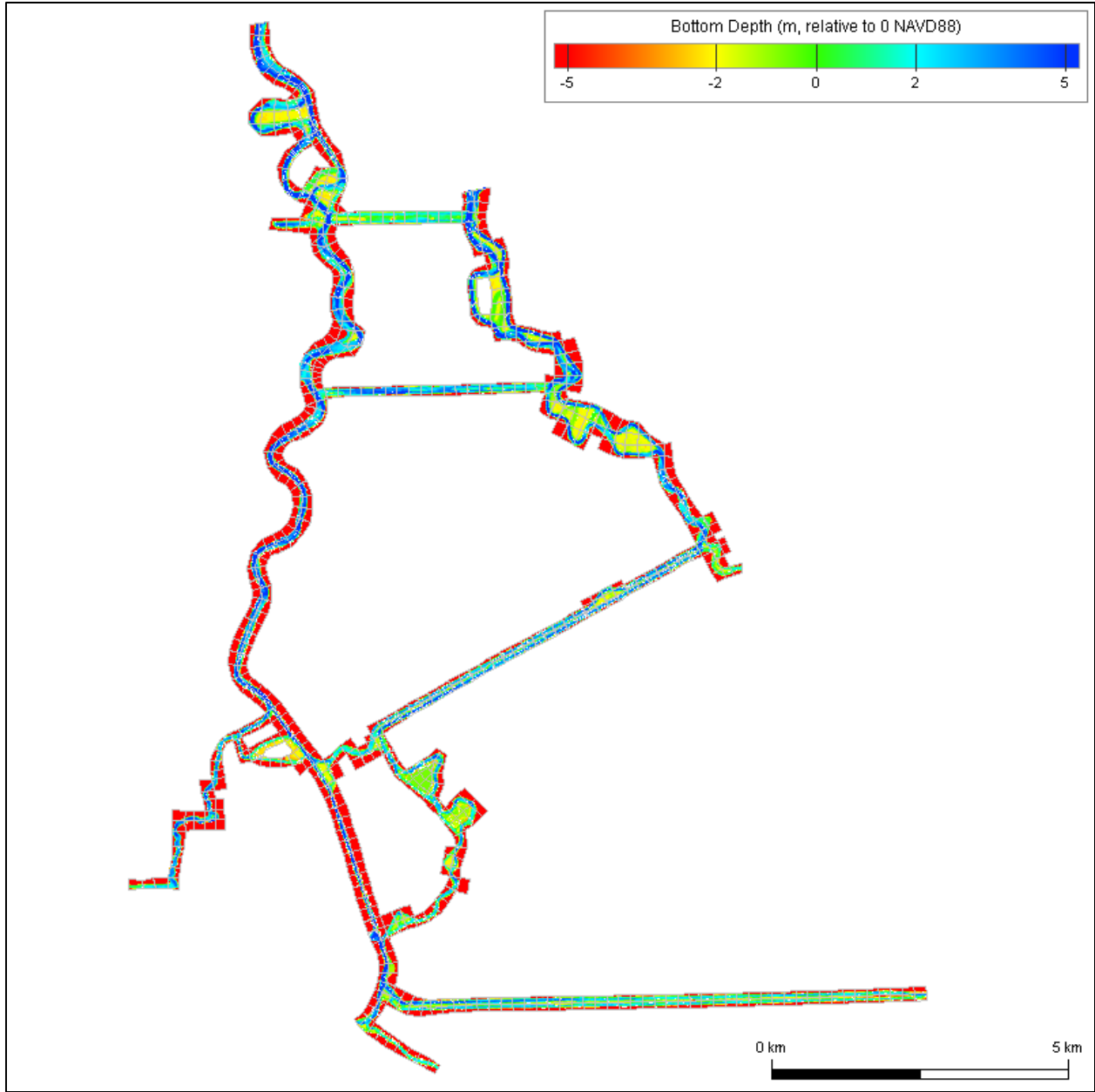


Figure 19 RMA 3D San Francisco Estuary Model grid section clipped to correspond to south Delta control volume downstream of temporary agricultural barriers.

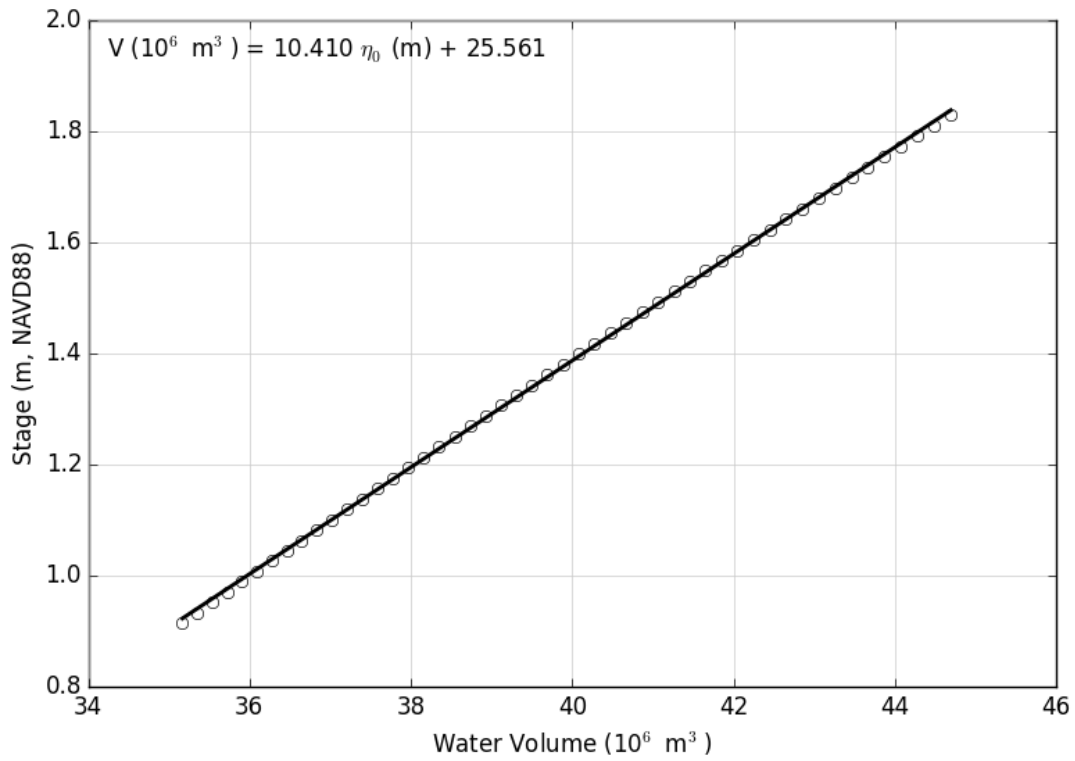
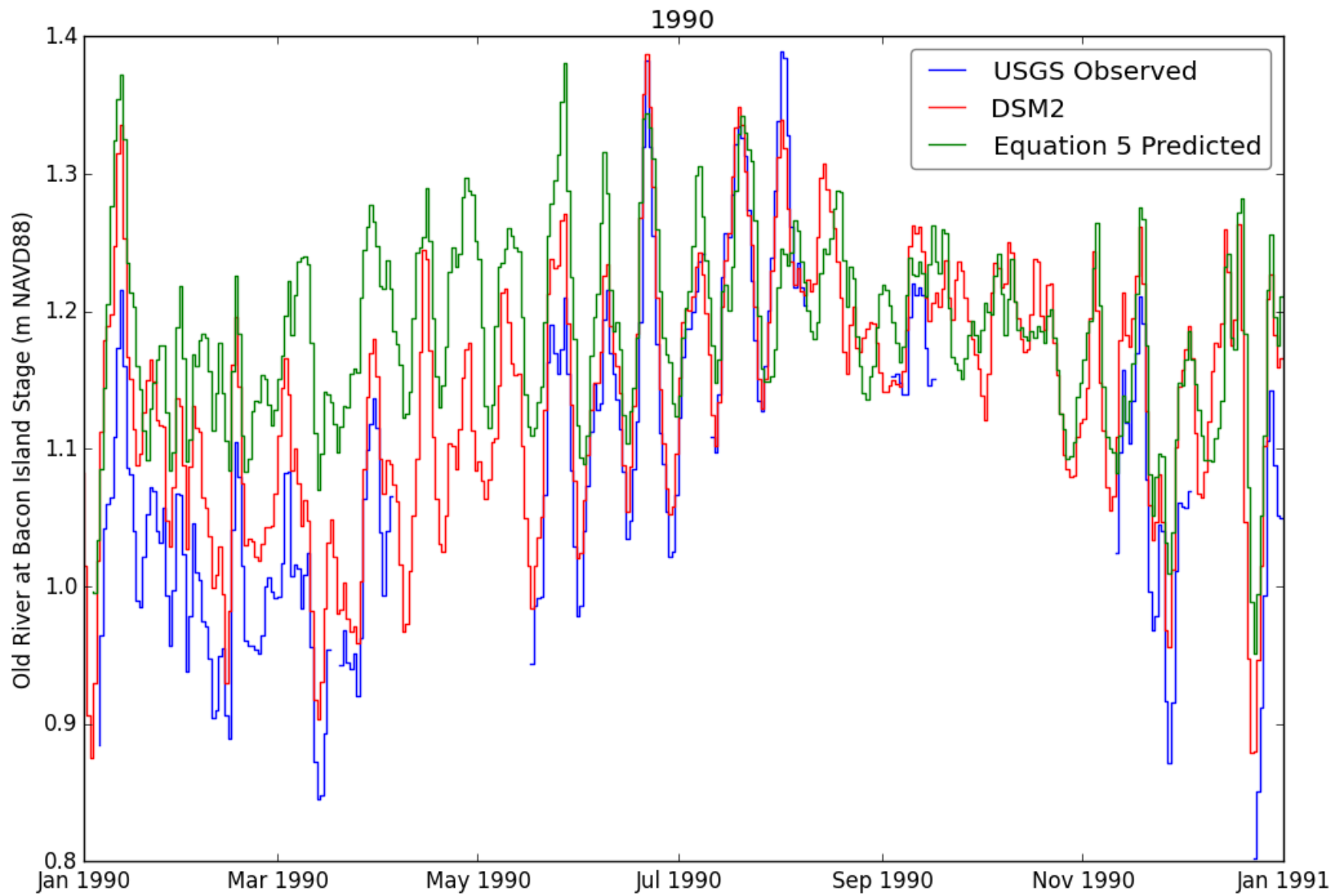
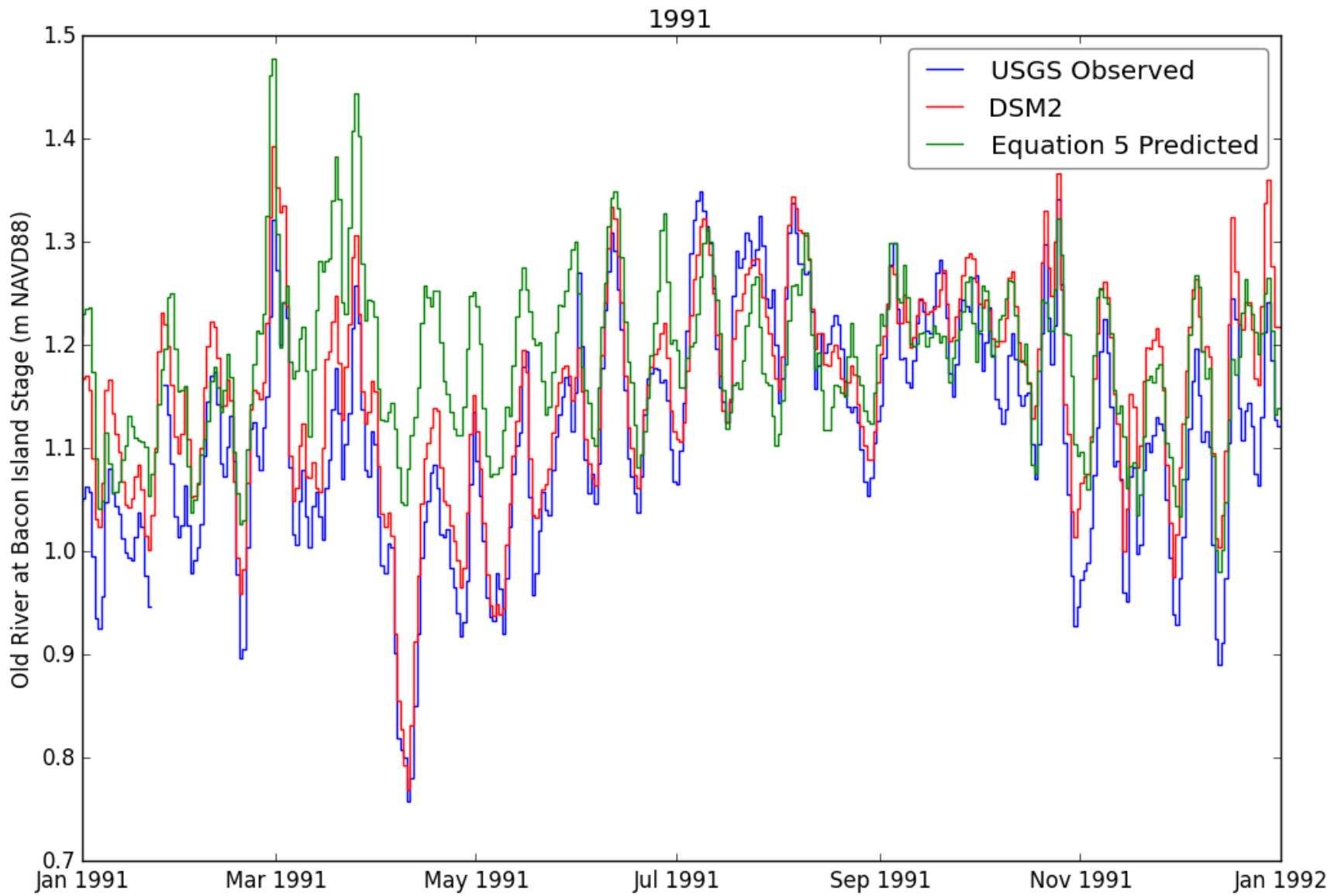
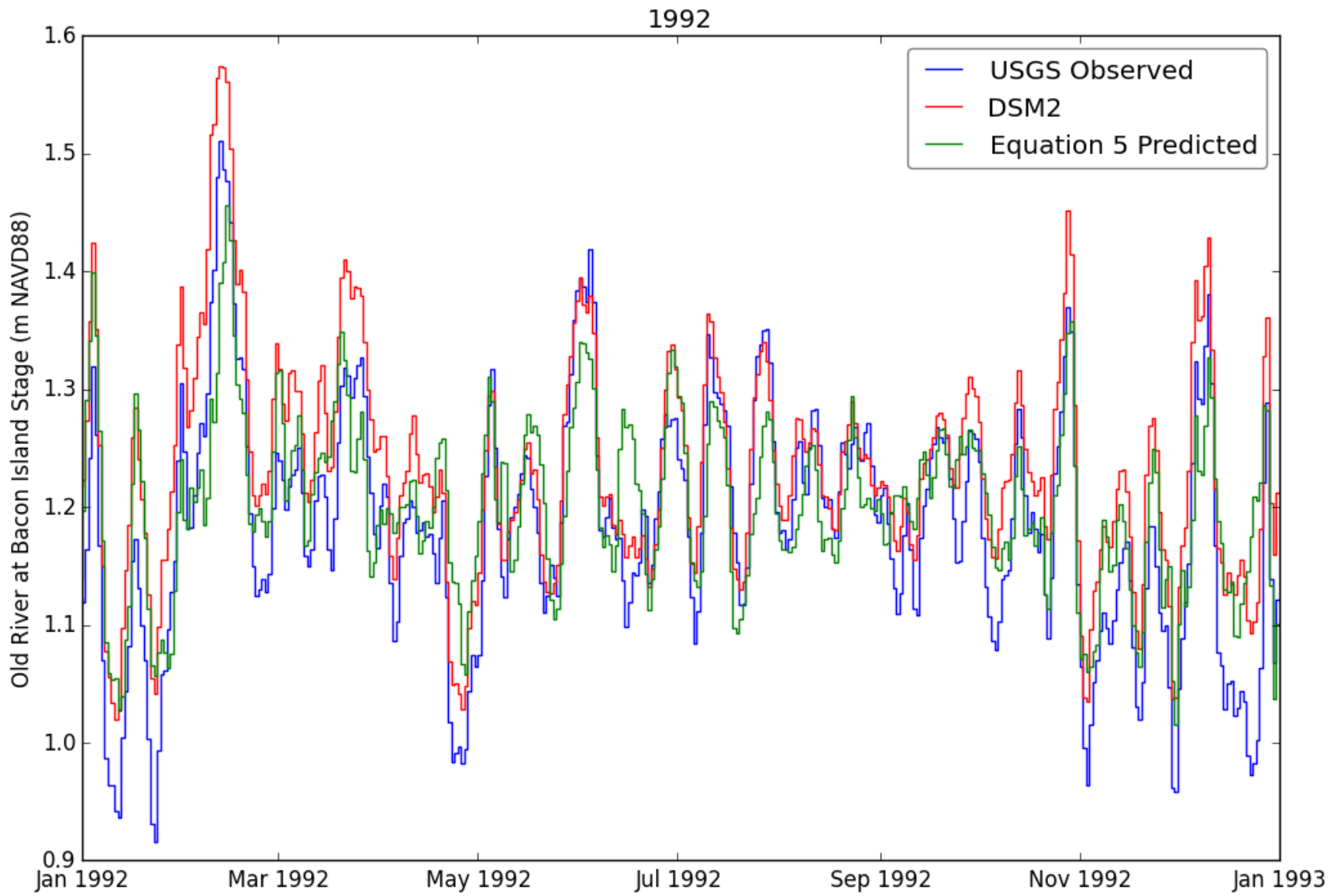


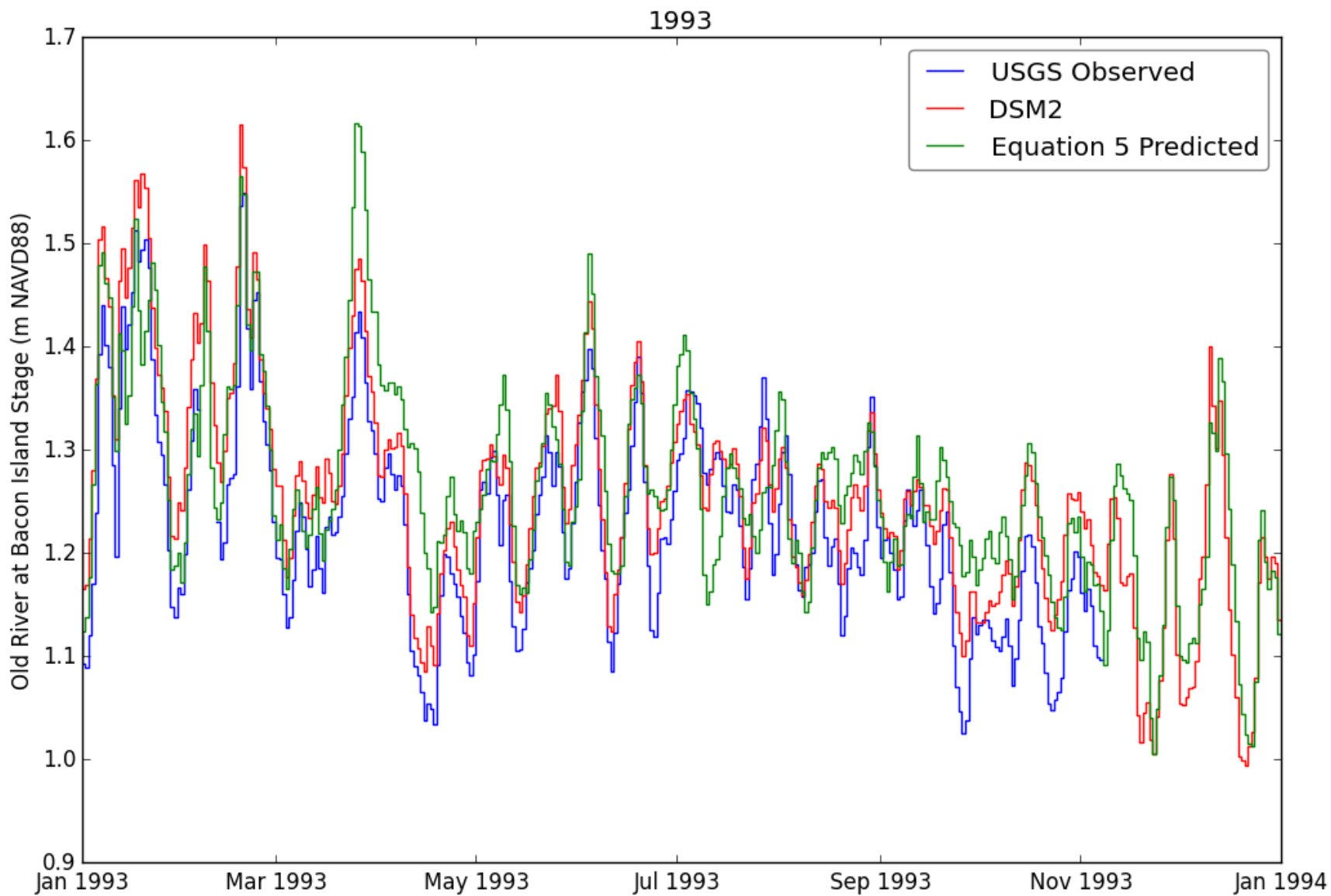
Figure 20 Hypsographic curve data and linear fit for the south Delta control volume region downstream of temporary agricultural barriers.

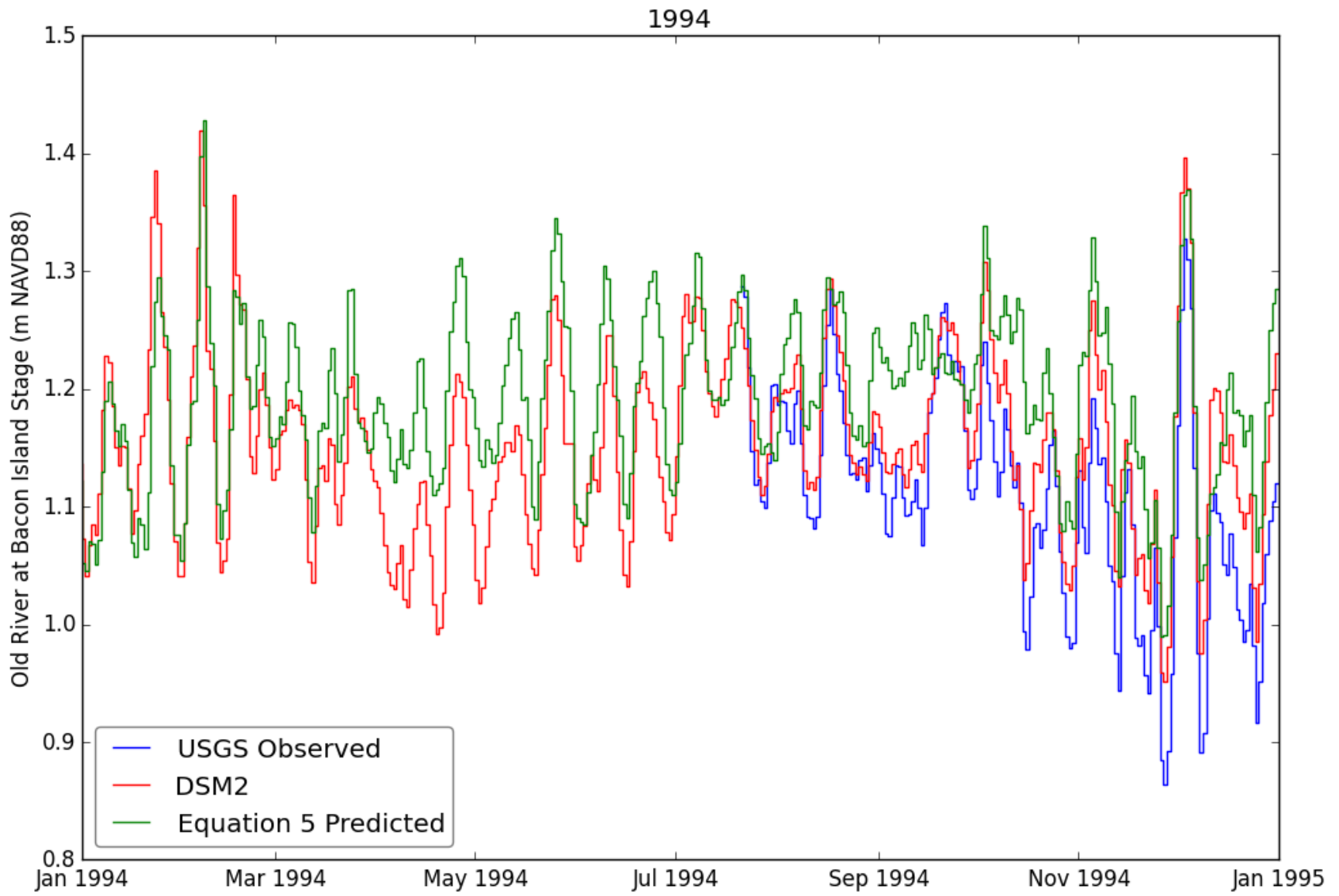
Appendix B: Yearly Old River at Bacon Island Stage Comparison Plots

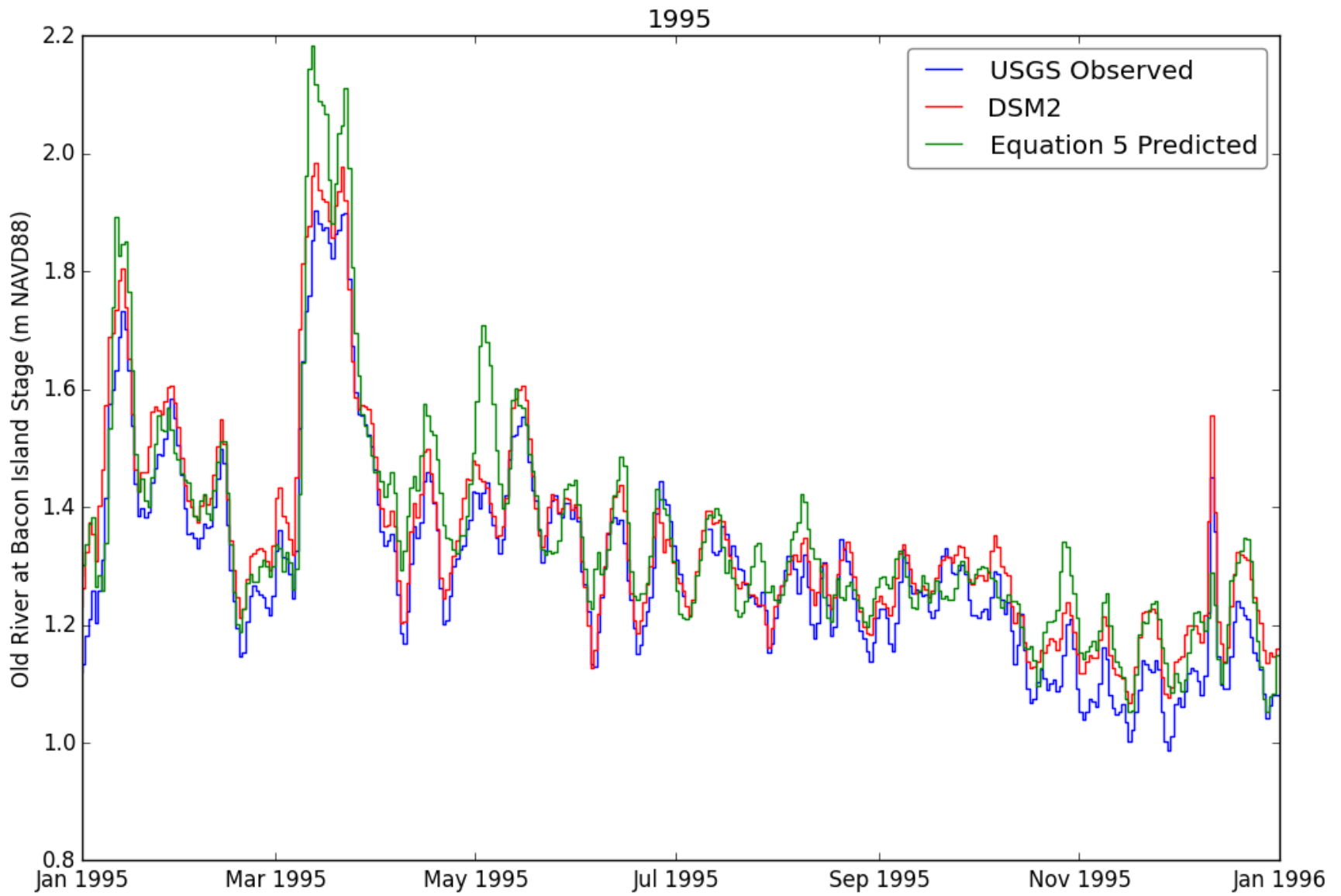


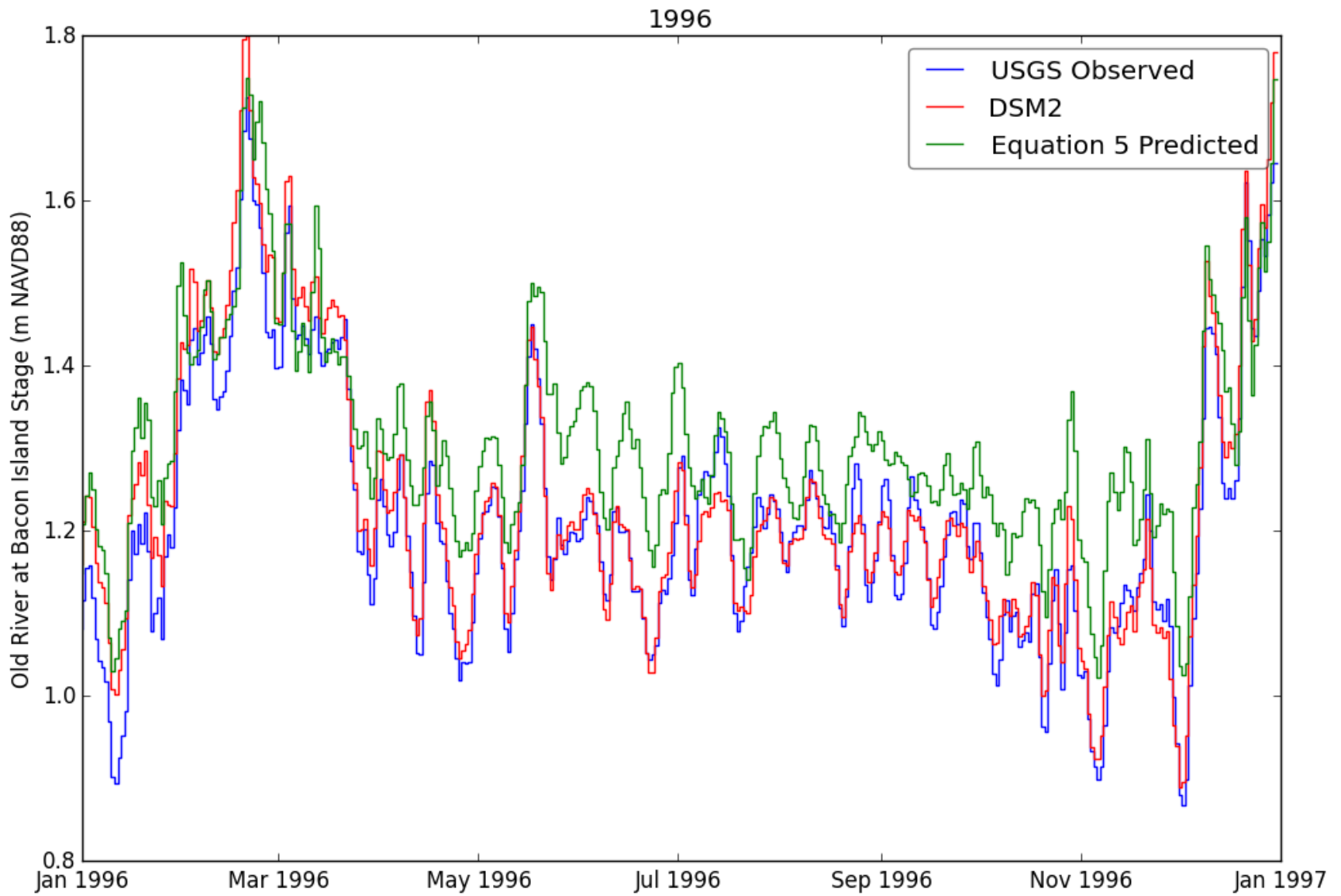


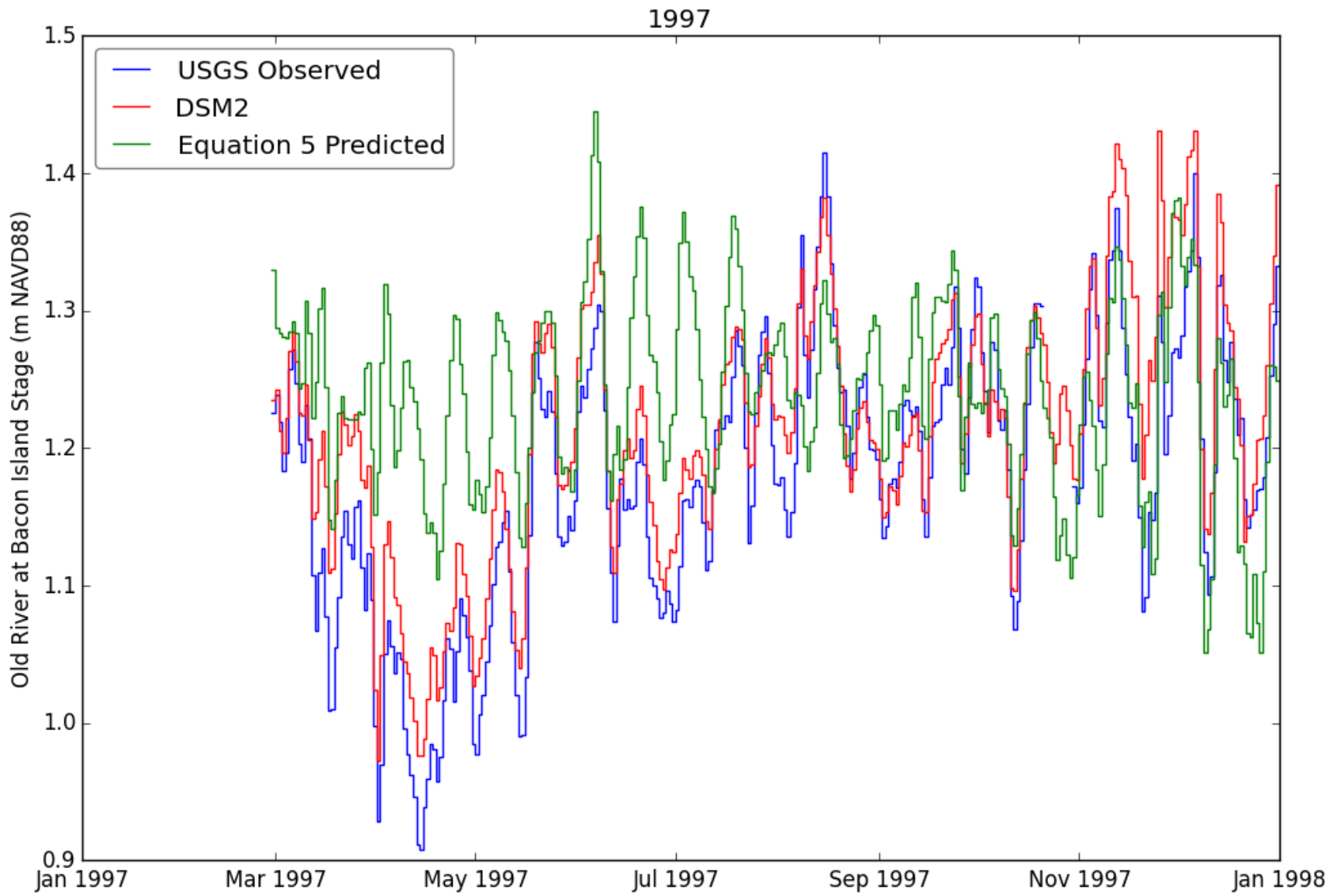


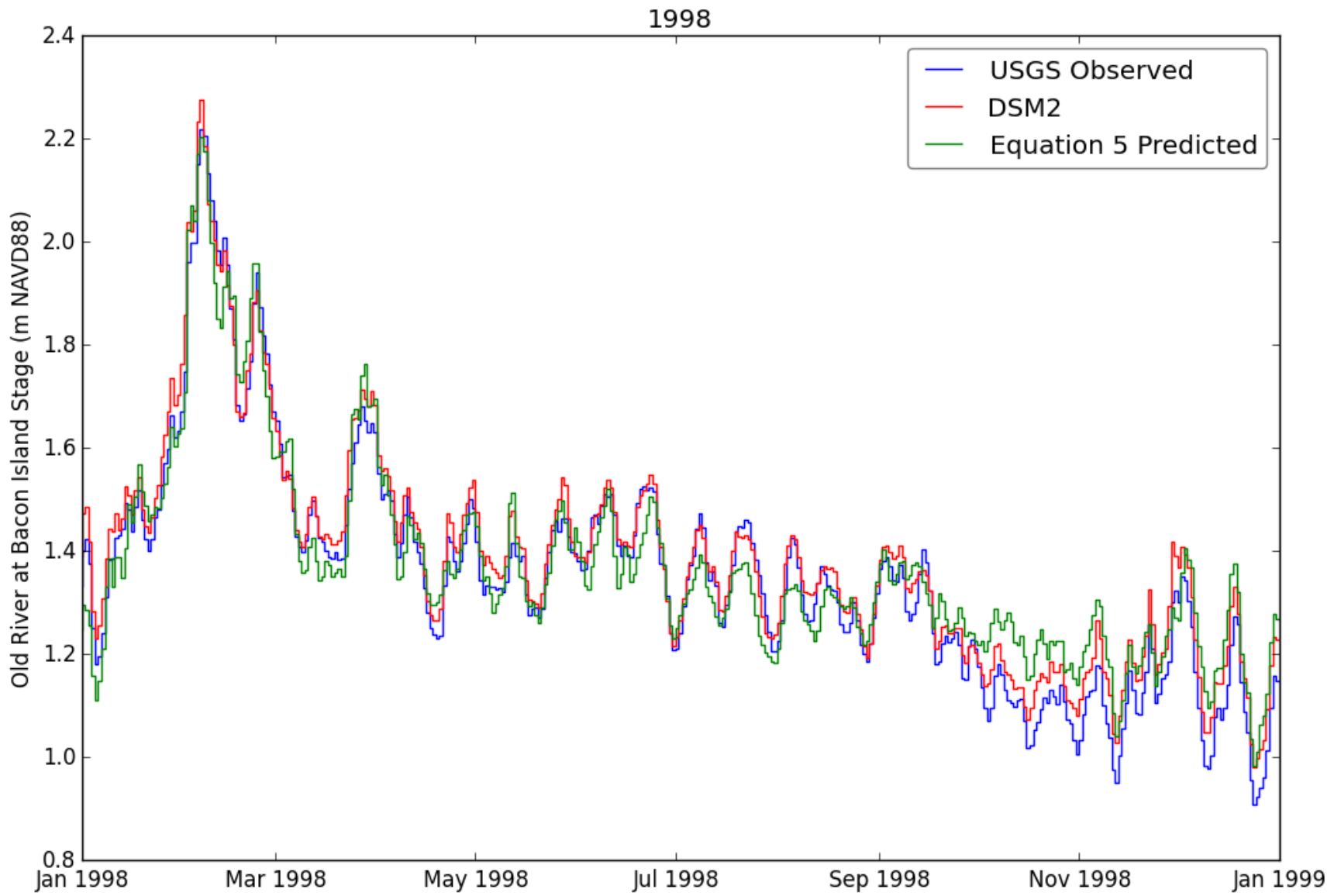


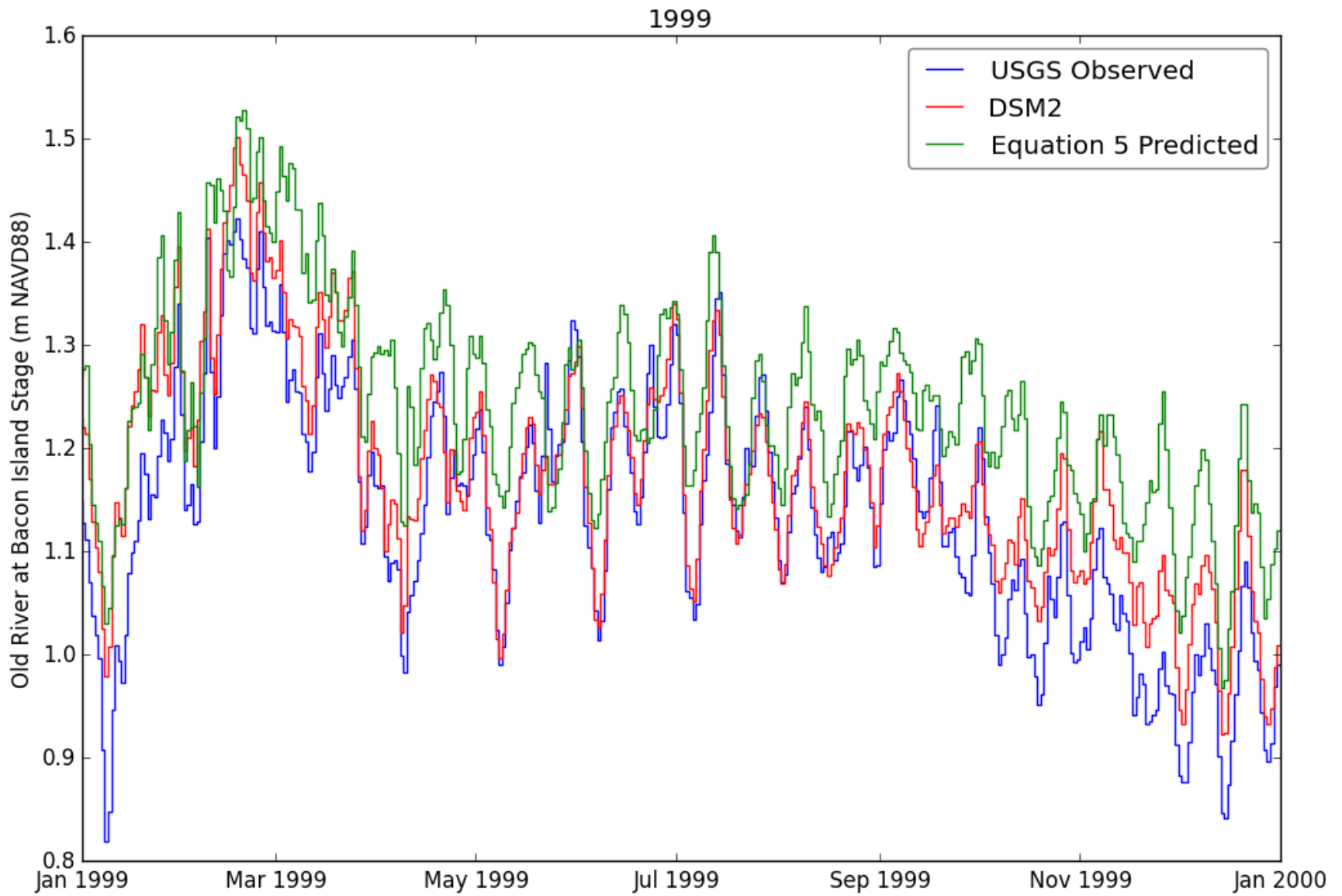


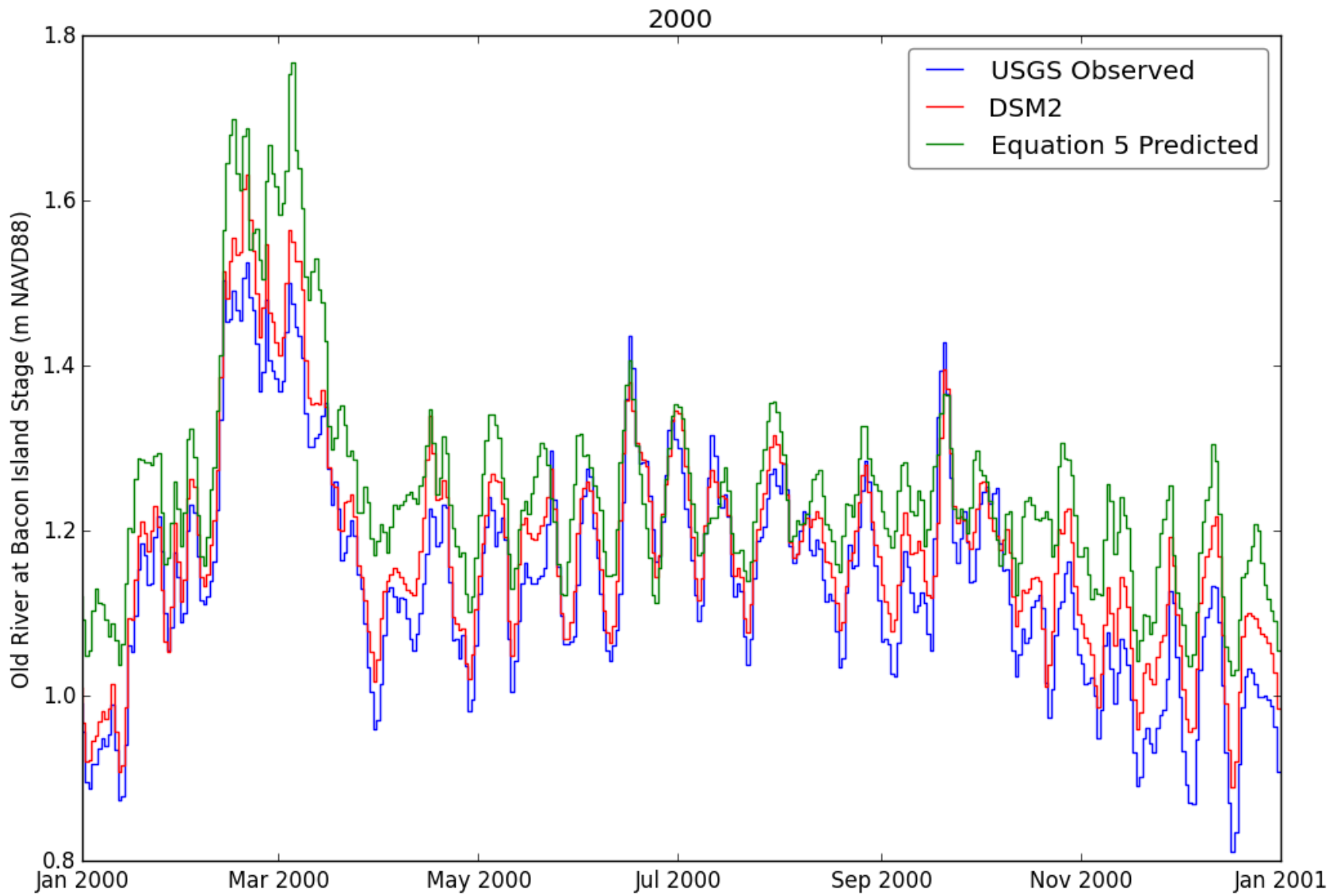


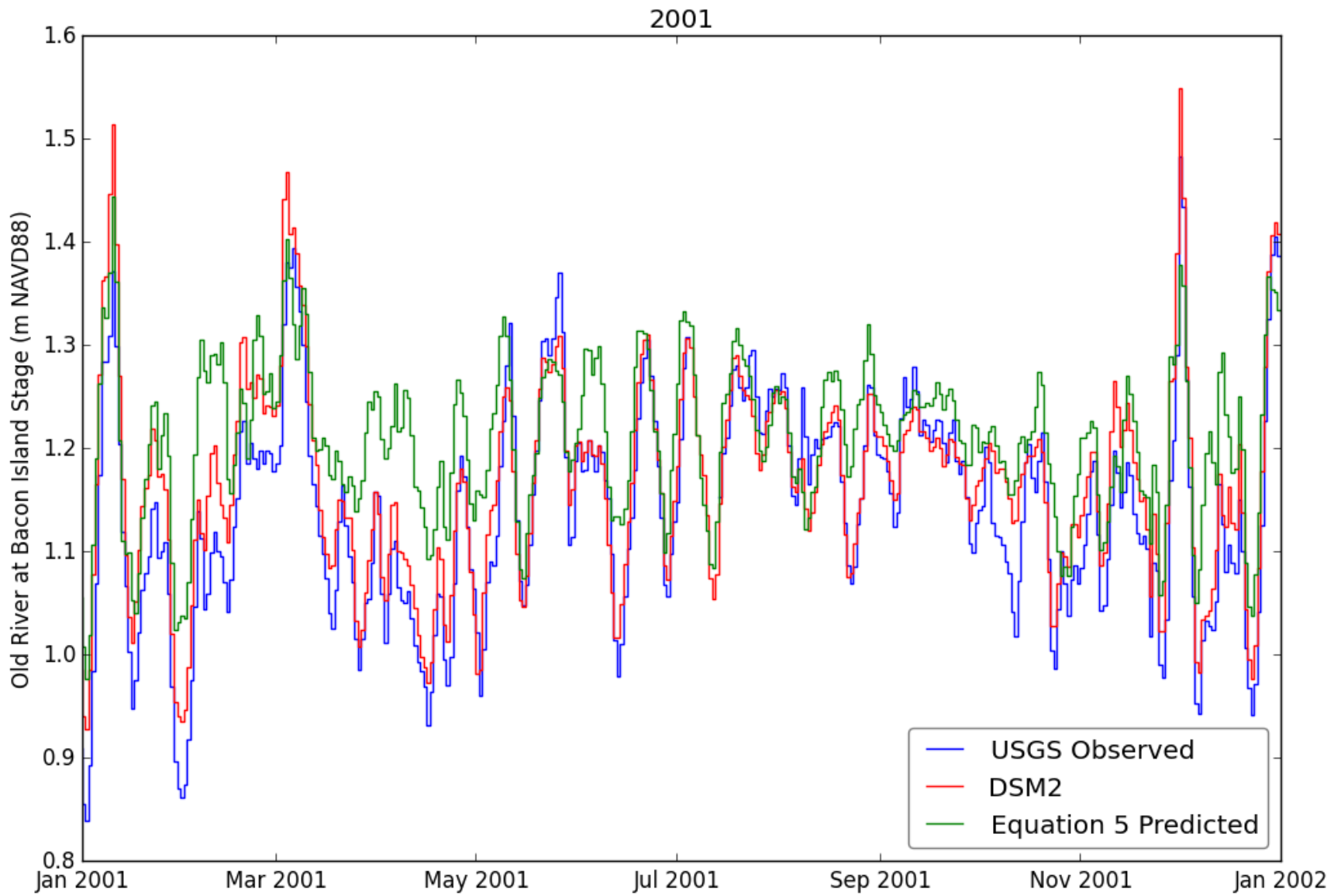


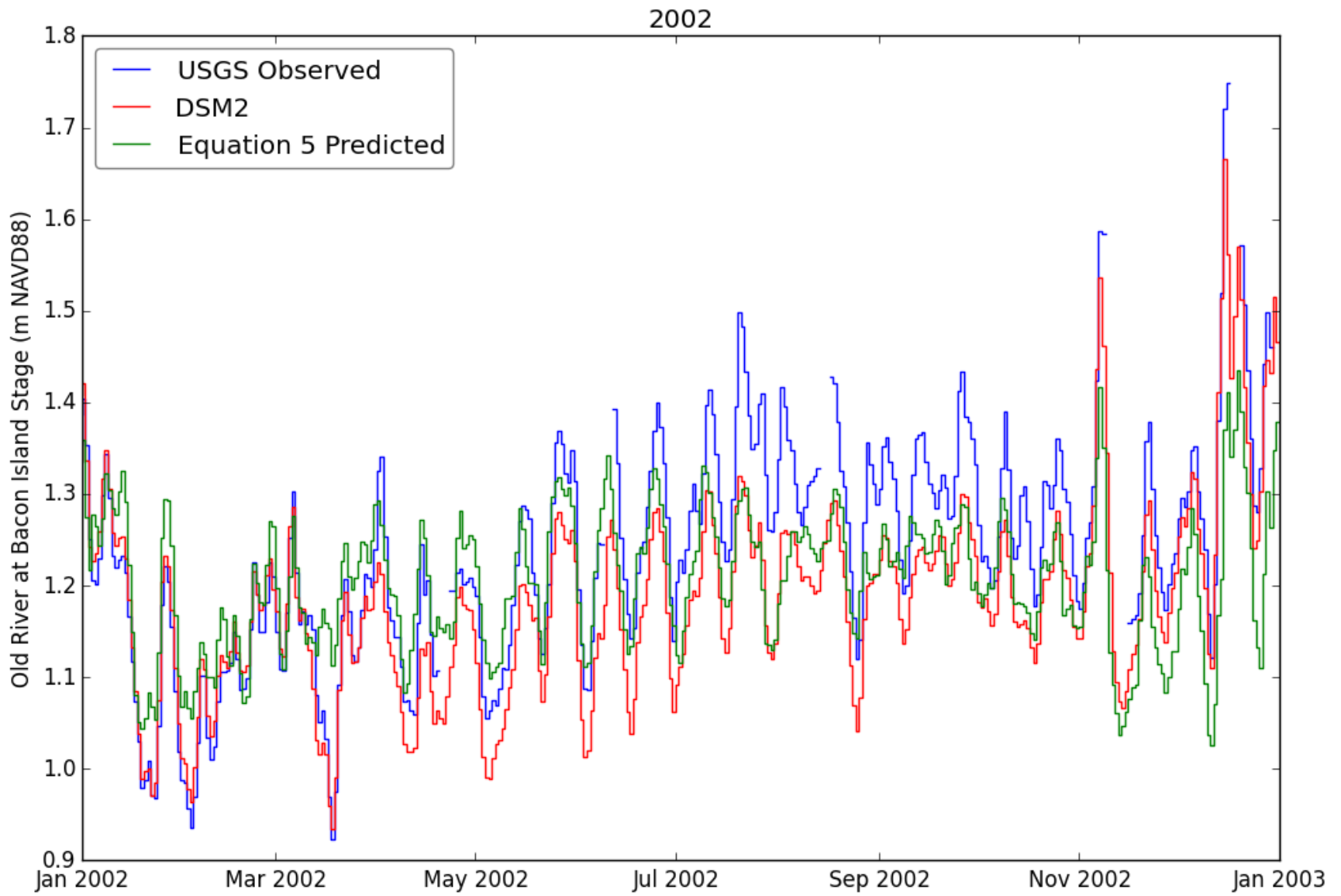


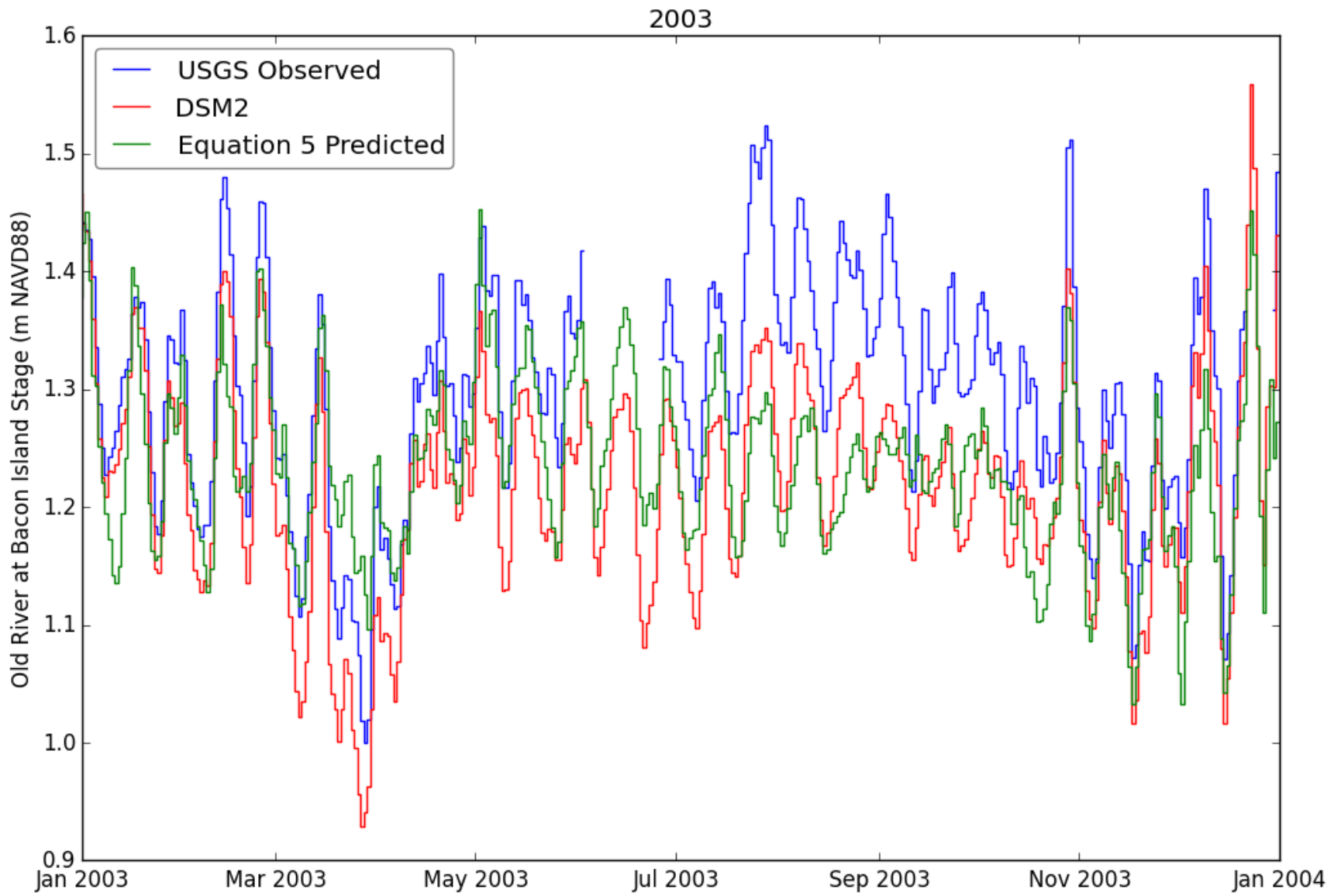


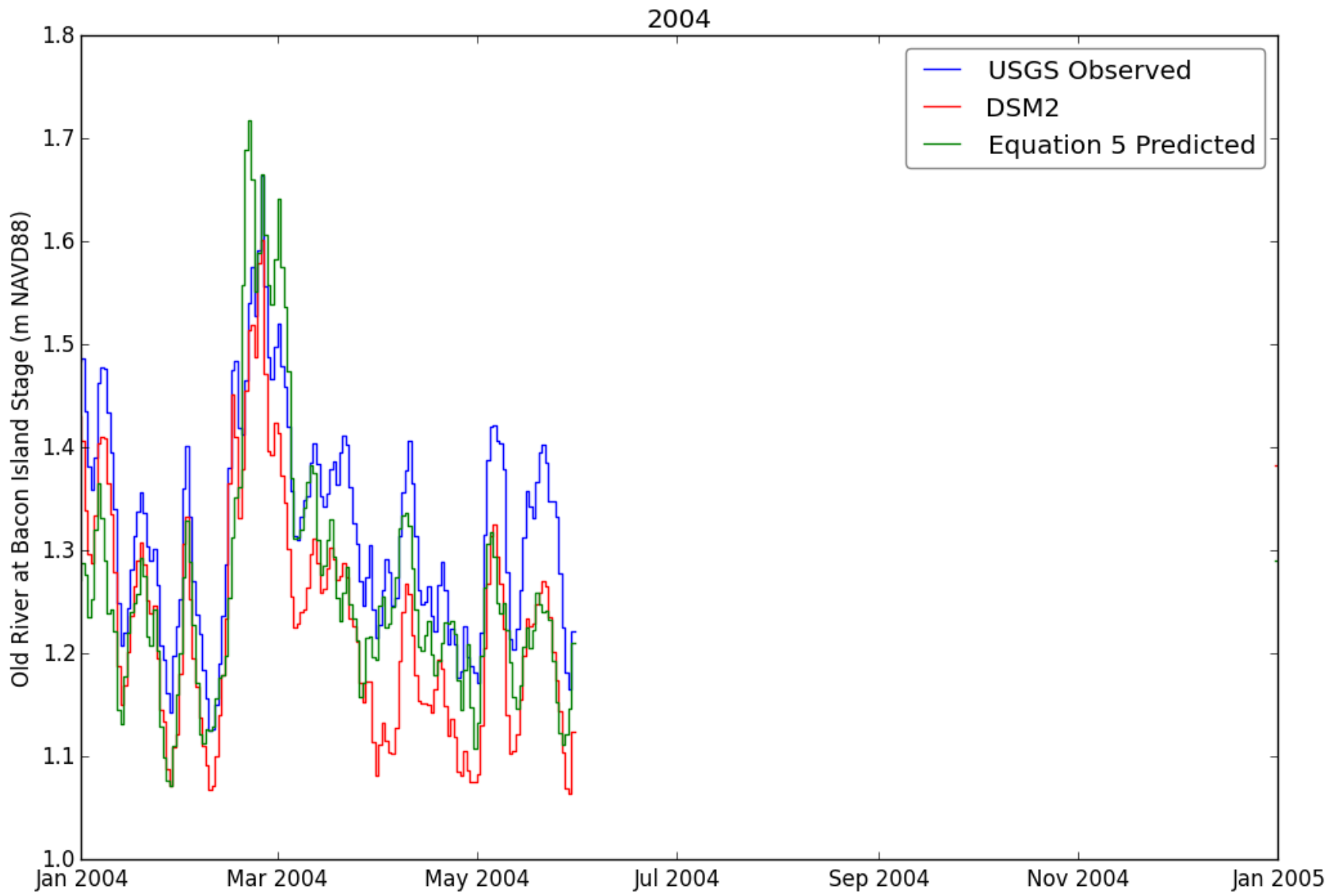


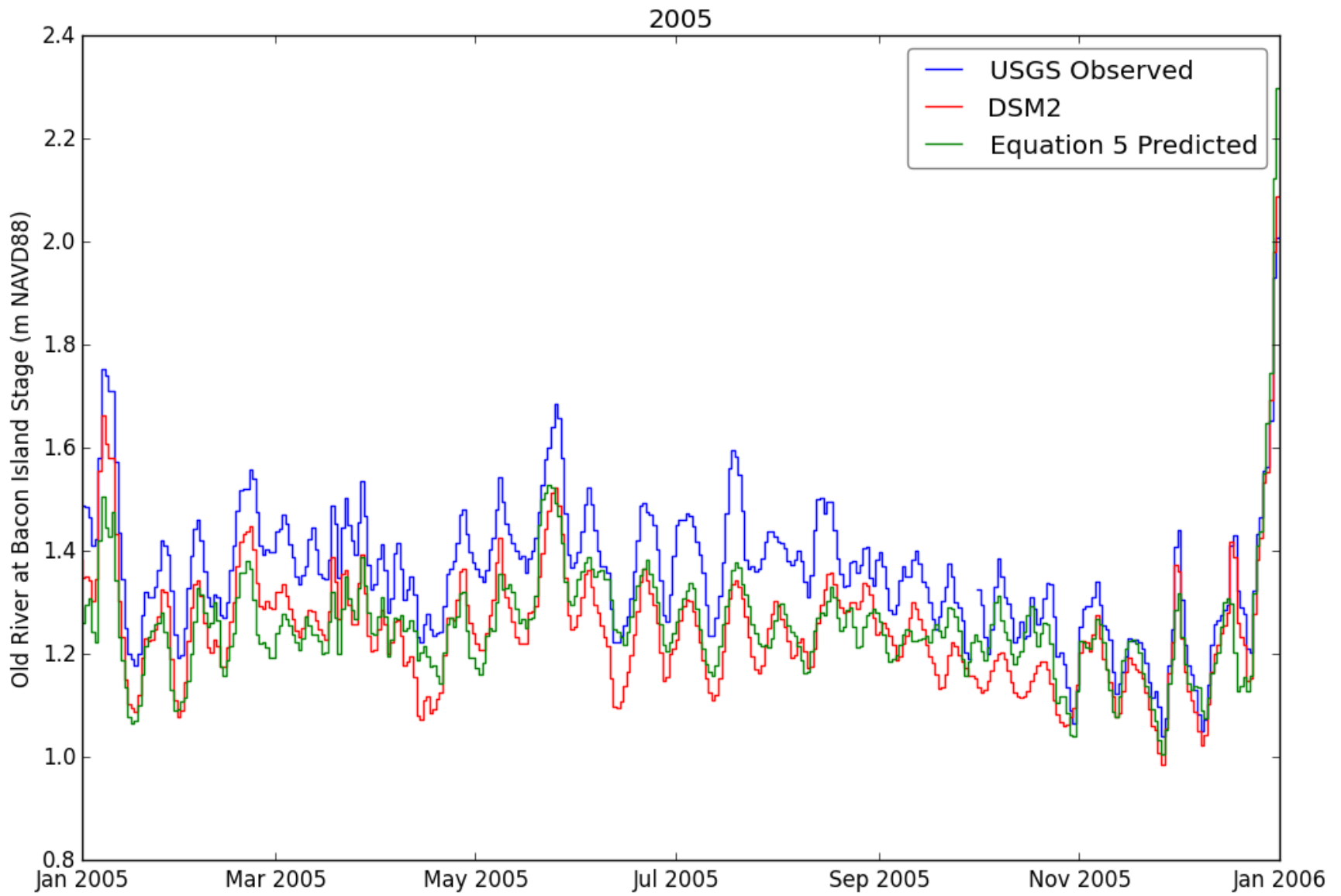


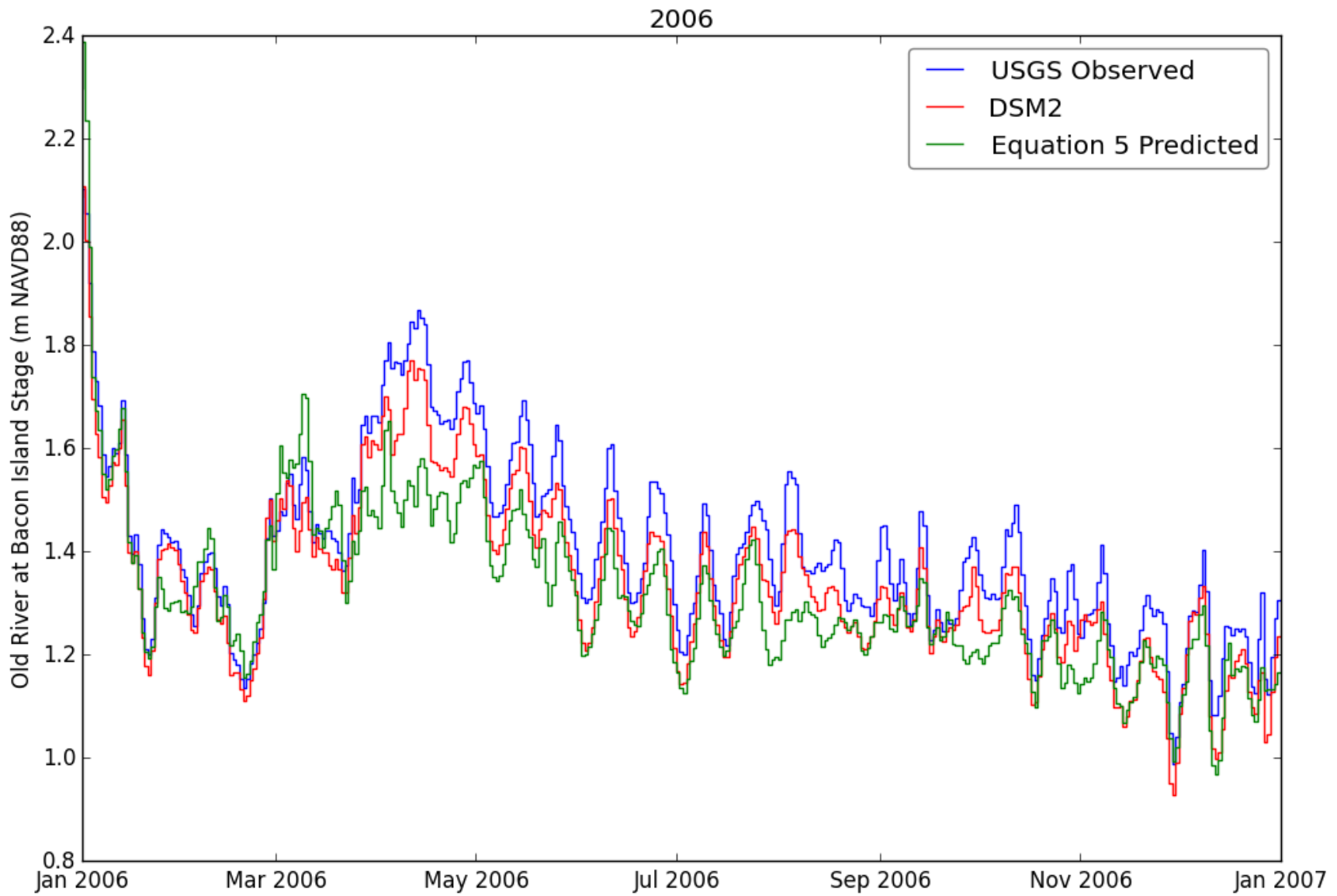


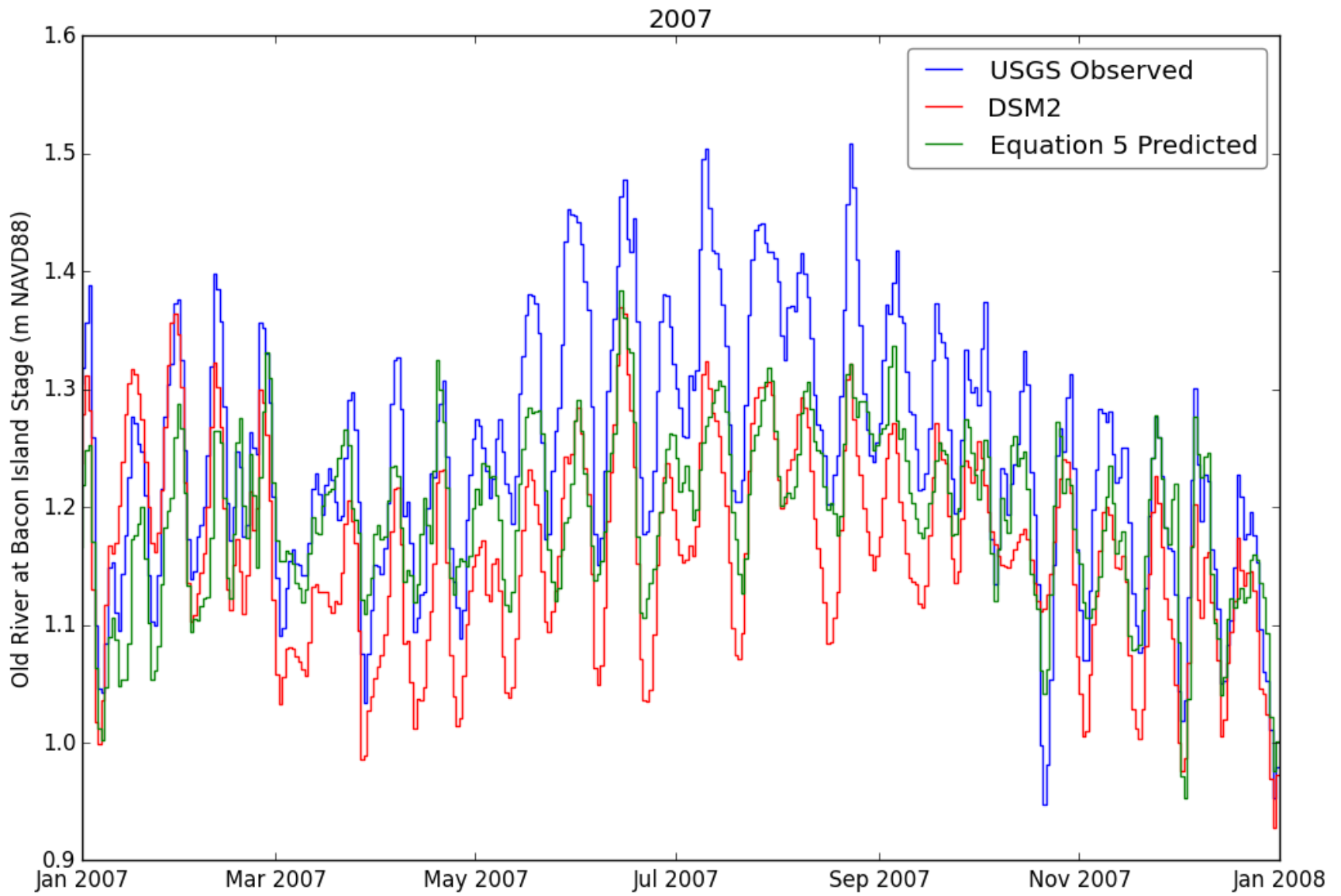


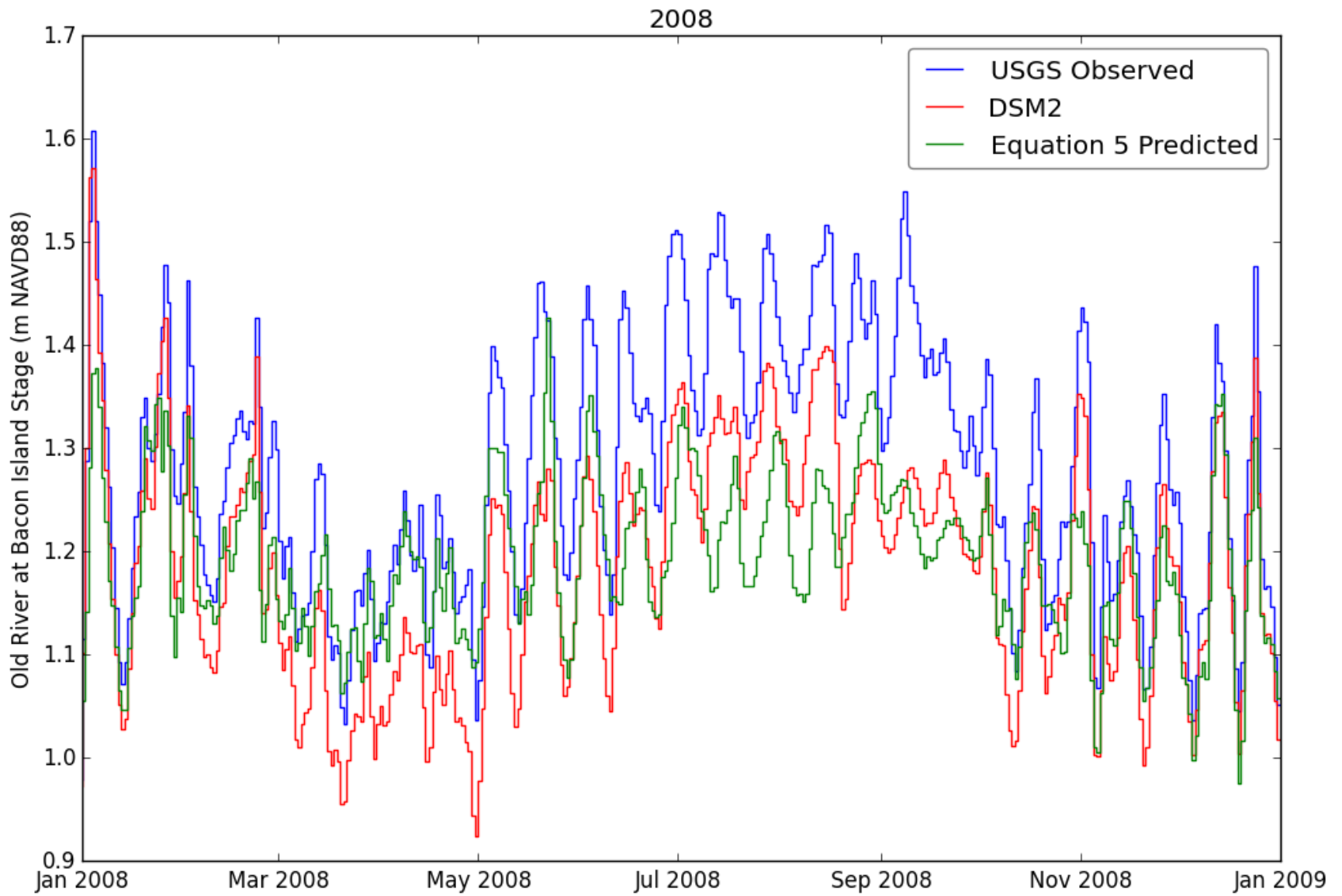


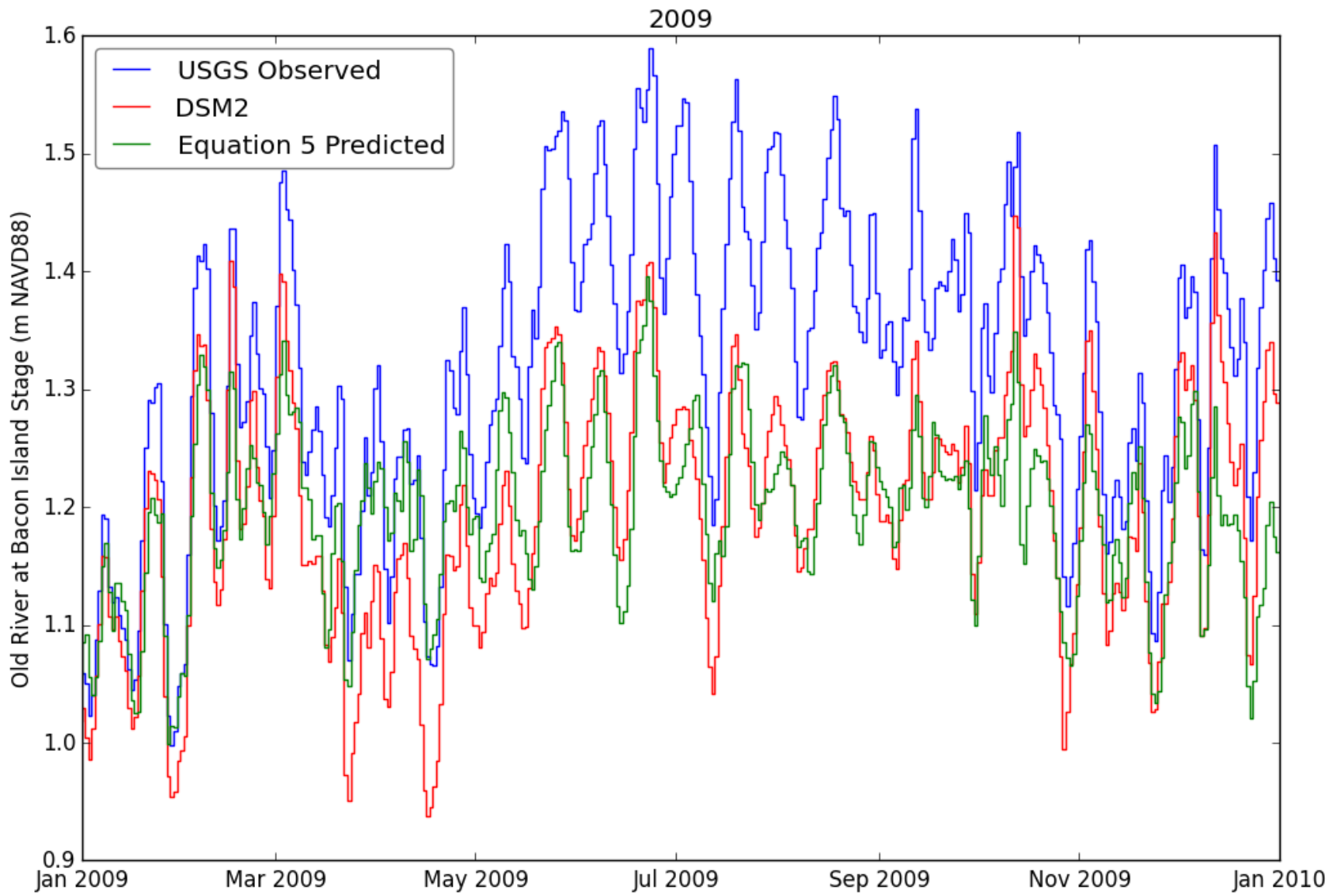


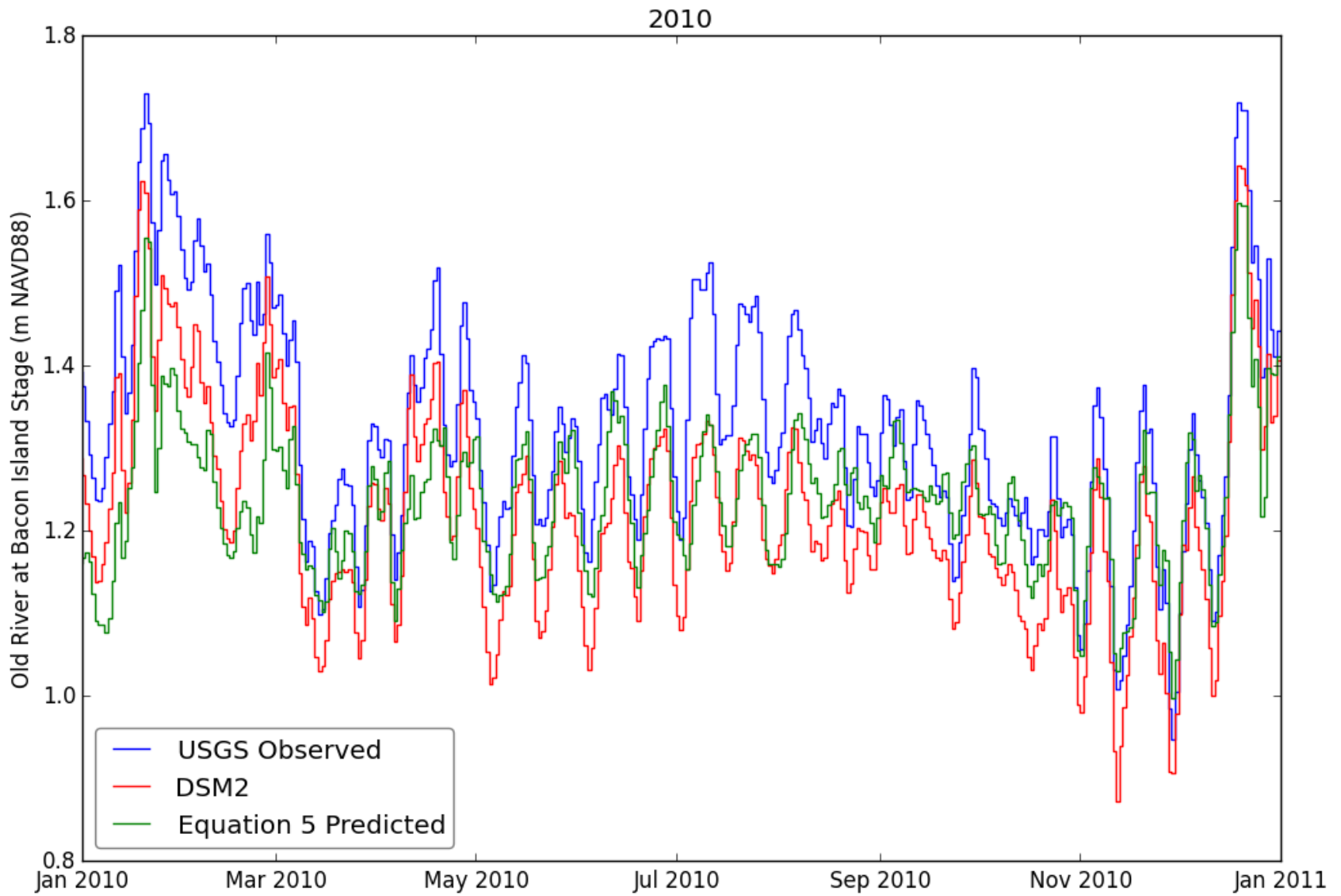


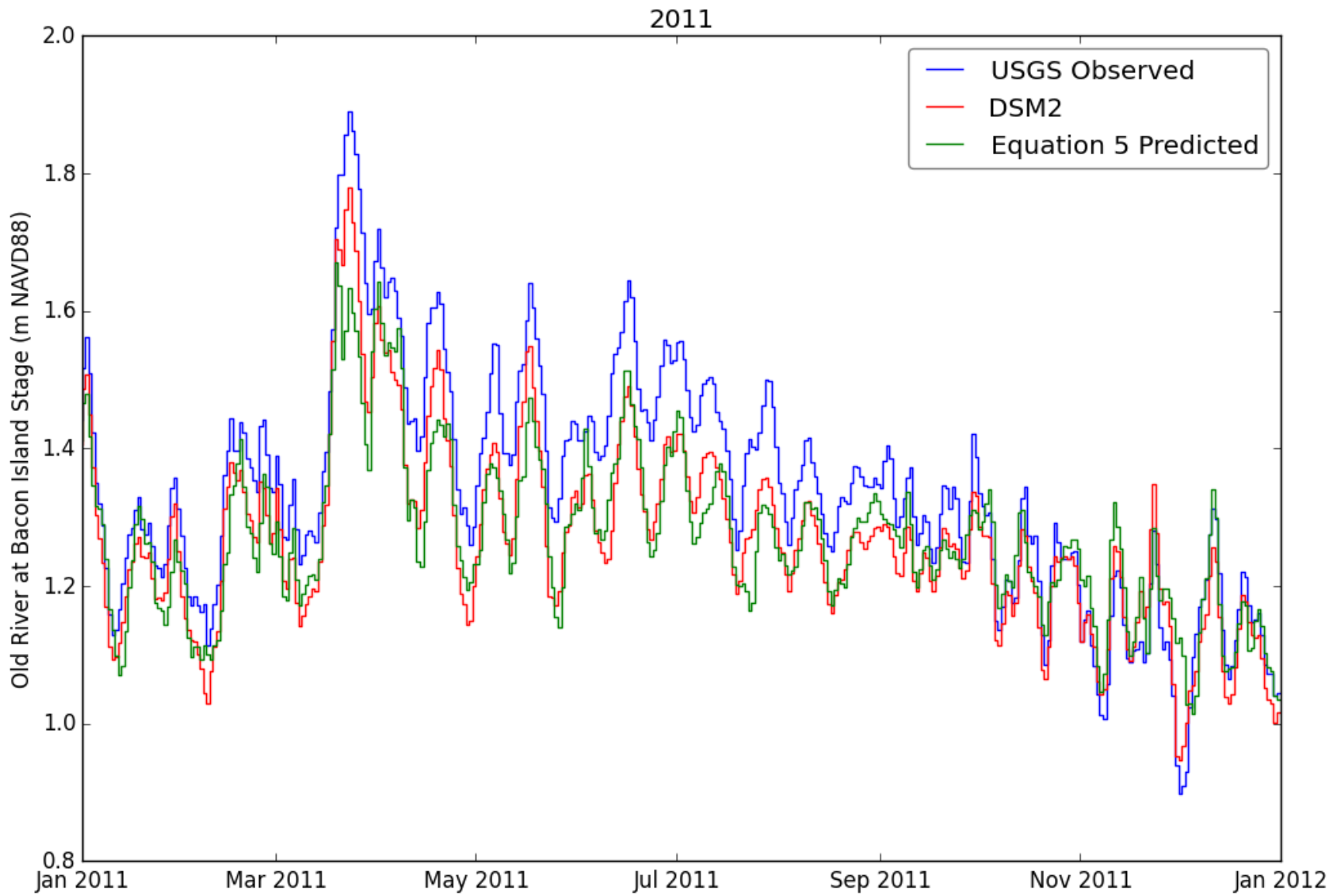


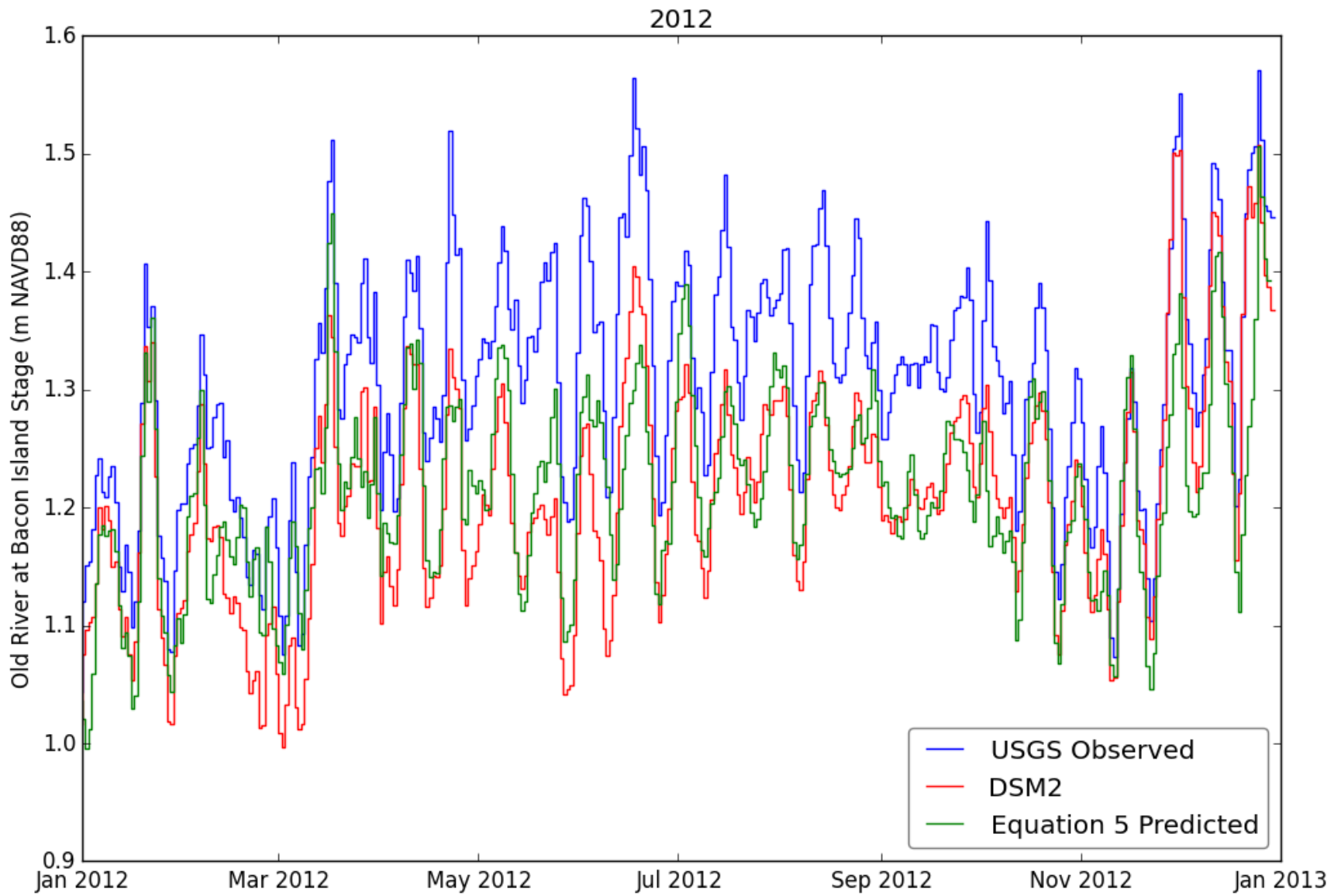












Appendix C: Yearly OMR Flow Comparison Plots

